Advanced Vehicle Powertrain Design using Model-Based Design

David Andrew Ord

Thesis submitted to the faculty of the Virginia Polytechnic Institute and State University in partial fulfillment of the requirements for the degree of

Master of Science
in
Mechanical Engineering

Chair: Douglas J. Nelson
Alexander Leonessa
John B. Ferris

May 5, 2014
Blacksburg, VA

Keywords: model-based design, hybrid electric vehicle, plug-in, architecture selection, greenhouse gases, petroleum, fuel economy, powertrain modeling

ADVANCED VEHICLE POWERTRAIN DESIGN USING MODEL-BASED DESIGN

David Andrew Ord

ABSTRACT

The use of alternative fuels and advanced powertrain technologies has been increasing over the past few years as vehicle emissions and fuel economy have become prominent in both manufacturer needs and consumer demands. With more hybrids emerging from all automotive manufacturers, the use of computer modeling has quickly taken a lead in the testing of these innovative powertrain designs. Although on-vehicle testing remains an important part of the design process, modeling and simulation is proven to be an invaluable tool that can be applied anywhere from preliminary powertrain design to controller software validation.

The Hybrid Electric Vehicle Team (HEVT) of Virginia Tech is applying for participation in the next Advanced Vehicle Technology Competition. ***EcoCAR 3*** is a new four year competition sponsored by the Department of Energy and General Motors with the intention of promoting sustainable energy in the automotive sector. The goal of the competition is to guide students from universities in North America to create new and innovative technologies to reduce the environmental impact of modern day transportation. ***EcoCAR 3***, like its predecessors, will give students hands-on experience in designing and implementing advanced technologies in a setting similar to that of current production vehicles. The primary goals of the competition are to improve upon a provided conventional, internal combustion engine production vehicle by designing and constructing a powertrain that accomplishes the following:

- Reduce Energy Consumption
- Reduce Well-to-Wheel (WTW) Greenhouse Gas (GHG) Emissions
- Reduce Criteria Tailpipe Emissions
- Maintain Consumer Acceptability in the area of Performance, Utility, and Safety
- Meet Energy and Environmental Goals, while considering Cost and Innovation

This paper presents a systematic approach in selecting a powertrain for HEVT to develop in the upcoming competition using model-based design. Using a base set of powertrain component models, several powertrain configurations are modeled and tested to show the progression from a basic conventional vehicle to several advanced hybrid vehicles. Each model is designed to generate energy consumption data, efficiency, emissions, as well as many other parameters that can be used to compare each of the powertrain configurations. A powertrain design is selected to meet the goals of the competition after exploring many powertrain configurations and energy sources. Three parallel powertrains are discussed to find a combination capable of meeting the target energy consumption and WTW GHG emissions while also meeting all of the performance goals. The parallel through the road hybrid is sized to meet most power needs with an electric motor and a smaller IC engine. Lastly, the battery and motor size are increased to allow a charge depleting mode, adding stored grid electricity to the energy sources. This electric energy only mode is able to displace a large amount of the fuel energy consumption based on the SAE J1711 method for determining utility factor weighted energy consumption of a plug-in hybrid vehicle. The final design is a Parallel Plug-In Hybrid Electric Vehicle using E85 fuel and a 7 kWh battery to provide an all-electric charge depleting range of 34 km (21 mi)

ACKNOWLEDGEMENTS

I would first like to thank Argonne National Laboratory for the Model Based Design Curriculum Project, and supporting partners The MathWorks, National Science Foundation, and The U. S. Dept of Energy for supporting this work. Next I would like to thank General Motors, the United States Department of Energy, and Argonne National Labs for sponsoring and organizing the EcoCAR 2 competition as well as other related programs. The opportunity to participate in such a program has shaped my academic experience as well as my career path into something I am proud of. Next I would like to thank the Hybrid Electric Vehicle Team at Virginia Tech for providing me support and friendship that I will value for years to come. I would also like to thank my family and friends for supporting me throughout my academic career. Finally, I would like to thank Dr. Nelson for being a great mentor and friend.

TABLE OF CONTENTS

LIST OF TABLES

LIST OF FIGURES

LIST OF ABBREVIATIONS

APP	Accelerator Pedal Position
AVTC	Advanced Vehicle Technology Competition
BAS	Belted Alternator Starter
BEV	Battery Electric Vehicle
BMEP	Brake Mean Effective Pressure
BPP	Brake Pedal Position
BSFC	Brake Specific Fuel Consumption
CD	Charge Depleting
CS	Charge Sustaining
ECU	Electronic Control Unit
EREV	Extended Range Electric Vehicle
ESS	Energy Storage System
EV	Electric Vehicle
FTP	Federal Test Procedure
GHG	Greenhouse Gas
GVWR	Gross Vehicle Weight Rating
HEV	Hybrid Electric Vehicle
HEVT	Hybrid Electric Vehicle Team
HIL	Hardware In the Loop
HVSC	Hybrid Vehicle Supervisory Controller
HWFET	Highway Fuel Economy Test
ICE	Internal Combustion Engine
LHV	Lower Heating Value
MIL	Model In the Loop
MPG	Miles Per Gallon
MPGGE	Miles Per Gallon Gasoline Equivalent
PE	Petroleum Energy
PEU	Petroleum Energy Use
PHEV	Plug-In Hybrid Electric Vehicle
PID	Proportional Integral Derivative
PTTR	Parallel Through The Road
SHEV	Series Hybrid Electric Vehicle
SIL	Software In the Loop
SOC	State of Charge
TE	Thermoelectric
UDDS	Urban Dynamometer Driving Schedule
UF	Utility Factor
WTW	Well to Wheel

1. INTRODUCTION

1.1. Introduction to EcoCAR

The purpose of the study (Ord et al., 2014) is to use modeling techniques to design a powertrain to meet the performance and energy consumption goals for ***EcoCAR 3***. In this study, energy requirements at the wheels for drive cycles are evaluated by a "glider" model. Once the energy requirements are established, powertrain configurations are evaluated by several MATLAB/Simulink component models. Some models, such as the conventional vehicle model, employ more than one modeling technique in order to evaluate the validity of the results. The powertrain configurations evaluated include:

- Conventional – IC Engine, Driveline
- Battery Electric – Traction Motor, Battery, Driveline
- Series Hybrid – IC Engine, Generator, Traction Motor, Battery, Driveline, Supervisory Controls
- Parallel Hybrid – IC Engine, Motor/Generator, Battery, Driveline, Supervisory Controls

These configurations are evaluated using different modeling techniques that include:

- Model Based Design – MATLAB driven Simulink models, including a driver model
- Single Step Evaluation – Excel spreadsheets of powertrain losses and consumption

The single step evaluation method is used for comparison purposes from the work contained in White's thesis (White, 2014). Powertrain models include separate components to keep track of the energy loss as the system power flow progresses. The components generally use power or torque and speed. While using power to evaluate individual components is certainly easier and provides useable results, torque-speed provides more accurate results with a more in-depth look into the function of the individual components. With several sources of results to model each of the listed powertrain configurations, a preferred configuration is selected to meet the consumption and performance goals for ***EcoCAR 3***.

EcoCAR 3 has specific minimum modeling design targets. These targets are summarized in Table 1-1. Although these targets may not be the final targets for the actual competition, they do serve as acceptable guidelines for powertrain modeling. The goal of the study is to not only meet the requirements listed in Table 1-1, but to exceed them using scalable modeling methods that will provide a solid basis to design a future advanced technology vehicle.

Table 1-1: Vehicle Design & Modeling Requirements

Performance/Utility Category	Vehicle Modeling Design Targets
Energy Consumption (unadjusted energy use on combined Federal Test Procedure [FTP] city and highway cycles)	Less than 370 Wh/km (600 Wh/mi) combined city and highway (55%/45% respectively)
GHG emissions (WTW combined city and highway cycles)	Less than 120 g of carbon dioxide equivalent (CO_2 eq)/km (200 g CO_2 eq/mi)
Interior size/number of passengers	Minimum 4 passengers
Luggage Capacity	More than 230 L (8 ft^3)
Range	> 320 km (200 mi) combined city and highway
Top Speed	> 135 kph (85 mph)
Acceleration time of 0 to 97 kph (0 to 60 mph)	< 11 seconds
Highway gradeability (at gross vehicle weight rating [GVWR])	> 3.5% grade @ 97 kph (60 mph) for 20 minutes

1.2. Hybrid Electric Vehicles

As the push for green energy continues to gain momentum in today's industry, the automotive industry is a primary focus of more efficient and eco-friendly machines. Consumers are looking for more efficient vehicles to save money as well as reducing greenhouse gas emissions that petroleum based fuels produce. In addition to consumer demands, government mandates have forced automotive manufacturers to move towards using alternative fuels and increasing the efficiency of their petroleum vehicles. Hybrids are now coming into the main focus of automotive manufacturers and will play a vital role in moving forward towards more efficient vehicles.

The basis of a hybrid vehicle is the use of two or more energy sources on board the vehicle. The general assumption is that the two fuels used are petroleum, whether it be gasoline or diesel, and electricity. With electricity and petroleum both being used in a powertrain, the use of electricity can vary in different forms of hybrid vehicles. A more complex, yet more efficient powertrain will include a large battery and electric motor, while a conventional vehicle with a larger starter motor for engine stop-start capabilities is considered a micro-hybrid.

Electrification of a powertrain can increase the efficiency of the powertrain by reducing fuel consumption in several different ways. As mentioned previously, a small motor can be used to quickly start the engine when it comes to a stop for a short amount of time, such as at a stop sign. The benefits of this function is clear because idle fuel use is essentially wasting fuel. In addition to reducing idle fuel use, a larger electric powertrain allows the on board engine to operate more efficiently. Many vehicles today have larger engines that generally will not operate in an efficient region during day-to-day use. With an electric motor large enough to assist the engine, the controller can choose an efficient operating point while the electric motor either assists the engine or loads the engine to get to that point. Another function in hybrid vehicles is regenerative braking. In a conventional vehicle, brake energy is completely lost using friction brakes. With regenerative braking,

electric motors are used to slow the vehicle for at least some portion of the driver demand, capturing some of the otherwise wasted energy for later use.

The powertrain that requires the largest battery and electric machines is a plug-in hybrid. With a plug-in hybrid, full electric capability is possible for a relatively short range, allowing limited use of fuel on short commutes, as well as the previously discussed advantages when using fuel is required. Grid electricity can be used to charge the vehicles at home or work.

1.3. Model-Based Design

With more advanced powertrains becoming a prominent part in automotive standards, the need for advanced methods of powertrain design become a necessity. While a main purpose of model-based design is to design and validate control systems, the advanced use of models can also be applied to powertrain design.

The ability to create realistic vehicle models has opened the opportunity to test powertrain layouts in a simulation setting. An important aspect of this is component sizing to meet vehicle specification goals. By varying component sizes, numerous powertrain configurations can be tested and validated to ensure that a more efficient and feasible powertrain is designed. Using model-based design allows preliminary comparisons to be made between powertrain configurations, particularly if specific performance, energy consumption, or efficiency goals are required for a design. The use of model-based design at this phase in the design process improves the overall efficiency of the design process. Using models serves as an alternative to experimentally analyzing components and powertrains, which can be time consuming and costly.

1.4. Objectives

The primary goal of this research is to show a model-based design process used in developing numerous powertrain configuration models and demonstrating the ability to generate useful data and select an appropriate design to meet specified goals. The powertrain requirements defined by ***EcoCAR 3*** listed in Table 1-1 are used as performance, energy consumption, and emissions goals for the design process.

The equations and methods used in creating specific components that are to be used in the models are first defined and explained. Then, using the component models, a base conventional vehicle model is constructed and compared with various component sizes and modeling methods to validate results, and demonstrate the ability and trade-offs of component sizing. In order to show the advantages of vehicle electrification, a battery electric vehicle is modeled with several component sizes as well. Finally, several types of hybrid vehicle powertrain configurations are constructed and tested. The control strategy for each system is varied and explained in section 3 to show different methods and advantages of specific controller functions. Different hybrid powertrains are modeled to demonstrate the variation and possibilities of hybrid vehicles, as well as the trade-offs in component sizing and vehicle operation. A final evaluation and selection is made at the end of the paper to select a powertrain design to be constructed for the future ***EcoCAR 3*** competition.

1.5. Powertrain Efficiency

To meet the energy consumption goal in Table 1-1 the powertrain needs to achieve a certain overall powertrain efficiency. The minimum required powertrain efficiency η_{PT}, can be calculated using the energy consumption goal provided in Table 1-1, along with either the combined city and highway net tractive energy (road load), or the positive propel tractive energy at the wheels. The following equation shows the calculation for both cases.

$$\eta_{PT}^{+} = \frac{E_{tr}^{+}}{E_{in}} \qquad OR \qquad \eta_{PT}^{\text{net}} = \frac{E_{tr}^{net}}{E_{in}} \qquad \text{Equation 1-1}$$

In these equations, the superscripts $+$ and net represent propel and net road load. E_{in} and E_{tr} represent input energy and output tractive energy, respectively. Input energy could represent either fuel energy used or AC grid electrical energy. In the case of a conventional vehicle with no regenerative braking, the propel energy efficiency may be used because all of the brake energy is lost to the friction brakes, making the required powertrain efficiency higher to meet the design target. However, in the case of a vehicle with regenerative brake energy capture, net tractive energy may be more representative and credits 100% brake energy at the wheel. This definition lowers the efficiency required to meet the energy consumption goals. Both definitions are used in this work.

1.6. Fuel Properties

One important consideration during vehicle powertrain modeling is the energy source(s) used in the vehicle. Of the ***EcoCAR 3*** fuels considered in this work, each has its own perks and pitfalls. Grid electricity, although it has a higher WTW GHG factor, often ends up providing a marginal decrease in overall GHG emissions due to the higher efficiencies of electric drivetrains over combustion engines. E85 also provides an improvement in WTW GHG emissions, but has a lower energy density than E10 gasoline. Finding a combination of fuels that can minimize environmental impact is a detailed and difficult problem. Table 1-2 lists the different fuels that are used in the study, as well as important properties needed for calculating fuel consumption and GHG emissions (EcoCAR 2, 2013; GREET, 2013). For reference, a gallon of gasoline is considered to contain 33.3 kWh to express energy use in mpgge (miles per gallon of gasoline equivalent).

Table 1-2: Fuel Properties

Fuel	WTW GHG [g/kWh]	Upstream PE Content [kWh PE/kWh]	Downstream PE Content [kWh PE/kWh]	WTW PEU [kWh PE/kWh]	LHV [Wh/kg]	Density [kg/L]
E10	322	0.044	0.94	0.984	11440	0.746
E85	261	0.056	0.26	0.316	7960	0.787
B20	288	0.049	0.81	0.859	11550	0.855
Grid Electricity	648	0.034	0	0.034	---	---

2. LITERATURE REVIEW

2.1. King Paper (King and Nelson, 2013) on Model-Based Design of a PHEV

A paper by King and Nelson (King and Nelson, 2013) shows an application of model-based design in primarily designing and validating a control strategy for a plug-in hybrid vehicle. The primary goal of the paper is to show the application of model-based design in a controller design and validation role, while it is mentioned that model-based design was also used in the powertrain selection process for EcoCAR 2.

Initially, the powertrain that is being tested is described and listed along with the components that are to be included and controlled in the study. The control system architecture is defined and then the focus for the remainder of the paper is on the development of the hybrid vehicle supervisory controller (HVSC). Then, using the developed HVSC strategy, several testing methods are used to validate the control strategy and show it is ready for vehicle implementation.

One important concept to understand is the control system architecture as described in the paper because it is directly relatable to the models and controls being used to develop the powertrain models being used in this work. The communication between components is an essential aspect of model-based design on not only a physical and mechanical level, but on a signal basis as well. As described in the paper, the need for a HVSC is essential in properly managing the components present in any hybrid vehicle. Therefore to generate a useful model to design a powertrain, the control aspect needs to be accurately represented as well, although the complexity of the control strategy may be simplified.

The paper then briefly describes the control strategy that is to be implemented and tested on the HVSC. Using an optimization method, the operating mode of the vehicle can be determined by choosing between a series or parallel operating mode. Although the vehicle models presented in this work do not have a series or parallel operating mode, there are several different operating modes contained within each powertrain design. Understanding the methods used in designing the operating strategies described by King offered insight into the operating strategy implemented into the HVSC used in this research.

The paper then describes validation methods for the series control strategy. This includes several tests involving appropriate mode selection and torque distribution behavior of the system. The importance of using model-based design as a diagnostics and safety tool is highlighted by testing the operation of a brake test, showing the traction motor command drops once the brake pedal is engaged at any point.

This research is primarily focused on higher level signals on the basis of torque and energy consumption, and not concerned with lower level systems such as safety and diagnostics. Although the paper is primarily focused on the function of a control strategy, it is useful and insightful to observe the methods used for developing a hybrid vehicle control strategy and apply them to the hybrid models that have been developed in current research.

2.2. White Master's Thesis (White, 2014) on Energy Flow Through Advanced Powertrains

In this master's thesis by White (White, 2014), a new proposed tool used for advanced powertrain development is described. The motivation for the tool is described not as a vastly complex and difficult to understand "black box" tool, but more of a learning tool for students and professionals who seek a better understanding of the energy flow through a battery electric vehicle (BEV) and series hybrid electric vehicle (SHEV) powertrain configurations. With White's involvement in the EcoCAR 2 competition and university students, the ability for unfamiliar students to understand the model is essential in the tool's success.

The thesis starts by modeling a simple BEV powertrain using a 1 Hz Excel spreadsheet model. The models in the tool are "backwards" oriented, meaning the required energy at the wheels for the drive cycle is first calculated, then the losses are accounted through the powertrain moving backwards back to the energy source. Following the BEV study, White describes different SHEV models with varying component sizes and two control strategies. The first control strategy is a simple thermostatic controller. This is used in current work as well for a SHEV. The second control strategy used in White's work is a load following strategy. A load following strategy bases the engine power command on an engine operating line that has relatively high engine efficiency to meet driver demand. This has advantages over a thermostatic controller because a thermostatic controller only has a constant power command, so the engine may have to remain on longer than it needs to, which will burn more fuel.

Using the SHEV models, a study is done to explore a parameter known as Power Split Fraction. This parameter governs how much of the engine power output is used to propel the vehicle versus how much is stored in the battery. This is an interesting and useful study because the operation and usage of the engine is a defining factor in the overall powertrain efficiency. More efficient use of the engine and the energy produced by the engine will lead to a better powertrain.

White's master's thesis introduces a tool similar in motivation to the models being used in current work. However the current work involves more complex control strategies and vehicle architectures designed in MATLAB/Simulink that may be harder to initially comprehend for new users.

2.3. Mahapatra (Mahapatra et al., 2008) Paper on Model-Based Design in HEV's

The purpose of the paper by Mahapatra (Mahapatra et al., 2008) is to describe the motivation and importance of using model-based design throughout the design process of a hybrid electric vehicle. While Mahapatra does recognize that model-based design is regularly used for controller design and validation, the paper states that is a useful tool for evaluating the capabilities of components in different powertrain configurations. This is directly applicable to the current work because Mahapatra describes a process similar to one that is carried out in this thesis.

The paper begins by addressing the importance of model-based design in a design environment, especially for complex hybrid vehicle powertrains. Along with controller design, model-based design can assist in validating powertrain capabilities by attempting to reach specified improvement goals for a vehicle. The paper then begins to describe a system level model with high level components such as an engine, motor, and planetary gear set. Using the simplified model described, design goals are specified and tested to attempt to improve the efficiency of the powertrain. A relatively simple control strategy for a parallel hybrid is described as the HVSC being used for the displayed model.

Once the model being used is described, Mahapatra begins to compare the simplified model used versus a much more complex model. The behavior of the simplified model and the complex model are shown to be generally similar, although not exactly the same. An insightful point brought up in the paper is the advantages of starting with a simplified model rather than a vastly complex model. With a high level simple model, the run time of the model is very low compared to the complex model and allows more iterations to be carried out in a shorter period of time. This is very important in the early stages of the design process where the general behavior of the model is more important than the exact numbers being generated. The point made by Mahapatra is applied in this thesis by the use of simplified models for powertrain design. While more complex models are available for use, the complexity they provide is not applicable in high level design.

This research carries out a design process related to the one described by Mahapatra in using simplified model-based design models throughout the entire design process. A powertrain and simplified control strategy is developed in high level systems to generate useable and efficient modeling. The advantages of simplified models are defined in the final section of Mahapatra's work. By reducing model complexity, run time is reduced which is important when results are not required to be precise, but rather give a general understanding of the powertrain capability. Reducing model complexity also yields higher user understanding of the powertrain. Modeling is often viewed as a "black box" where inputs sometimes have to be assumed and no knowledge of how the outputs are generated is found. Simplified models allow the trace of data so the user can comprehend the workings of the model.

2.4. Wang (Wang et al., 2011) Paper on Hybrid Vehicle Control Systems

A paper by Wang (Wang et al., 2011) describes a design method using model-based design for a series hybrid electric vehicle in a real-world industry environment. The move towards using model-based design is described as a necessary and beneficial move away from solely doing on-vehicle testing. Having an initial controller simulation validation phase reduces the amount of time spent performing often slow and error filled testing on vehicle. Wang's affiliation with the Ford Motor Company provides a unique insight into a manufacturer's point of view on using model-based design as a tool for advancing production of hybrid electric vehicles.

The paper begins by describing the development methodology used in generating the control software for a HEV. The process starts with using model-in-the-loop (MIL) testing, which involves testing the controller software with a vehicle plant model on a purely software platform. Using MIL testing allows for faster than real time testing, which can

quickly identify and eliminate errors found in both the plant model and the control code. Once the algorithm is optimized inside of an MIL environment, hardware-in-the-loop (HIL) testing is performed using an actual controller to be implemented into a vehicle. HIL testing is done in real time and ideally accurately mimic performing on-vehicle testing in terms of controller validation. However, Wang does go on to say that while HIL testing is valuable in quickening the design process, some nuances cannot be simulated on a machine (such as noise and vibration) thus on-vehicle testing is always going to be the final and most essential step in the design process. The importance of high fidelity model in controller validation is also addressed by citing issues with on-vehicle testing that cannot be identified in a simulation environment.

After the discussion about the advantages and shortcomings of model-based design, Wang continues to describe factors that are included in designing an efficient control strategy for a series hybrid electric vehicle (SHEV). By studying the engine and generator efficiencies and combining them into an overall efficiency, the desired efficiency islands can be specified as to where the engine-generator (genset) should ideally be operated. A similar method of combined efficiency is used in this current work when developing a SHEV as well. The methods used in designing an efficient control strategy provides further ideas in how to design the operating modes for the hybrid powertrain models used in this thesis.

The paper then displays test results by running several different drive cycles and shows the operating points and mode selection of the control strategy. Wang shows that model-based design methodology is highly valuable in the vehicle control system design especially in validation efficiency. Using model-based design in controller validation is proven to reduce the amount of time spent doing on-vehicle testing which yields overall a higher efficiency for the design process. The paper also described the advantages of thermostatic and load-following strategies which are both used in the series models in this thesis.

2.5. Simpson (Simpson and Walker, 2003) Paper on a Parametric Analysis Technique for HEV Powertrain Design

The paper by Simpson (Simpson and Walker, 2003) proposes a new method for fuel cell and hybrid vehicle design. It is stated that by using approximately 30 parameters to fully characterize the vehicle platform, powertrain data can quickly and reasonably accurately generated. This would serve as a useful tool in model validation as well as a novel method in approaching hybrid vehicle powertrain design. Simpson states that generally, quasi-static models provide reasonable data but do not provide insight into how the system generates the data, so users are generally steered away. The method proposed details each component's definition and what parameters are to be used for each component in designing a powertrain.

The paper then describes the shortcomings of quasi-static models that are to be addressed by the new method. Specifically, the avoided reliance on drive cycle analysis because it does not always provide accurate driving conditions on a daily basis, and simplicity of the models so the user can easily understand the fundamentals of the models. The paper then goes on to describe all of the component models that are to be used for the design and modification of a fuel cell series hybrid. Although the components of the powertrain are

well defined, the paper does not address the control strategy being used to obtain the performance and energy consumption numbers presented in the paper.

With the vehicle and components defined, the paper then begins to present validation data for a fuel cell vehicle taken from Virginia Tech. The results are identical but do have a significant degree of error that Simpson does address and attributes to the overall simplicity of the model. A sensitivity analysis is then carried out using direct impact factors such as component efficiencies, as well as indirect impact factors such as vehicle mass. This is useful in defining which parameters have the greatest impact on fuel economy. By identifying which parameters have the greatest impact on fuel economy, the parameters that must be most closely quantified and validated in order to reduce the error of the model are identified. Beyond this, the sensitivity analysis shows which factors the powertrain designer should focus on.

While the paper does describe a unique method in designing a powertrain, the control strategy and validation of the tested hybrid vehicle is not addressed. This paper will address some of the shortcomings of Simpson's paper by addressing several powertrains to validate component models, as well as describing the control strategies used in each hybrid powertrain designed.

2.6. Marco Paper (Marco and Cacciatori, 2007) on Model-Based Design in HEV Design

The purpose behind the paper by Marco and Cacciatori (Marco and Cacciatori, 2007) is to demonstrate how model-based design can be used in several methods to reduce the design time of a hybrid electric vehicle. The first section of the paper focuses on architecture selection by using high level models in drive cycle testing. A brief discussion of forwards and backwards oriented models displays the advantages and disadvantages of each, and the primary purpose that each method should be used for. An example using a fuel cell LIFEcar project is shown using a backwards oriented model to show tradeoffs in component sizing. Although Marco and Cacciatori does not address the control strategy used in the study, which is important in deciding whether the vehicle is operating properly and efficiently, the purpose of the study is clear. By varying powertrain efficiency, vehicle weight, and aerodynamics, different results can be drawn about what is the optimum setting for the LIFEcar project.

The paper then goes on to describe how using modeling techniques is advantageous for control design as well, however does not go into detail about specific hybrid controller design or optimization methods for powertrain operation. This research demonstrates both the use of model-based design in primarily designing and comparing different powertrain configurations while also the ability to design and employ higher level control strategies.

The paper then describes tools that can be used for developing control architecture and strategy development. The vehicle control system tools such as UML and SysML are given as examples. A high level Simulink model is shown as a base for a possible executable control software, however the actual strategy to be used is not discussed. An example of a visual logic structure is also given in the paper as an example of what has to be considered when designing a control strategy. However, no control architecture or strategy is proposed

or discussed. Marco and Cacciatori do show the use of model-based design as a tool for powertrain development, which is the primary goal of this thesis. However in order to properly use model-based design in a hybrid setting, the control strategy used in testing needs to be described as it can drastically affect the operation of the vehicle. The current work describes several control strategies used in different hybrid powertrain configurations, as well as details the goals of each strategy.

2.7. Literature Review Summary

This literature review looks at work done in the past and present in a similar setting for using model-based design for powertrain design. Marco and Cacciatori describes the usefulness of model-based design in a powertrain design environment and not strictly in its primary role of control validation. Wang gives an interesting view into the automotive industry and how essential using model-based design throughout the design process in addition to controller validation. Mahapatra reiterates the importance of model-based design and also provides insight on the complexity of the model versus the effectiveness and time spent running models. Prior work has shown that using model-based design in powertrain design is a useful tool in minimizing time spent in the design process as well as being used in controller validation. This thesis builds upon the ideas portrayed in the literature by using model-based design to select an appropriate powertrain to meet the proposed goals. The models are not designed to be vastly complex, but complex enough to provide accurate results while promoting understanding of the workings of an advanced vehicle powertrain. Consistently through all of the papers, the idea of simplified models being used as a base for design is illustrated. While simple models may not be able to be used for more complex tasks such as controller validation, they do provide insight into the workings of a powertrain and help the user understand how the components are interacting. As tasks become more demanding, higher fidelity models are implemented to model more complex systems. This research starts at the base of the model-based design concept by generating simple models to gain general insight into the capabilities of the modeled powertrains.

3. COMPONENT MODELS

To construct the vehicle powertrain configurations being evaluated, several component models are generated using different metrics. The initial models are generated using power to drive the models.

3.1. Glider Model

A glider model is generated in order to calculate the current vehicle velocity while also finding the energy requirements at the wheels. A glider model is the equivalent of the characteristics of a vehicle, such as the aerodynamics and mass of the vehicle, but does not include any of the powertrain components. The base equation for the glider model is seen in Equation 3-1:

$$F_{TR} = F_{rr} + F_{gr} + F_{aero} + F_i \qquad \text{Equation 3-1}$$

Where F_{TR} is the tractive effort at the wheels, F_{rr} is the rolling resistance, F_{gr} is the force generated by a grade (uphill, downhill), F_{aero} is the aerodynamic drag, and F_i is the inertial force of the vehicle. Figure 3-1 illustrates the forces described in Equation 3-1.

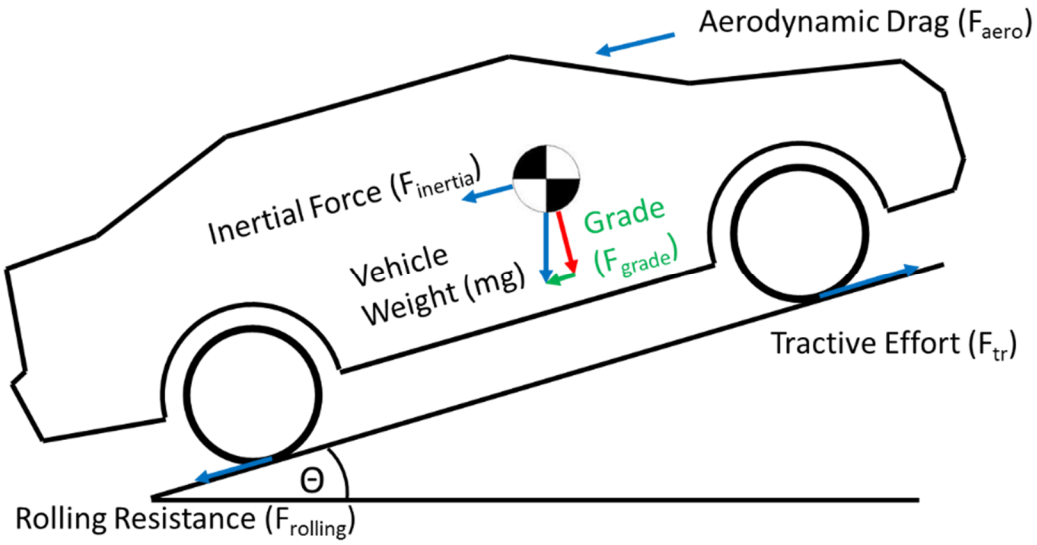

Figure 3-1: Tractive Forces Acting on a Vehicle in Motion

Each of these forces makes up a component of the tractive force required to propel the vehicle. The road load is defined as:

$$F_{rl} = F_{rr} + F_{aero} \qquad \text{Equation 3-2}$$

Road load consists of the rolling resistance force and aerodynamic force. This method for calculating the road load is an alternative to using a quadratic involving several variables specific to a vehicle. Equation 3-3 shows this alternative method.

$$F_{rl} = f_0 + f_1 V + f_2 V^2 \qquad \text{Equation 3-3}$$

The characteristic values in this equations, f_0, f_1, f_2, are values generated for a specific vehicle and similar to the values found in EPA for vehicle parameters. The EPA uses *A, B,* and *C* to define a specific vehicle. This means that the values do not scale with mass, making them more difficult to use for modeling purposes.

The rolling resistance force F_{rr} describes the resistance encountered at the wheel of a vehicle generated by the contact patch on the tire. The calculation for the rolling resistance is simple and does not depend on the velocity of the vehicle for our purpose.

$$F_{rr} = C_{rr} mg \qquad \text{Equation 3-4}$$

Equation 3-4 describes the rolling resistance, where C_{rr} is the coefficient of rolling resistance, m is the vehicle mass, and g is the gravitational constant. The coefficient of rolling resistance is generated based on specific tire tread, pressure, and numerous other factors. This constant remains static in this modeling.

The grade force is calculated using Equation 3-5:

$$F_{gr} = mgsin\alpha \qquad \text{Equation 3-5}$$

Where α is road angle. Grade force accounts for the resistance or in a downhill case, the assistance that gravity produces on the vehicle. Aerodynamic drag is calculated by Equation 3-6:

$$F_{aero} = \frac{1}{2}\rho C_d A_f V^2 \qquad \text{Equation 3-6}$$

Where ρ is air density, C_d is the coefficient of drag, A_f is the frontal area of the vehicle, and V is the current velocity of the vehicle. Once again, the vehicle is parameterized by picking specific values for C_d and A_f, to generate results based on a vehicle of choice. This force is heavily dependent on velocity, as it contains a V^2 term.

The final force, and the most significant force is the inertial force of the vehicle, described in Equation 3-7:

$$F_i = m_i a_x \qquad \text{Equation 3-7}$$

Where m_i is the inertial mass of the vehicle, and a_x is the longitudinal acceleration of the vehicle. The inertial mass takes into account the rotating inertia of the components of wheels. tires and brakes of the vehicle, and therefore is slightly larger than the actual mass of the vehicle (~4%).

In order to run the components of the model, the current velocity of the vehicle is needed. The glider model does this by first reorganizing Equation 3-1 and solving for acceleration:

$$a_x = \frac{dv}{dt} = \frac{F_{TR} - (F_{rr} + F_{gr} + F_{aero})}{m_i} \qquad \text{Equation 3-8}$$

Integrating by time yields vehicle velocity. The tractive effort is provided by the powertrain of the vehicle based on the driver demand, which is discussed later.

3.2. Power Loss Modeling

The method of power loss modeling is introduced by Zhang and Mi (Zhang and Mi, 2011). Being a reliable and simple method to generate useful results, power loss models are generated for each powertrain component. A power loss model views each component from a high level power-in, power-out perspective. Although using a power loss model loses a significant amount of the component information, it provides a semi-accurate view on the end results of the component. Each power loss model can be derived from Equation 3-9:

$$P_{in} = P_{out} + P_{loss} \qquad \text{Equation 3-9}$$

Where P_{in} is the power going into the component, P_{out} is the power leaving the component, and P_{loss} is the power lost during component operation. Different applications of this equation based on components will be discussed later. Most of the components in the simplified powertrain structures can be modeled using this equation. The loss term is found by solving Equation 3-10:

$$P_{loss} = C_0 + C_1 P + C_2 P^2 \qquad \text{Equation 3-10}$$

Where C_0, C_1, and C_2 are all constants that correspond to specific components. For example, if a motor is modeled using the power loss method, it would have its own set of constants, while an engine would have a different set of constants. These constants form an operating line that corresponds to some operation of the component, and may be the most efficient. Figure 3-1 shows an example of a bidirectional motor loss curve estimate of a UQM 125 motor. Table 3-1 shows the coefficients used to model the UQM 125.

Table 3-1: UQM 125 Motor Parameters

	UQM 125 Motor
Peak Power	125 kW
C0 (kW)	0.6
C1 (kW/kW)	0.02
C2 (1/kW)	0.0015

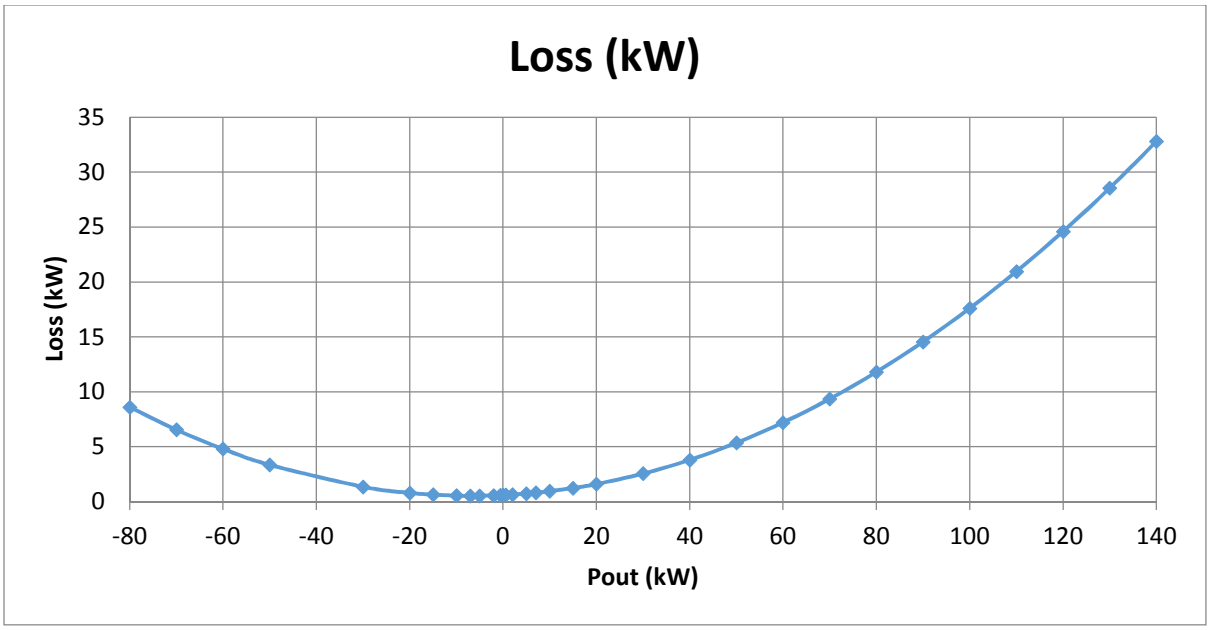

Figure 3-2: UQM 125 Bidirectional Motor Loss Curve

The power loss equation, in the case of a motor (explained in section 3.5) is a function of P_{out}. Bidirectional loss is important in components such as an electric motor and a driveline because in a hybrid, power will be transferred in either direction because of propelling the vehicle or braking. The quadratic behavior shows higher loss at higher power outputs. The negative side of the graph will continue to increase, however such a high negative demand is rare and the presented curve is sufficient for the operating range of an electric motor. Figure 3-2 shows the relationship between P_{out} and its dependent result P_{in}.

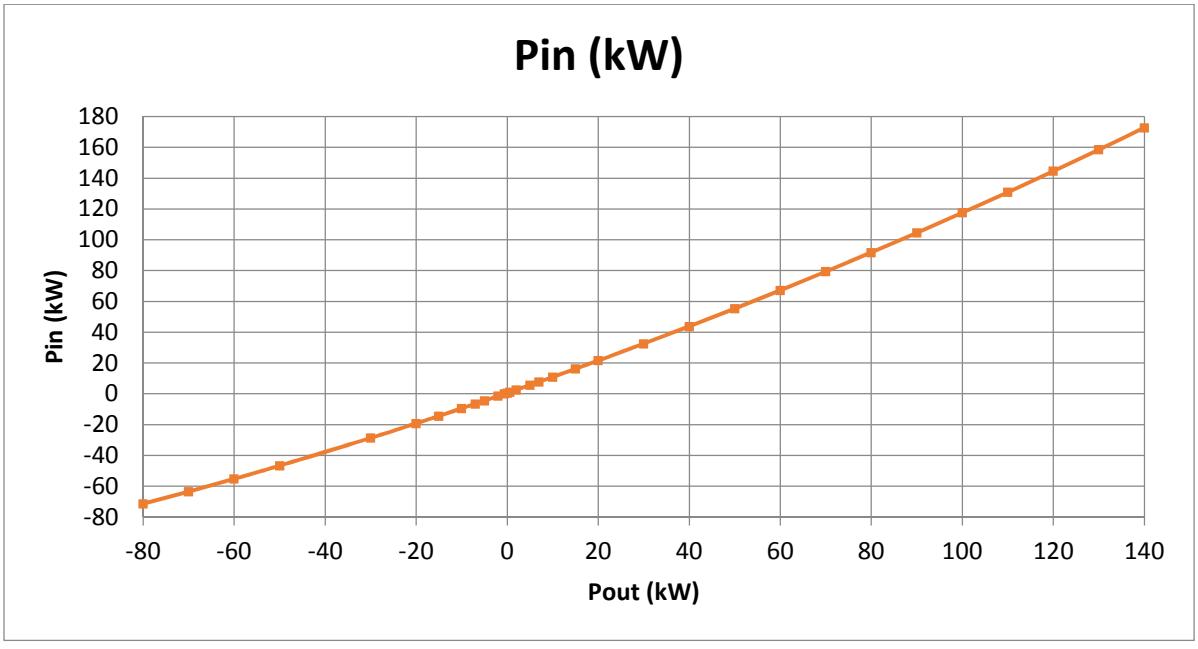

Figure 3-3: UQM 125 Power Input

From Figure 3-2, it can be seen that the electric motor has a relatively high efficiency. Because of bidirectional capability, efficiency must be defined in two ways:

$$\eta_{propel} = \frac{P_{out}}{P_{in}} \ (\boldsymbol{a}) \qquad \eta_{brake} = \frac{P_{in}}{P_{out}} \ (\boldsymbol{b}) \qquad \text{Equation 3-11 a-b}$$

With Equation 3-11b being used for the negative, or regen braking portion of demand, and Equation 3-11a being used for the propel portion of demand, Figure 3-3 shows the efficiency estimate for the UQM 125.

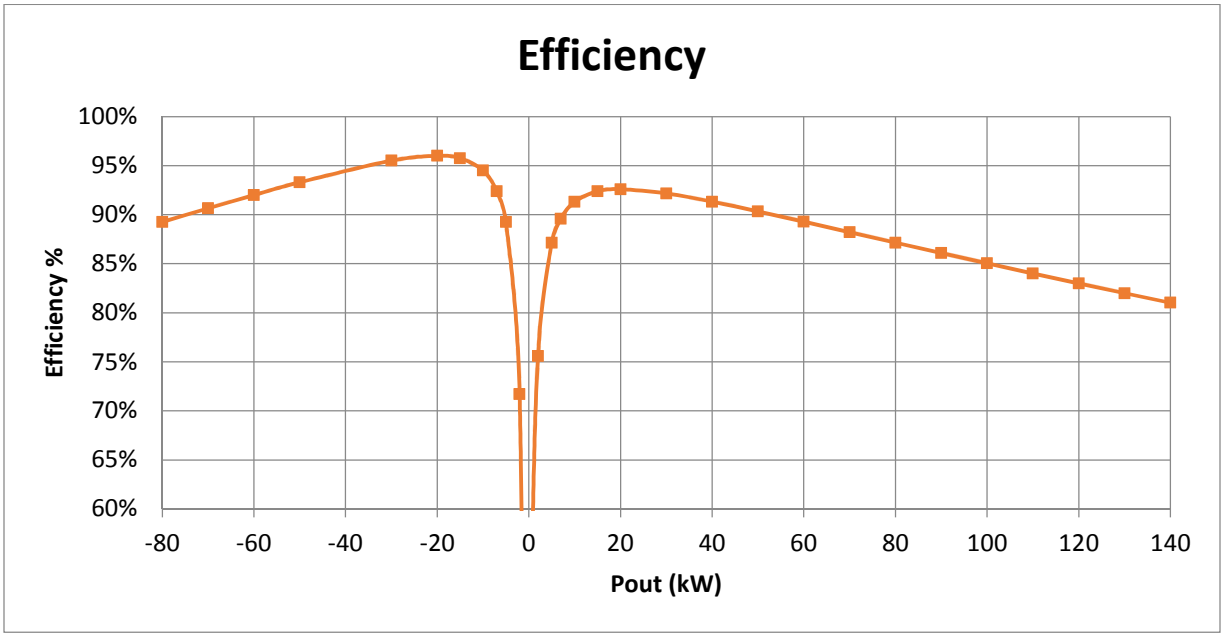

Figure 3-4: UQM 125 Efficiency

The efficiency plot shows a valley when there is no power output demand. This indicates the motor is off and the region around zero with low efficiency is generally not used. The graphs is this section show similar behavior to all of the bidirectional components, such as a generator or a driveline. An engine is not bidirectional, so the general behavior may be similar, except with higher losses and no braking demand.

Modeling using a power loss method has several advantages. Using these equations is simple and it is easy to scale these components as well. However, it only provides a rough estimate of the power consumption and does not take into account the actual operation of the component, but rather just the energy consumption. For the purposes of energy requirement modeling, it is sufficient but may provide generous results because the way the equations are structured, the models may be operating at their most efficient points at all times, which may not be accurate.

3.3. Engine Model

The engine is modeled using two different methods, a power loss method as previously described, and a torque-speed based model. In this variation of the power loss model, the

output power of the engine is known. This is because in order to meet the driver demand, a specified amount of power needs to be commanded.

To do this, an accelerator pedal position (APP) is found using a simple PID controller using the error between current vehicle speed and desired vehicle speed from an input drive cycle. The APP is then multiplied by the maximum power output of the engine to obtain a corresponding percentage of the maximum power, or driver demand. This serves as P_{out}. Figure 3-5 is a visualization of the power loss engine model.

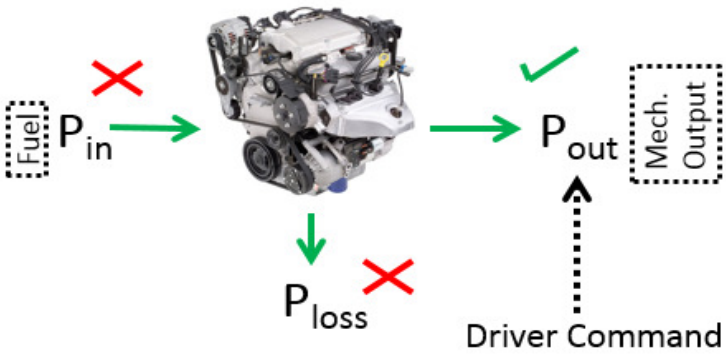

Figure 3-5: Power Loss Engine Model

With P_{out} being known from calculating driver demand, which is also the mechanical output of the engine, it must be used to solve for the unknowns P_{loss} and P_{in}. Equations 3-12a-b show how to find the unknown power in and power loss. Power loss is a function of power output in this case.

$$P_{in} = P_{out}(Known) + P_{loss}\ (\boldsymbol{a})$$
$$P_{loss} = C_{0,eng} + C_{1,eng}P_{out} + C_{2,eng}P_{out}^2\ (\boldsymbol{b})$$

Equation 3-12 a-b

Equation 3-9a is used to solve for P_{in} which is the power entering the system. In the case of the engine, this power comes from fuel. Energy can be calculated by Equation 3-13.

$$E_{in} = \int P_{in}dt$$

Equation 3-13

Being able to solve for E_{in} allows the model to calculate the fuel consumption for different fuel sources, based on the energy content value of the fuel desired. Using the same method, the total energy loss of the engine can also be calculated for future reference, and then compared to different engine sizes, models, and other components in the vehicle. Using Equation 3-13 with P_{out} instead of P_{in} to find the total output energy E_{out} allows the model to find the average engine efficiency over an entire drive cycle.

$$\eta_{avg} = \frac{E_{out}}{E_{in}}$$

Equation 3-14

An example of a set of coefficients for a generic 1.8 L engine power loss model is in Table 3-2. The following figures show the same engine model behavior.

Table 3-2: 1.8 L Engine Power Loss Coefficients

	1.8 L Engine
Peak Power	100 kW
C0 (kW)	5.4
C1 (kW/kW)	1.5
C2 (1/kW)	0.006

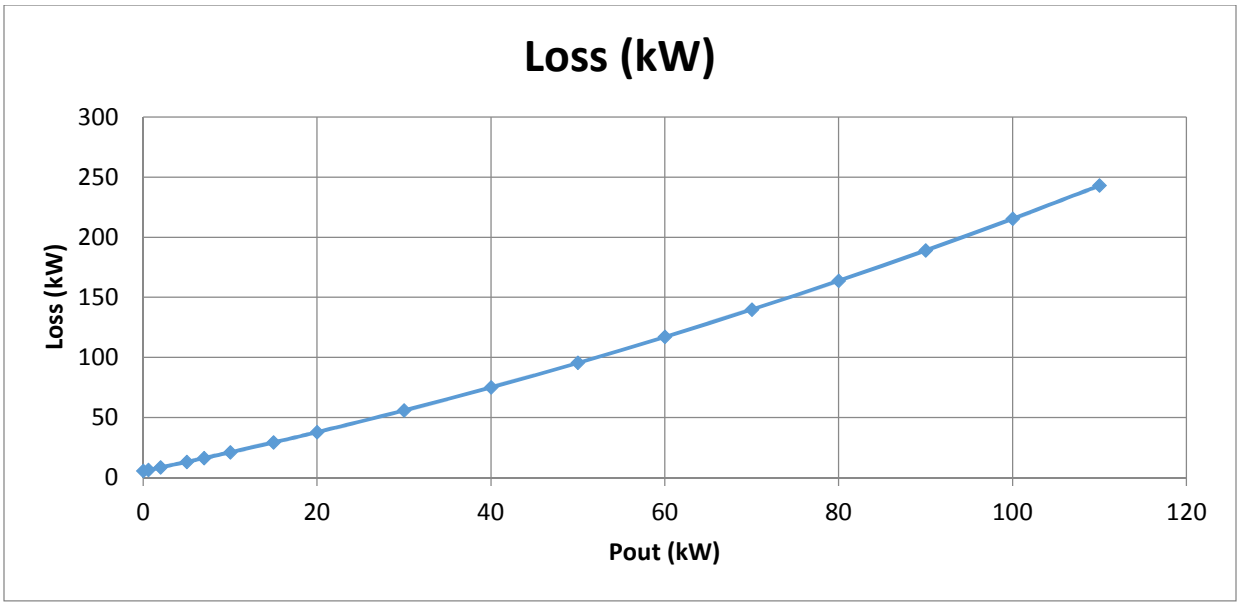

Figure 3-6: 1.8 L Power Loss Engine Loss Curve

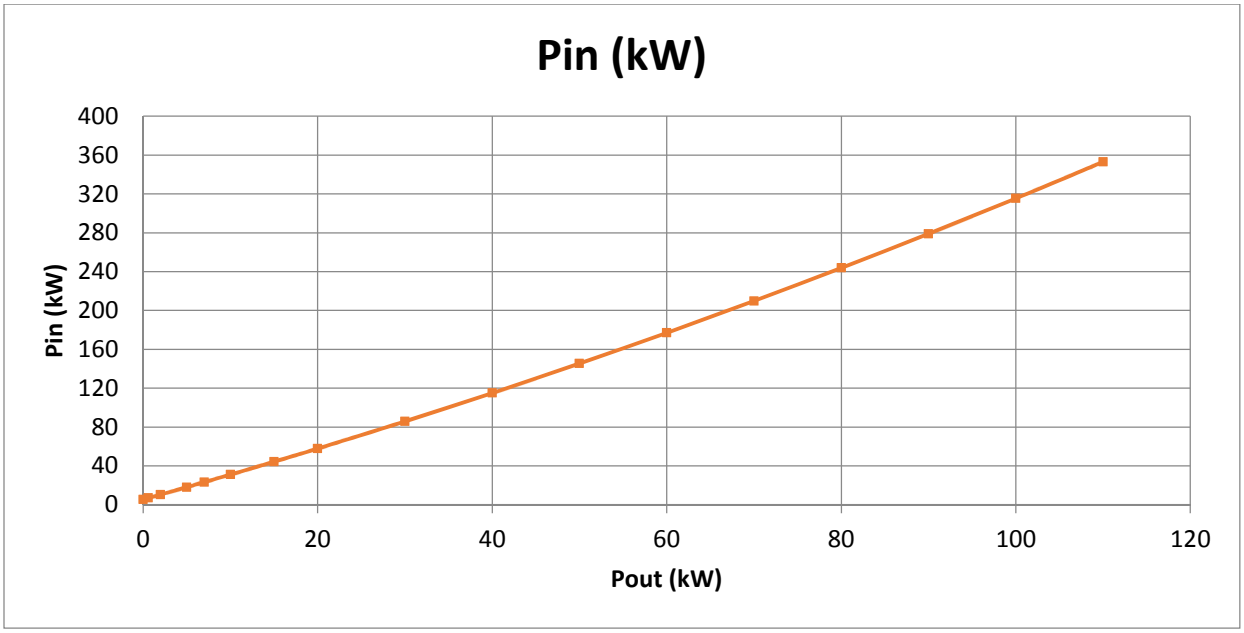

Figure 3-7: 1.8 L Power Loss Engine P_{in} Curve

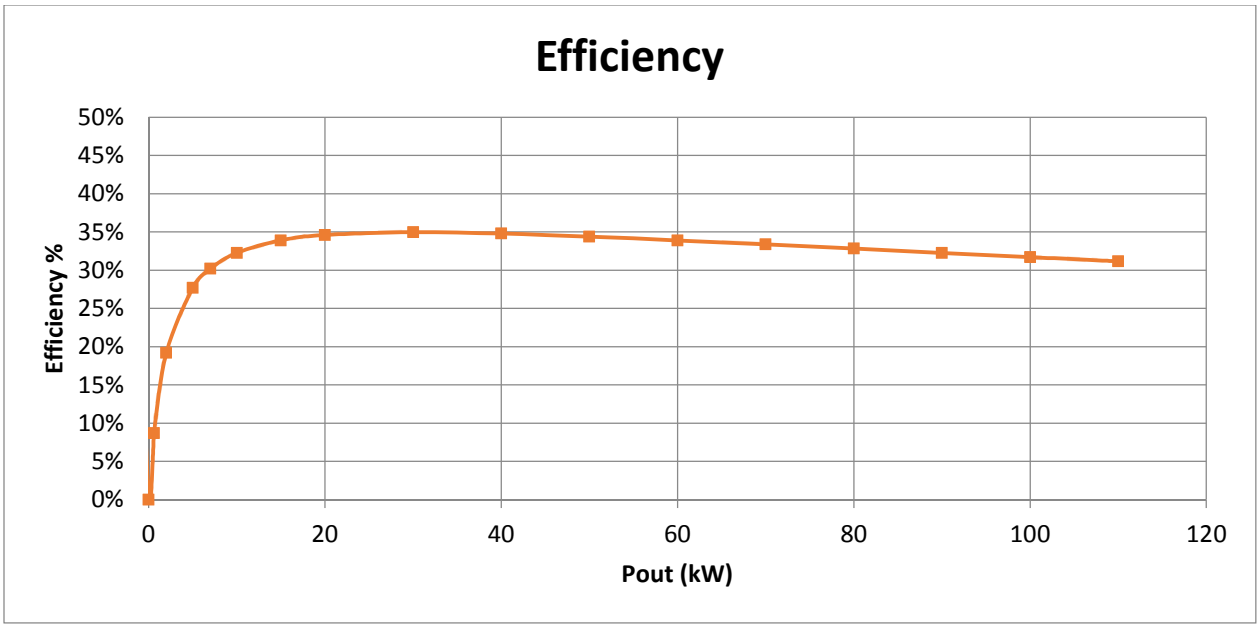

Figure 3-8: 1.8 L Power Loss Engine Efficiency Curve

The general behavior of the curves is similar to that of the motor described in the previous section without the ability of bidirectional power flow. However, as expected, the losses are much higher for the internal combustion engine. The high engine losses lead to a lower engine efficiency. This is a main point of utilizing electric machines, they are much more efficient than engines. The coefficients in Table 3-1 are for a specific engine and engine operation. These coefficients are easily manipulated to match a different engine operation to produce more realistic numbers. This is further discussed in the conventional vehicle modeling section (Section 5).

The second method used to model engines is a torque-speed based model that solves for the efficiency of the engine. In order to generate a driving torque, a maximum torque-speed curve is implemented to limit the engine based on the current speed of the vehicle. Similar to before, an APP is multiplied by the maximum torque provided by this curve or the maximum torque from the power limit of the specified engine. Equation 3-16a shows the base form of the engine efficiency equation using brake mean effective pressure (BMEP) (Alley et al., 2013). In order to make the equation easier to scale for the purpose of our study, the equation is rewritten in the form of Equation 3-16b by using the identity of BMEP for a 4 stroke engine (Equation 3-15). By rewriting Equation 3-16a, the displacement volume (in Liters) of the engine is exposed. This will be used throughout the study in order to scale the engine efficiency based on the displacement of each engine used.

$$bmep = \frac{2\pi 2T_{eng}}{V_d} \qquad \text{Equation 3-15}$$

$$\eta_{engine} = bmep * \frac{\eta_{thermo}}{fmep_0 - bmep} \ (\boldsymbol{a}) \qquad \eta_{engine} = \frac{\eta_{thermo}}{1 + \frac{fmep_0 V_d}{4\pi T_{eng}}} (\boldsymbol{b}) \qquad \text{Equation 3-16 a-b}$$

Here, η_{therm} is the thermodynamic efficiency of the specified engine, which is assumed a constant. $fmep_0$ is the friction mean effective pressure (kPa) at zero power, V_d is the volumetric displacement (L) of the engine and T_{eng} is the output torque (Nm) of the engine, which was previously calculated. In this model, engine efficiency is only a function of torque and not speed. This assumption is only valid within a certain operating range of the engine. This region is below the maximum torque of the engine for a higher efficiency. At very low and very high speeds, the assumption becomes invalid. Because the operating range used for drive cycles does not generally involve high speeds, the assumption is valid for the models used. In these zones, the lines of constant efficiency for engines is relatively constant across the engine speeds. For the different engines described throughout this thesis, Table 3-3 describes the values used.

Table 3-3: Parameters for Engine Efficiency Models

Engine Type	**Indicated Thermo Eff**	**Friction fmep0**	**Maximum Thermal Eff**	**Bmep for Max Eff**
Units	%	kPa	%	kPa
Base SI	40.0	145	35.0	1000
Improved SI	44.0	140	38.5	960
CIDI TC	45.5	200	40.6	1650

Using torque and speed instead of just power introduces several different needs for the model. In order to calculate current engine speed, a simple shifting strategy has to be developed for the driveline model. A different driveline model is also needed to provide power loss calculated in terms of torque. The driveline and shifting strategy are discussed further in the next section.

3.4. Driveline Model

To simplify the model, the transmission and differential are lumped together in a model labeled the driveline. The driveline, in order to properly interact with the engine, is modeled in both terms of power and torque-speed. As opposed to the engine, P_{in} is now the known variable in the power loss equation because it has been previously calculated at the engine. To solve for P_{out}, or the output of the driveline, Equations 3-16 a-b is used.

$$P_{in}(Known) - P_{loss} = P_{out} \ (\boldsymbol{a})$$
$$P_{loss} = C_{0,DL} + C_{1,DL}P_{in} + C_{2,DL}P_{in}^2 \ (\boldsymbol{b})$$

Equation 3-16 a-b

Where P_{loss} is now a function of P_{in}. With the output power of the driveline now known, tractive effort can be calculated by simply dividing by the current vehicle speed provided by the vehicle glider model. Force limitations are also implemented inside of the driveline to mimic transmission limitations. The tractive effort found in the driveline is the tractive effort that is be used to "drive" the glider model.

For models using the torque-speed based engine discussed earlier, a torque-speed based driveline model is needed. To calculate the torque loss of the driveline, an equation similar to the power loss equations is used.

$$T_{loss} = C_0 + \frac{C_1 T_{in}}{T_{ref}} + \frac{C_2(s - s_{ref})}{s_{ref}} \qquad \text{Equation 3-17}$$

Where s is speed in RPM, T_{ref} and s_{ref} are values that are specific to different drivelines, but are simply reference speed and torques. The reference speed and torque can be used to modify the behavior of the driveline depending on the input of the driveline. For example, a driveline attached to a large engine will operate in a different range than a small motor. These constants can be modified fit the input of the general operating range of the input component. The C constants are similar to the previous models in that they are specific to a certain vehicles driveline and have been generated to model losses based on component data. Table 3-4 shows the coefficient values for both power loss and torque-speed models used in the study.

Table 3-4: Driveline Characteristics for Torque-Speed and Power Loss

Driveline Characteristics			
Torque-Speed	Value	Power Loss	Value
C0 (Nm)	8	C0 (kW)	0.6
C1 (Nm/Nm)	10	C1 (kW/kW)	0.007
C2 (Nm/RPM)	4	C2 (1/kW)	0.00037
Tref	200	--	--
Sref	2000	--	--

In order to scale torque and speed through the driveline, a simple shift strategy is developed to calculate the current gear ratio. To keep the model relatively simple, the shift strategy is based only on the current speed of the vehicle and does not consider driver demand. Speed windows are generated for typical use of each gear. For example, first gear is used for speeds under 10 mph, and second gear is used for speeds above 10 mph but below 25 mph. This gives a useful shifting strategy that can be used across several different vehicle configurations. The shift strategy is valid to use for drive cycles because of the non-aggressive drive cycles being used in the study. The ability to modify the shifting windows easily also allows specific shifting based on the drive cycle being tested. Each drive cycle used in this study has a specific set of shift windows, including an acceleration test. Table 3-5 shows the shifting windows used for each drive cycle. Table 3-5 shows the different behavior of the driveline. The higher demand acceleration tests and US06 cycle has much higher shifting points for each gear. The acceleration shift points are taken from gathered data of an acceleration test using the transmission being modeled (6T30).

An example of the shifting strategy can be seen in Figure 3-1, an acceleration test of a conventional vehicle model. The speed windows chosen also consider the RPMs of the engine to ensure the maximum speed is not exceeded. If this maximum speed is

approached, the gear will shift. In the acceleration test (Figure 3-9) the engine is taken to red line before shifting for maximum performance.

Table 3-5: Shift Points for Different Drive Cycles

Gear	Limit	Drive Cycle			
		UDDS	***HwFET***	***US06***	***Acceleration***
1st	Lower	0	0	0	0
	Upper	10	5	15	25
2nd	Lower	10	5	15	25
	Upper	20	15	30	42
3rd	Lower	20	15	30	42
	Upper	30	25	45	65
4th	Lower	30	25	45	65
	Upper	40	35	55	87
5th	Lower	40	35	55	87
	Upper	50	45	60	89
6th	Lower	50	45	60	89
	Upper	--	--	--	--

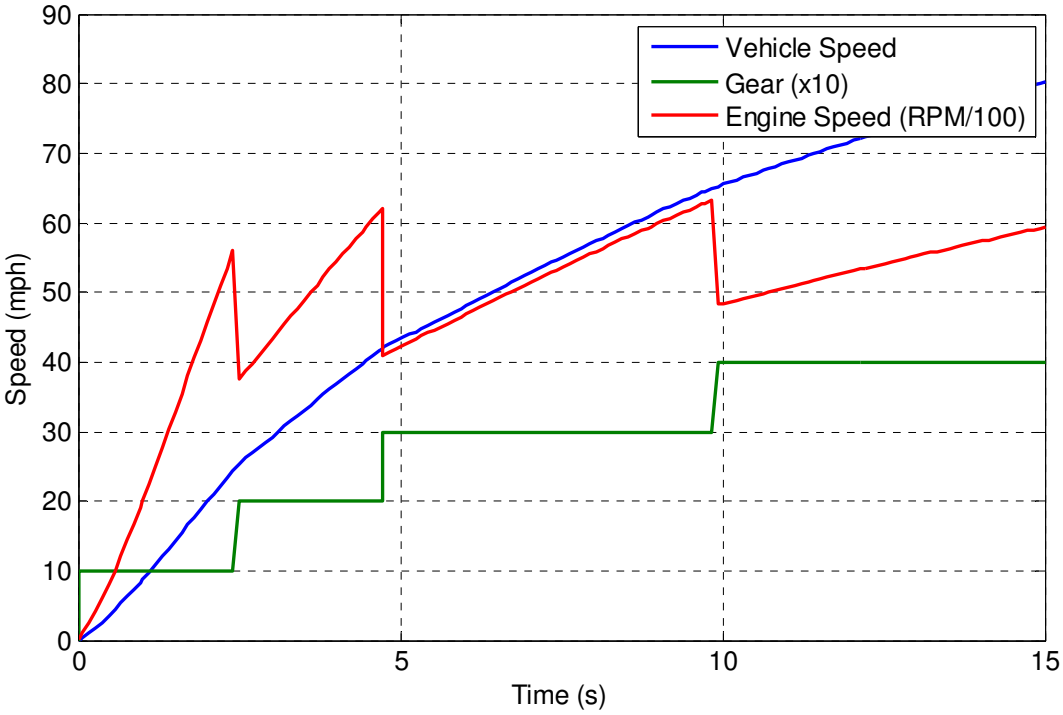

Figure 3-9: Acceleration Speed Trace displaying the Shifting Strategy

The speed windows for each gear are easily modifiable as well, to help meet performance demands specified by the ***EcoCAR*** competition. In this case, the speed window could be

increased for each gear. Note that a speed-based shift schedule for acceleration performance is significantly different than for a fuel economy part load drive schedule.

3.5. Motor Model

The motor model used in the battery electric vehicle as well as the hybrid configurations is similar to the engine model used in the power loss case. Refer to Equation 11a-b for the power loss equations that are used to model an electric motor. Although the equations are the same for an engine and motor, the constants that define the power loss equation are different and correspond to a different curve than the engine. The example power loss model curves given in section 3.2 define a UQM 125 power loss motor model. The constants that define the curves for the UQM 125 as well as a comparison to the engine model constants are shown in Table 3-6.

Table 3-6: Comparison of Motor and Engine Loss Coefficients

	UQM 125 Motor	1.8 L Engine
Peak Power	125 kW	100 kW
C0 (kW)	0.6	5.4
C1 (kW/kW)	0.02	1.5
C2 (1/kW)	0.0015	0.006

Although the engine and motor use an identical method and equation in power loss modeling, the difference in coefficients is drastic because the engine produces significantly higher losses than the motor. This illustrates the flexibility of the power loss models that they are able to model different components similarly by simply modifying coefficients.

The torque-speed motor equation is defined by Equation 3-18.

$$P_{loss} = \left(\frac{T_{max}\omega_{max}}{T_{ref}\omega_{ref}}\right)\left(k_c T_{ref}^2 \left(\frac{T}{T_{max}}\right)^2 + k_i \omega_{ref}\left(\frac{\omega}{\omega_{max}}\right) + k_w \omega_{ref}^3 \left(\frac{\omega}{\omega_{max}}\right)^3 + C\right) \quad \text{Equation 3-18}$$

Where k_c, k_i, k_w ,and C are constants specific to an electric motor. T_{ref} and ω_{ref} are also constants associated with a specific motor. The motor loss equation is set up to help easily scale the power loss of an electric motor for sizing purposes. T_{max} and ω_{max} can be scaled up or down in order to vary the loss values of the motor. This is ideal for powertrain component sizing, and the purpose of the study. Table 3-7 shows the parameters used to model the UQM 125 using the torque-speed equation rather than the power loss equation.

Table 3-7: UQM 125 Torque-Speed Values

Constant	Value
k_c (s/Nm)	0.12
k_i (Nm)	0.01
k_w (s^2/Nm)	1.20E-05
T_{max} (Nm)	300
T_{ref} (Nm)	300
ω_{max} (rad/s)	838
ω_{ref} (rad/s)	838
C (W)	600

Once again, the motor model is easily scalable by only modifying the torque parameters. This same motor is used throughout the study in different sizes by manipulating the T_{max} parameter in Equation 3-18. Figure 3-10 shows the loss map for the UQM 125 specified by Table 3-5. The loss map is generated by using Equation 3-18 across the operating range of the UQM 125. The increased variability of the torque-speed models is evident by comparing the power loss curve from the power loss model to the power loss map. The extra degree of freedom provided by using the torque-speed equation gives the model a vastly wider operating range throughout an entire torque-speed map rather than along a specified line for the power loss models.

To calculate the efficiency of the motor, Equation 3-19 a-b is used.

$$\eta_{mot}^{+} = \frac{T_{mot}\omega_{mot}}{T_{mot}\omega_{mot} + P_{loss}} \ (\boldsymbol{a}) \qquad \eta_{mot}^{-} = \frac{T_{mot}\omega_{mot} + P_{loss}}{T_{mot}\omega_{mot}} (\boldsymbol{b}) \qquad \text{Equation 3-19 a-b}$$

The efficiency is defined by dividing the operating torque and speed, or power in Watts, by the operating power summed with the power loss. When the power flows in the opposite direction, such as in a regenerative braking case, the definition is flipped as seen in Equation 3-19b.

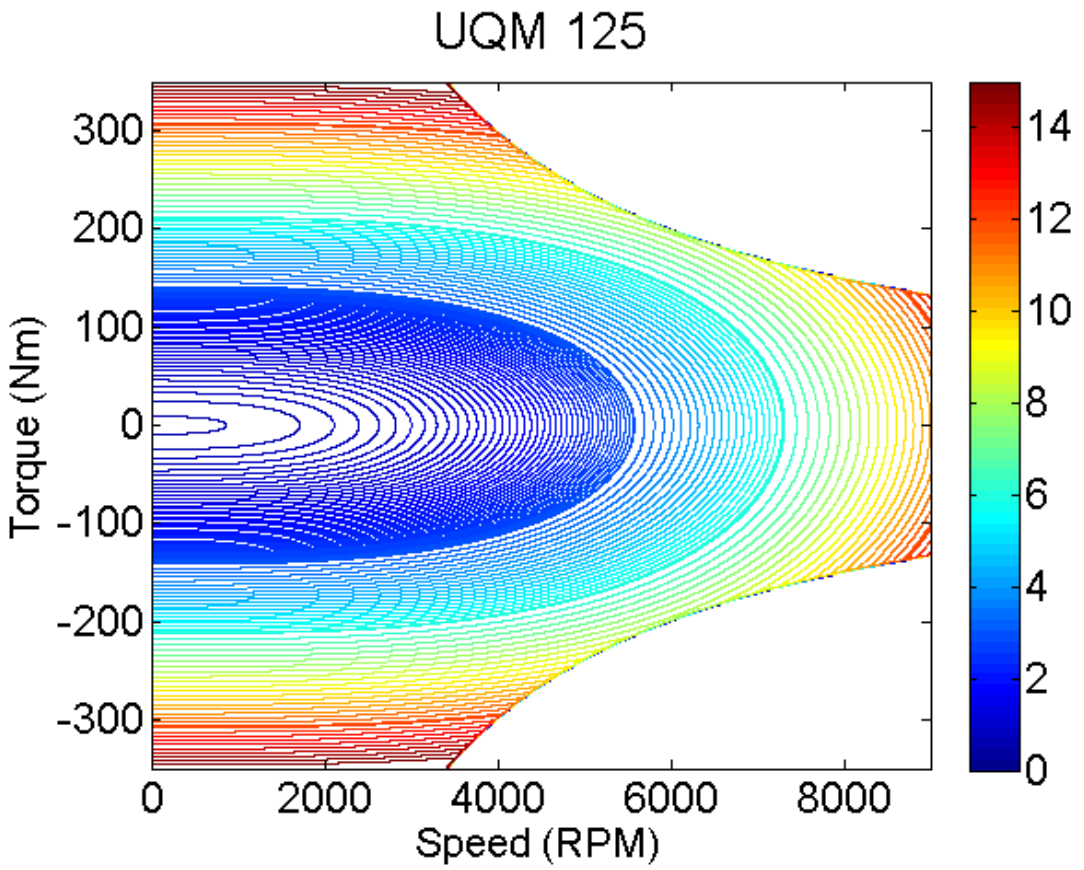

Figure 3-10: UQM 125 Motor Power Loss (kW) Map

Figure 3-11 shows the positive efficiency map for the UQM 125 generated using Equation 3-19a. Only the positive portion of the efficiency map is included because at very low speed and torque, the negative portion does not behave accurately. This is because in a region of low torque in the reverse direction, both P_{in} and P_{out} flow into the motor due to the motor losses. Because this region will generate a negative efficiency, it has been excluded from Figure 3-11.

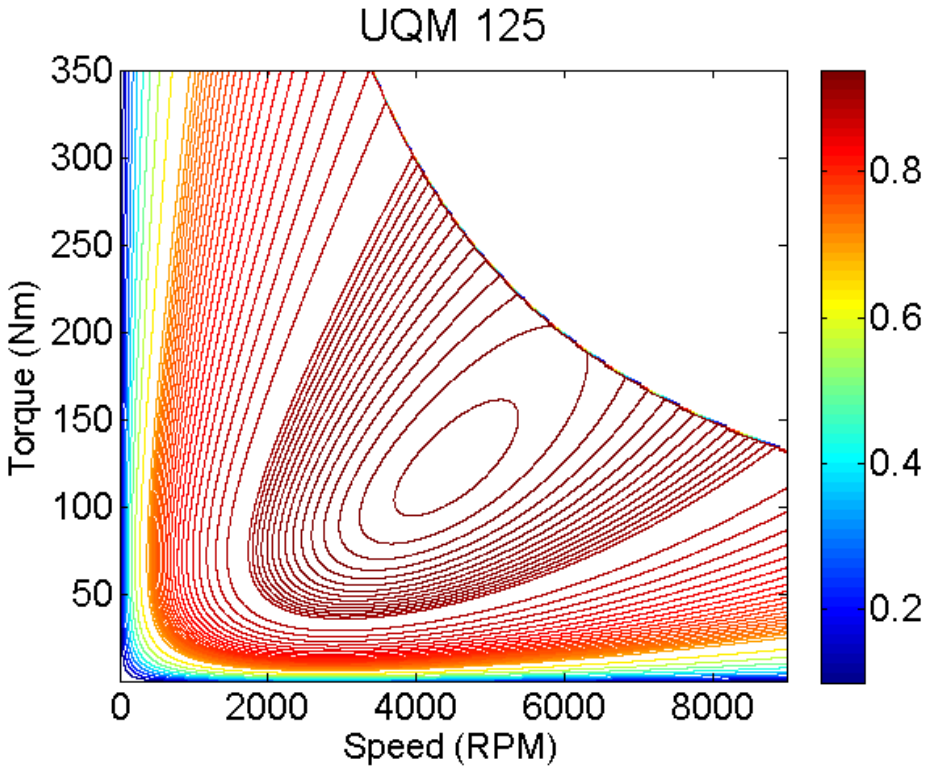

Figure 3-11: UQM 125 Motor Positive Efficiency Map

Figure 3-11 shows the most efficient operating region for the UQM 125 is near the power limit for the motor with an island of high efficiency at 4000 RPM, 130 Nm. Although operating the motor efficiently is important, the poor engine efficiency has significantly higher consequences than operating the motor inefficiently. For this reason, the efficiency of the engine is the primary focus of the control strategies.

Using the same set of equations, a generator model can also be generated. In terms of power loss, the fundamental equation is the same as the driveline (Equations 16a-b) because the generator is connected to an engine and the output power of the engine is already known. Once again, the constants associated with the loss equation are specific to the generator being modeled. A generator is only used in the series model seen later in the study. In the series study, the following parameters are used to specify the generator.

Table 3-8: Generator Motor Parameters for Series Cases

Constant	Value
k_c (s/Nm)	0.12
k_i (Nm)	0.01
k_w (s^2/Nm)	1.20E-05
Tmax (Nm)	240
Tref (Nm)	300
wmax (rad/s)	838
wref (rad/s)	838
C (W)	600

Note that all of the parameters are identical to the traction motor described in Table 3-7. By modifying only the maximum torque output, the behavior of the model is scaled to a smaller motor, including the loss characteristics and other aspects of the model.

3.6. Battery Model

For the electrified powertrain models, a simple internal resistance model for a battery is generated to calculate energy losses and state of charge (SOC). A schematic for the battery modeled is shown in Figure 3-12.

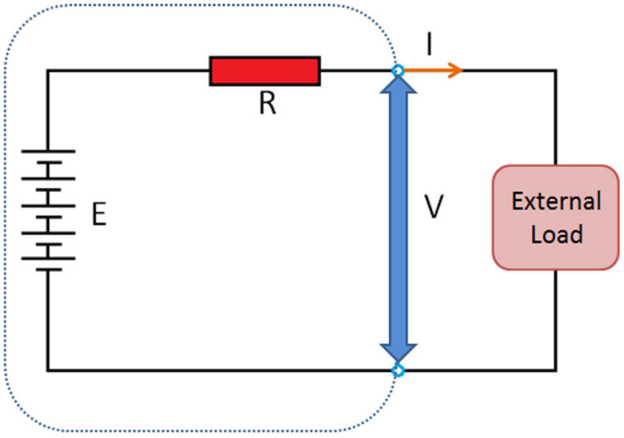

Figure 3-12: Simple Internal Resistance Model

In Figure 3-12, *R* represents the internal resistance of the battery modeled, *V* is the battery voltage at the terminals, and *I* is the battery current, and *E* is the energy source (at potential V_{oc}) of the battery. In order to find the change in state of charge of the battery based on a power demand, the output current of the battery is needed. Note that energy discharge is positive current, while charging is indicated as negative current. Power notation is the same as current, where positive power represents power discharge, and negative power represents power charge. Initially, Equation 3-20a-b represent the ideal power of the battery, and the means of calculating power loss of the battery.

$$P_{ideal} = IV_{oc} \ (\boldsymbol{a})$$
$$P_{loss} = I^2 R_{int} \ (\boldsymbol{b})$$

Equation 3-20 a-b

With these equations, it is easy to establish the actual power output of the battery at the terminals as Equations 3-21a-b.

$$P_{actual} = P_{ideal} - P_{loss} \ (\boldsymbol{a})$$
$$P_{actual} = IV_{oc} - I^2 R_{int} \ (\boldsymbol{b})$$

Equation 3-21 a-b

The power output, or in the case of regenerative braking, input for the battery is known by solving the power equations used previously to model a motor. To calculate the state of

charge, battery current is needed. Equation 3-22 solves for battery current using Equation 3-20b.

$$I = V_{oc} - \sqrt{\frac{V_{oc}^2 - 4R_{int}P}{2R_{int}}} \qquad \text{Equation 3-22}$$

Figure 3-13 shows the battery current versus the battery voltage for the battery model. When the battery charges (negative current) the voltage increases, while when the battery discharges (positive current), the battery voltage drops.

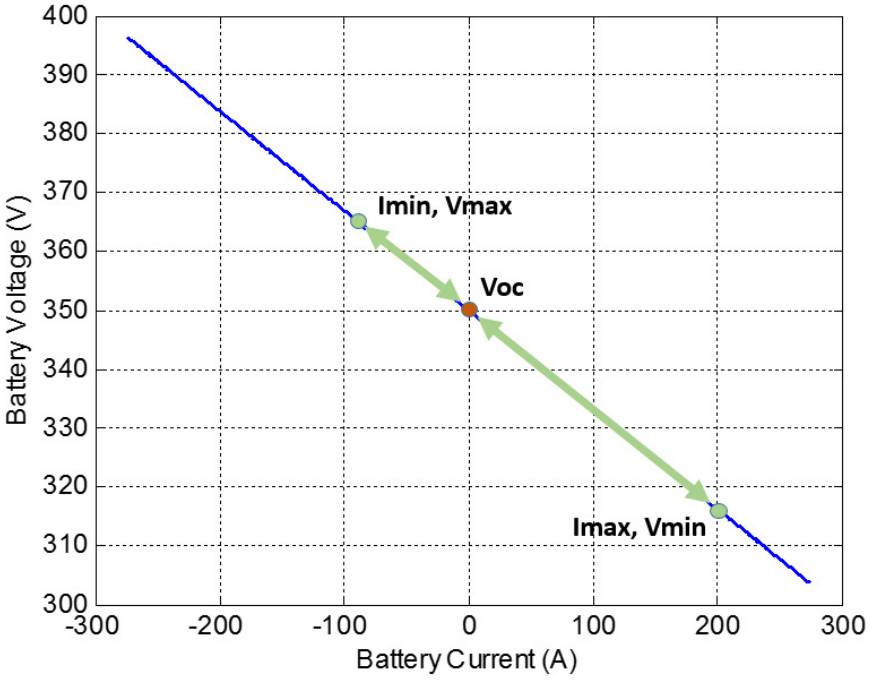

Figure 3-13: Battery Current and Voltage for UDDS Drive Cycle

Note that there are maximum and minimum voltage and current limits implemented in the battery model. This is essential in modeling to ensure the components perform similarly to actual components. These limits can be shifted along the operating line (the internal resistance defines the slope) while V_{oc} remains at zero current.

The voltage at the terminals of the battery can also be found by Equation 3-23.

$$V_{term} = V_{oc} - I_{bat}R_{int} \qquad \text{Equation 3-23}$$

With the battery current, the internal power and energy can be found by integration. This energy can then be subtracted from or added to an initial condition of energy capacity based on the battery size, as shown in Equation 3-24.

$$SOC_{new} = SOC_{old} + 100\left(\frac{dE_{int}}{E}\right) \qquad \text{Equation 3-24}$$

Note that the change in energy can be both positive and negative for the generated model in order to account for charging the battery with regenerative braking. Figure 3-14 shows an example of the battery model calculating the current for the first hill of the UDDS drive cycle.

Once again, positive current denotes battery discharge while negative current denotes battery charging. The current in Figure 3-14 shows the battery charging during braking because of regenerative braking with negative current. The battery is shown to discharge during periods of acceleration, indicating the motor is being used to propel the vehicle. The auxiliary load discharging the battery can be seen when the vehicle is at zero speed. The auxiliary load is modeled as a constant loss.

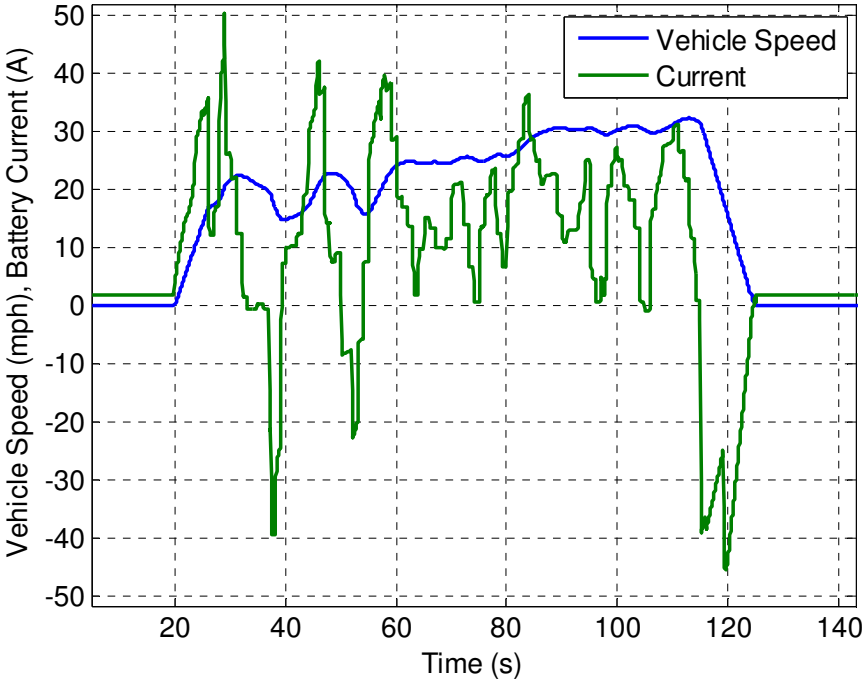

Figure 3-14: UDDS Hill 1 Battery Current

3.7. Driver Model

Each of the models used in the study use a driver model to generate a driver demand. The driver model uses a simple PID controller. The input to the PID controller is the speed error, or the error between the drive cycle "desired" velocity, and the current vehicle velocity. The output of the driver model is the accelerator pedal position (APP) as a percentage. Figure 3-15 shows a diagram of the PID controller used as a driver model.

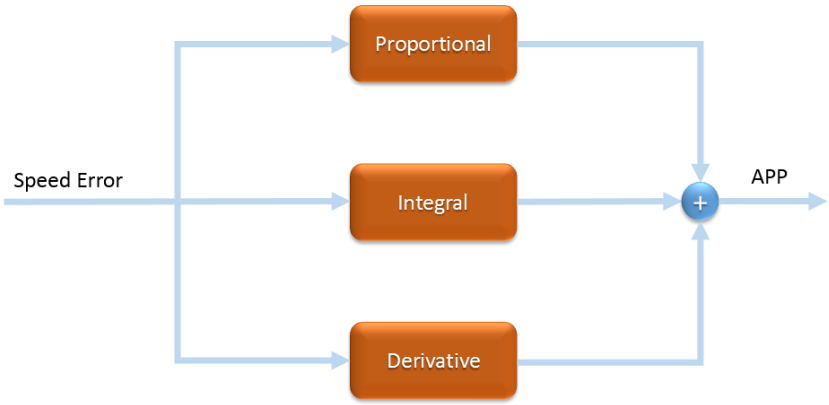

Figure 3-15: Vehicle PID Controller

In order to properly use the driver model, the proportional, integral, and derivative gains must be tuned properly to achieve the desired performance of the driver. The primary criteria for an acceptable set of driver model parameters is the ability to meet all of the drive cycle demands (particularly the more aggressive US06) without performing a trace miss. A trace miss is defined in this study as deviating from the drive cycle velocity by greater than 2 mph at any point. Table 3-9 shows the driver model parameters used for all test cases in this study.

Table 3-9: Driver Model Parameters

Parameter	Value
Proportional Gain (kp)	250
Integral Gain (ki)	10
Derivative Gain (kd)	5.00E-02

The dominant term in the driver model is the proportional term. The proportional term is the primary tunable parameter in the driver model because the proportional term has the highest influence on the behavior of the model. The integral and derivative terms are primarily used to smooth the behavior of the driver in cases where the output of the model may oscillate around a certain value. In order to tune the driver model, the Ziegler-Nichols tuning method is used. This method involves beginning with only a proportional terms, then finding the integral and derivative terms based on the oscillation of the PID output.

Figure 3-16 shows the driver model output for the first hill of the UDDS cycle. The error between the input drive cycle and the vehicle speed is very small. This shows the driver model settings are able to meet the demand for an input drive cycle.

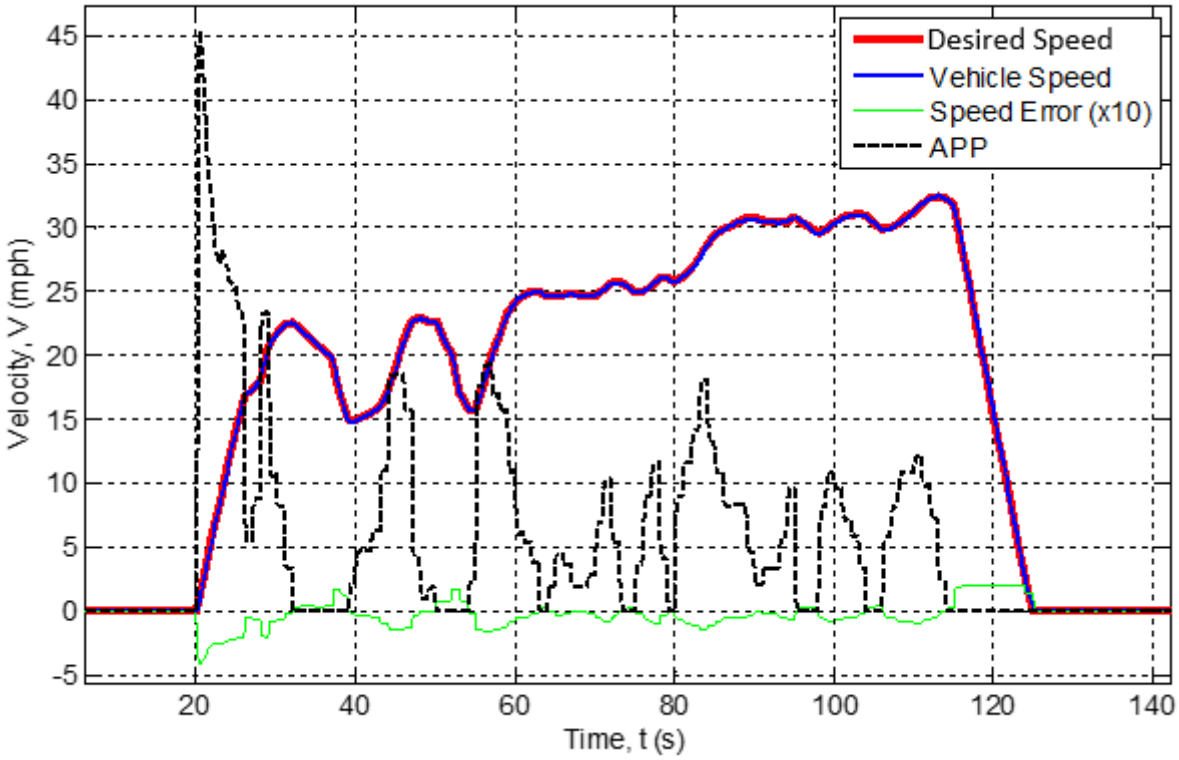

Figure 3-16: Driver Model Output for UDDS Hill 1

3.8. Hybrid Vehicle Supervisory Controller

Series Configuration

In order to have vehicle components interact with each other in an efficient manner, each component must be managed by a hybrid vehicle supervisory controller (HVSC). Figure 3-17: Flow Diagram of a Series HEV shows the flow of data, as well as torque and power in the Series model. Figure 3-17 also visualizes the operation of the Series model. The driver model and HVSC model are components of the model that are more involved with the data flow of the rest of the configuration, and manage or drive the rest of the vehicle. While these are not all the signals that are communicated in the model, the primary functions of each individual model are represented and the impact that each component has on the rest of the powertrain is displayed. The HVSC commands both the engine and generator to be on or off, as well as the power command of both. The strategy for determining the power command is discussed further in the remainder of this section.

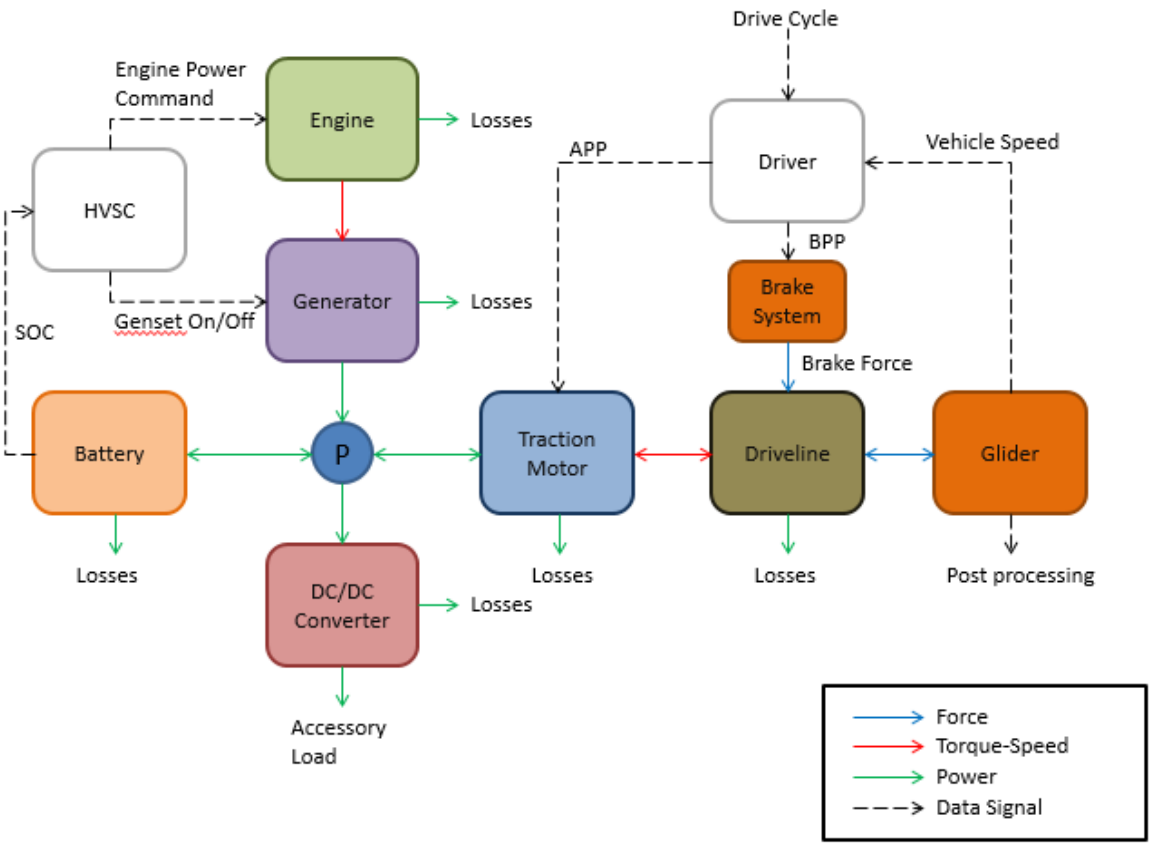

Figure 3-17: Flow Diagram of a Series HEV

Once the power output of the genset is calculated, the "power node" represented as a blue circle in Figure 3-17 directs where the energy is going by summing the power demanded by the driver, the power required to sustain the DC/DC converter for accessory loads, and the remainer that can be used to charge the battery. Equation 3-25 shows the power node equation.

$$P_{bat} = P_{dcdc} + P_{mot} - P_{genset} \qquad \text{Equation 3-25}$$

As stated in the previous section, negative current and therefore power denotes charging the battery. For this reason, the P_{genset} term is always negative. The power from the genset must first be converted to electrical energy before it can be used to propel the vehicle. This is a disadvantage with series hybrids and is discussed later on in the study. Equation 3-25 is used to account for several scenarios in a hybrid vehicle. The following figures illustrate the operation of the power node in different situations.

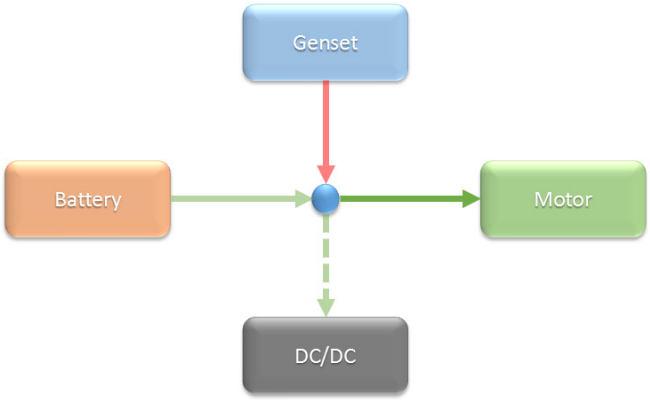

Figure 3-18: Series Propel Case: High P_{mot}

Figure 3-18 shows a propel case for the SHEV where the highest value on the right hand side of Equation 3-25 is P_{mot}. This is a general propel case that will be used during acceleration and other general driving cases. In Figure 3-18, green arrows denote positive values, while red denotes negative values. The DC/DC power line is denoted as a dashed line because it is not considered in the operation of the components, but still is present as a parasitic load. The above case illustrates that P_{mot} is higher than P_{genset} and in order to meet the motor demand, the battery must be discharged in addition to the power provided by P_{genset}.

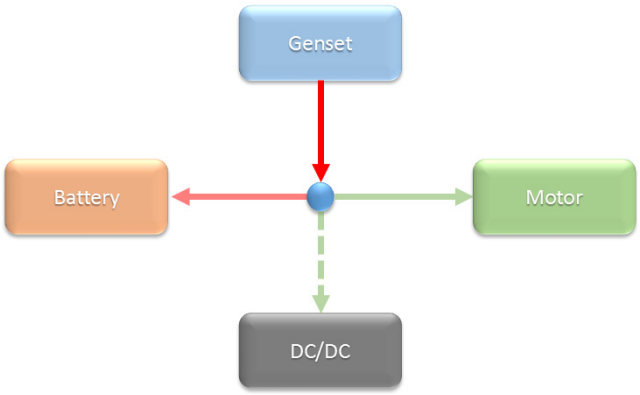

Figure 3-19: Series Propel Case: High P_{genset}

Figure 3-19 shows when P_{genset} is higher than the demand from P_{mot} and P_{dcdc}. In this case, the excess power after accounting for the motor and auxiliary load will be used to charge the battery. This situation is for a case of lower driver demand and when battery SOC is low.

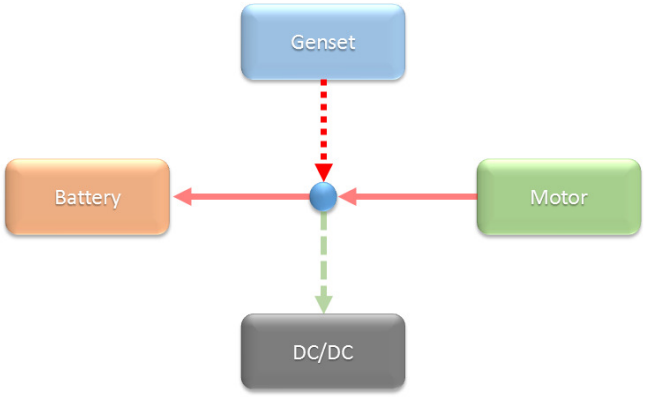

Figure 3-20: Series Regenerative Braking Case

Figure 3-20 shows a regenerative braking case for the SHEV. In this situation, the motor is being used to brake the vehicle, so the P_{mot} term is negative. P_{dcdc} is still a parasitic load taking power from the system. All of the energy from either the genset or the motor is being used to charge the battery. In this case, the genset may be switched off depending on battery SOC, so it is also possible that the motor is the only component charging the battery in this case.

The SOC is then transmitted to the HVSC so the operation mode can be determined. The traction motor uses the supplied power to transfer to the driveline for a simple single gear multiplication as well as account for the losses experienced in a transmission and differential. Once the power loss from the driveline has been accounted for, the current vehicle speed is used to produce the tractive force.

As discussed previously, the driver model is a PID controller used to read and follow an input drive cycle. The driver model produces an APP, or BPP if demand is negative, based on the error between the current vehicle speed and the desired vehicle speed. The APP or BPP is then commanded to the traction motor or the brake system.

In a series hybrid, controlling the multiple torque sources means modulating the output of the engine and the generator. In the case a plug-in hybrid vehicle, there are two higher level operating modes: charge depleting (CD) and charge sustaining (CS). In charge depleting mode, only electric energy is used to propel the vehicle, discharging the battery. In charge sustaining mode, the SOC of the battery is maintained within upper and lower bounds by a balance of charging and discharging the battery.

The goal of the HVSC is to minimize fuel consumption of the vehicle, while maintaining the battery within SOC limits. In the first model for the Series hybrid, a thermostatic control strategy is implemented. Figure 3-21 shows an example of the thermostatic control strategy. An upper and lower battery SOC limit is implemented and if the upper limit of the SOC is reached, the engine-generator (genset) is switched off. If the lower SOC limit is reached, then the genset is commanded to turn on. The power produced by the genset is set to a constant output of high efficiency for the combined engine and generator. This strategy has the advantage of always running the engine at its most efficient point, however,

has no regard to the actual energy demands of the vehicle and may, in some cases, fail to maintain charge sustaining mode.

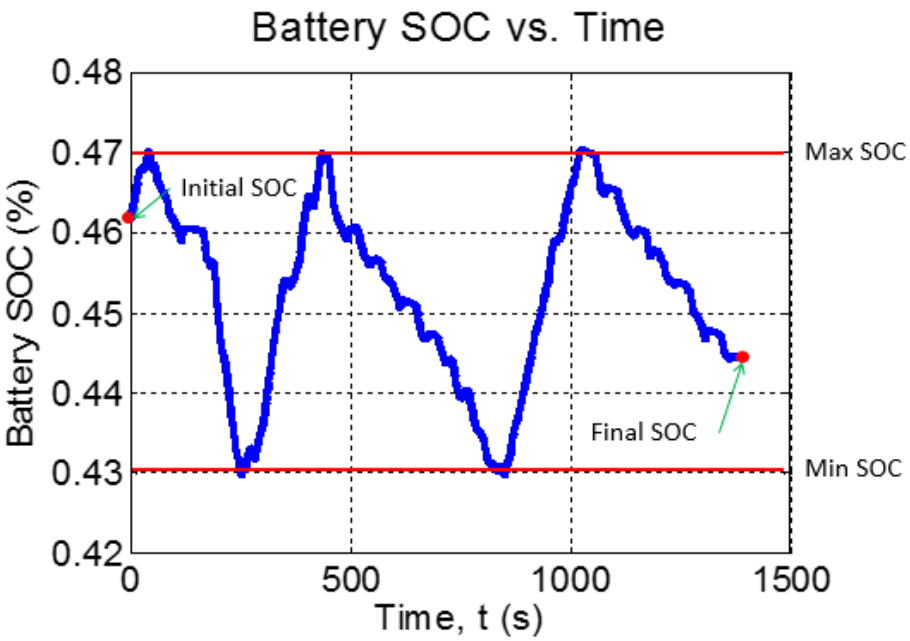

Figure 3-21: Example of a Thermostatic Controller

In order to generate meaningful, charge-balanced consumption values for the hybrid configurations, the initial SOC and final SOC need to be near equal. This is to ensure that the energy consumption numbers accurately reflect the performance of the powertrain. To maintain a charge balance, initial SOC values are iterated over repeating drive cycles until the initial and final SOC are close. Figure 3-22 and 3-22 (Alley et al., 2013) show the energy flow through a series hybrid vehicle for both propel cases and braking (regenerative) cases. An important distinction to make in comparing the energy flow diagrams is the direction of the energy flow. The inputs and outputs for each component are flipped, depending on the direction of the electrical energy flow.

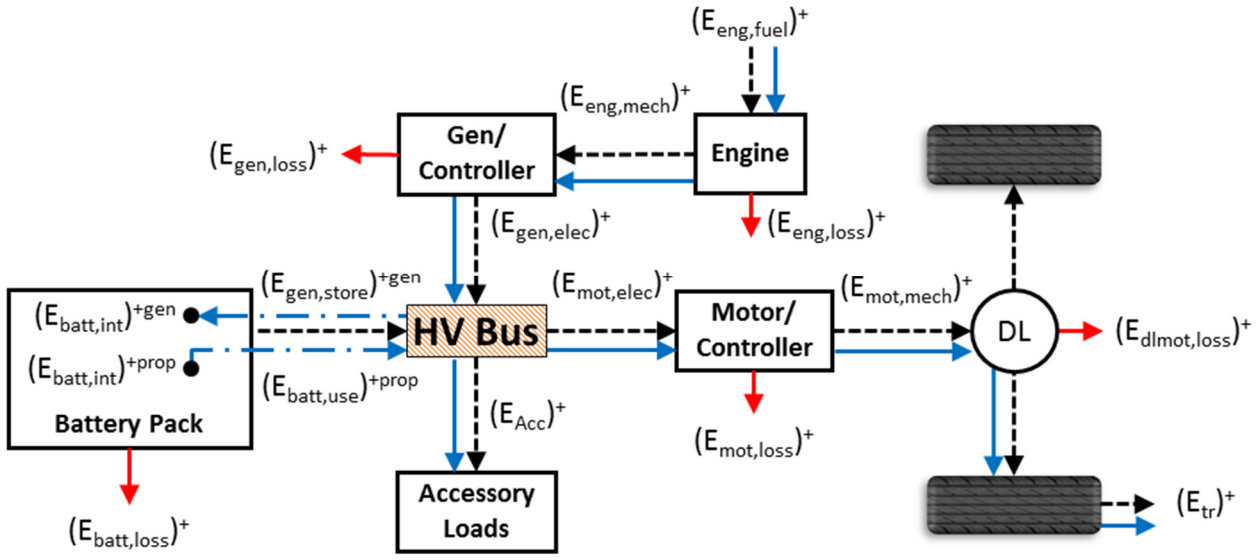

Figure 3-22: Energy flow for a Series hybrid configuration (propel case)

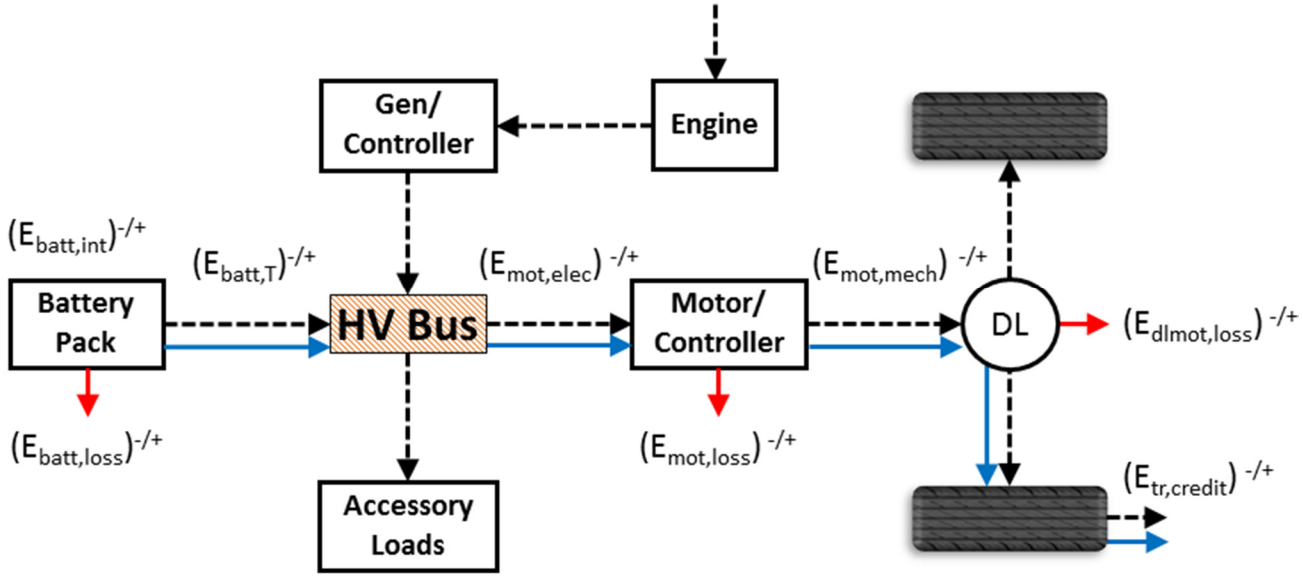

Figure 3-23: Energy flow for a Series hybrid configuration (regen reuse case)

Another function of the HVSC is engine start-stop capability. Engine start-stop capability is possible when a larger motor is attached to the engine so the engine speed can quickly rise and meet driver demand instantaneously from stop. The presence of a larger generator motor provides this capability. Figure 3-24 shows the engine start-stop function for a UDDS cycle. The engine on flag indicates where the engine is active and inactive. The logic in the HVSC for the series also contains a settling time for the engine. This means whatever state the engine is in (on or off), it will remain in that state for at least 30 seconds before exiting the current state. This is important to prevent constant engine activations and deactivations.

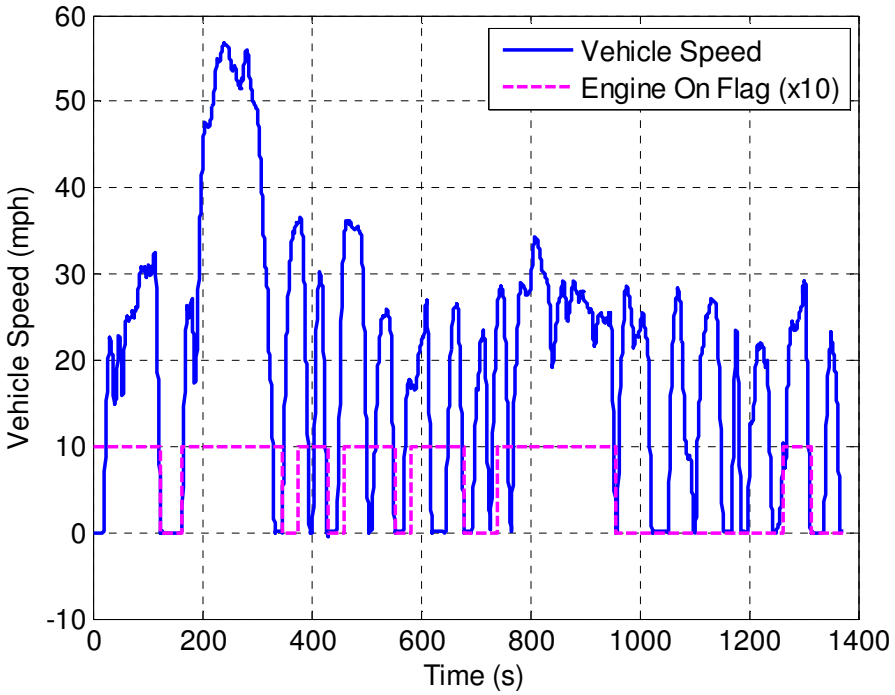

Figure 3-24: Engine Start-Stop for UDDS Drive Cycle

The load-following control strategy used for the Series cases in this work was built using Simulink Stateflow. The stateflow model accepts inputs of the current SOC, drive cycle time, power required by the motor and the power that the generator can provide at that instant. As discussed before, an additional parameter of minimum engine on/off time is programmed into this model and fixed at 30 seconds. The reason for having this parameter is to avoid instantaneous engine start-stops, which leads to inefficient engine operation, although the simple engine model does not account for engine start penalties. The stateflow block is programmed such that it directs the engine to turn on if either the SOC drops below minimum SOC limits or the battery cannot match the motor power demand. The engine "off" command is output only when both the SOC is above the minimum limit and the motor power demand is being met by the battery. The other block in the HVSC model is to decide the engine power command when the engine is turned on. This too depends on the current SOC and the current motor power demand. If the SOC is above minimum limits, the engine power command is the difference between the motor power demand and the peak power the battery can provide. If the SOC is below the minimum limit, the engine power command is based on the difference between the target SOC and current SOC using a proportional controller. In case both the motor power demand and the SOC make the engine turn on, the engine command gives priority to the vehicle demand with only a small portion dedicated to charging the battery.

Figure 3-25 illustrates the load following engine status logic. The three parameters in the center column of the figure (battery SOC, motor command, and vehicle velocity) are the parameters in which the engine state is determined. While the battery SOC and motor

command operate in parallel and are able to turn the engine on if either of the on conditions are met, the vehicle velocity cannot alone turn the engine on.

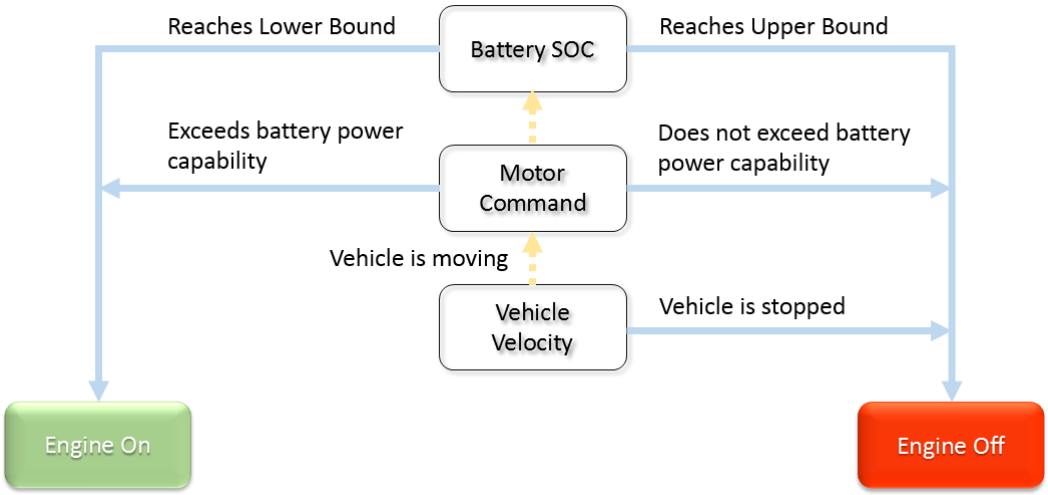

Figure 3-25: Load Following Decision Flow Chart for Engine On/Off

To demonstrate the control strategy operation, the following figures show the power values for the battery, motor, and generator in different drive cycle scenarios. Figure 3-26 shows the SHEV operating the first hill of the UDDS drive cycle.

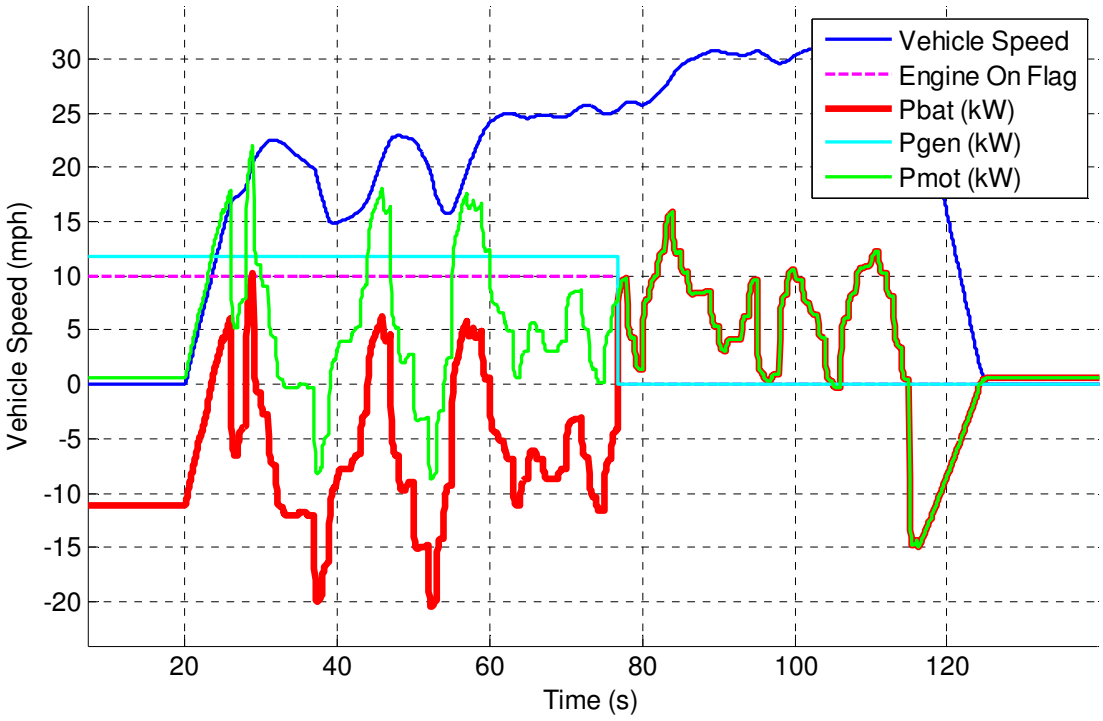

Figure 3-26: UDDS Hill 1, Load Following SHEV

This is a low demand hill for the vehicle. The initial state for the genset is on because of the current SOC. While the genset is on, it is operating constantly at the lower limit allowed (~10 kW). This lower limit is the implemented to prevent the engine from operating at a very low, inefficient power. However, around the 78 second mark, the genset shuts off. The battery power is sufficient to meet the relatively low driver demand. When the genset shuts off, motor power is equal to the battery power at the terminals because the motor is the only component operating with the battery. The accelerations and braking behavior is shown by using the motor to propel (positive power) and charge the battery in deceleration (negative power).

Figure 3-27 shows the more demanding US06 cycle. Hill 3 of the US06 has a dramatic acceleration at the beginning of the hill. This is evident by the spike in motor demand. To meet the motor power demand, the genset is switched on and operating at a higher power (~40 kW). As the speed begins to stabilize, the demand of the motor is reduced and the generator power slowly tails off. The negative spikes seen in the motor and battery are high speed braking events, which require a significant amount of power.

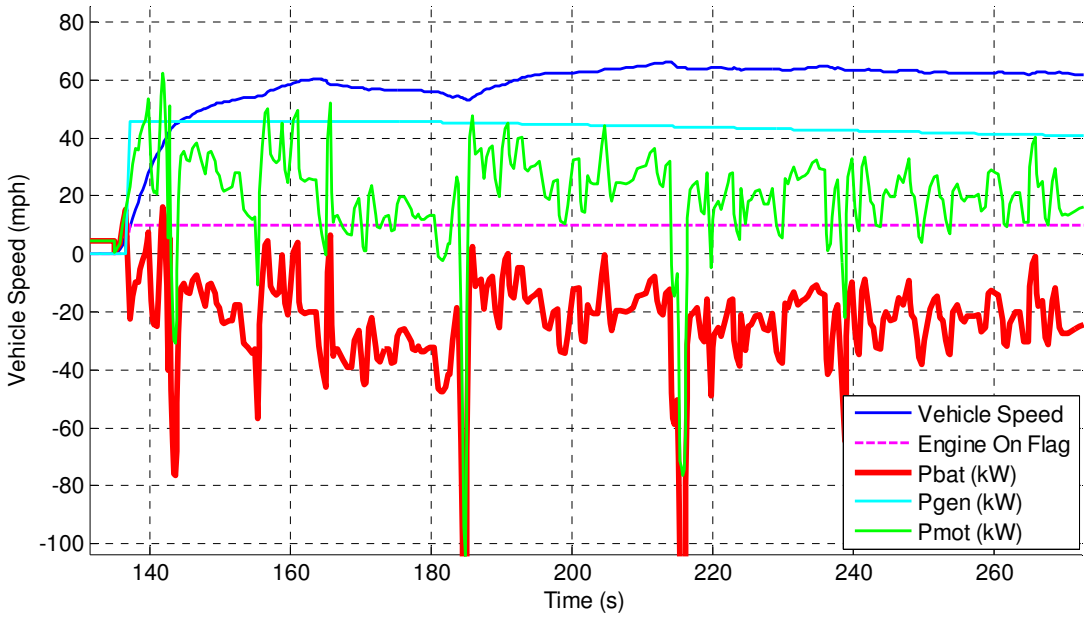

Figure 3-27: US06 Hill 3, Load Following SHEV

Figure 3-28 shows the first section of the highway fuel economy test (HwFET). The first section of the test is a lower speed, low acceleration test. The demand difference is evident by comparing the motor demand from the US06 (~80 kW peak) and from HwFET (~20 kW peak). The genset is used once again to help meet the demand of the motor. Once again, after a steady speed is established, the genset power begins to tail off, as motor demand beings to decline.

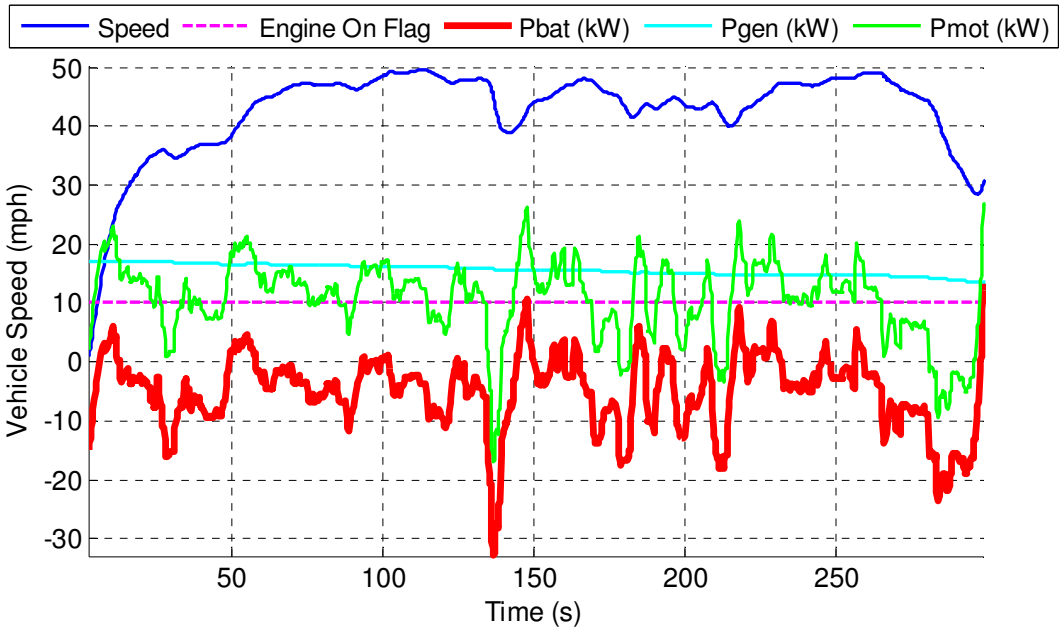

Figure 3-28: First Portion of HwFET, Load Following SHEV

As mentioned previously, this model is used to simulate charge balanced Series vehicle operation. The series models used in this thesis are simulated and the results compared to those of the 1 Hz thermostatic excel model seen in White's work. As discussed within the body of the thesis, the results match fairly closely, leading to the conclusion that both models produce accurate values. The tables in Appendix A show the values produced by the load-following model, while the thermostatic model results are contained within the body of the thesis.

Parallel Configuration

The control strategy used for the parallel models varies based on the component sizes because the capability of the motor changes drastically with the sizing. The parallel model is constructed as a parallel through the road (PTTR), where each axle of the vehicle has its own driveline model. The electric portion of the powertrain contains an electric motor of varied size, a battery model of varied size, and a base single speed transmission similar to that used in the BEV model. The mechanical portion (or engine axle) contains an engine model and a multispeed transmission similar to the model used in the conventional cases. Figure 3-29 (Alley et al., 2012) describes the energy flow for the PTTR configuration.

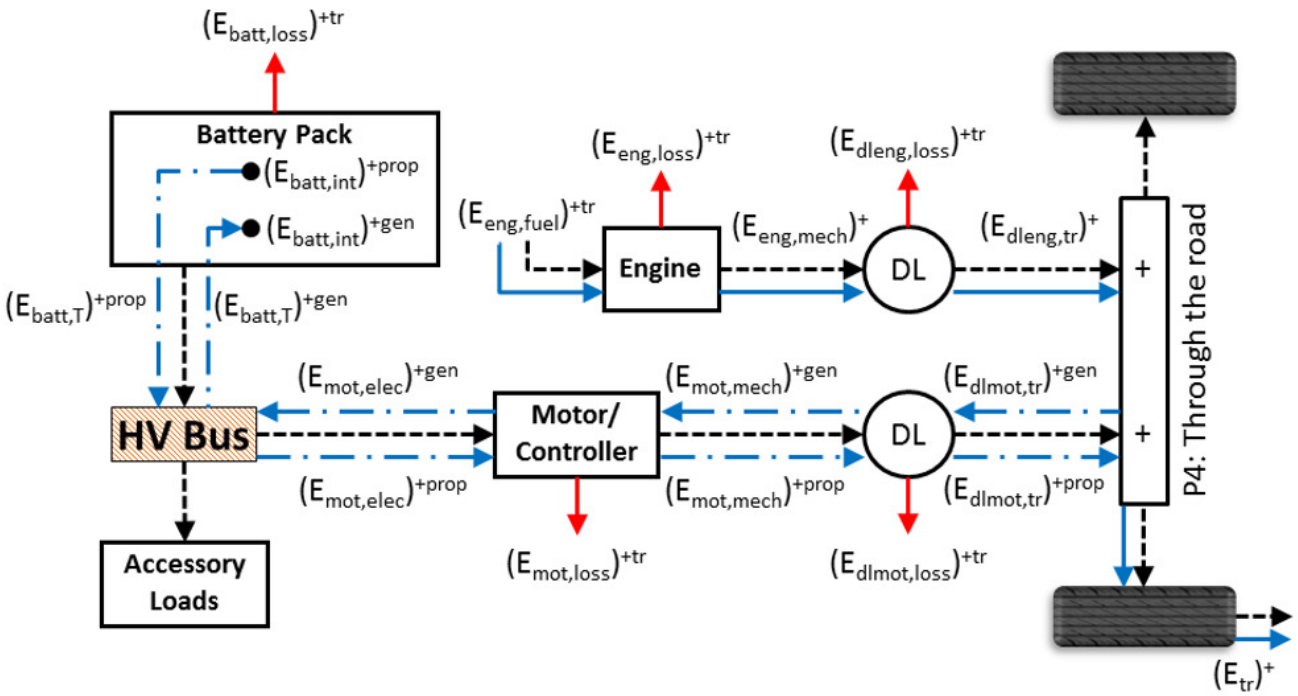

Figure 3-29: Energy flow for a PTTR hybrid configuration

The Charge Sustaining strategy for the parallel models uses the minimum BSFC line to determine the engine operating point. The minimum BSFC line represents the most efficient line of torque operation over a range of engine speeds. To use the engine efficiently at most points, the motor can either load the engine up to the BSFC line, or assist the engine to lower engine load back down to the BSFC line. Figure 3-30 graphically represents the efficient operation of the engine.

When driver demand is below the minimum BSFC line, the motor loads the engine to push the demand up to the minimum BSFC line. When driver demand is above the minimum BSFC line, the motor assists the engine to move the engine demand down to the minimum BSFC line. However, if driver demand cannot be met with the engine operating along the minimum BSFC line, a high demand state is entered. There are two high demand states, based on the current SOC. If SOC is above a certain threshold where the battery can freely discharge, the motor command is saturated to its full ability, while the remainder of the driver demand is taken by the engine. If the SOC is below a threshold that the battery cannot discharge a significant amount, the engine takes a majority of the driver demand and the motor command takes the remainder.

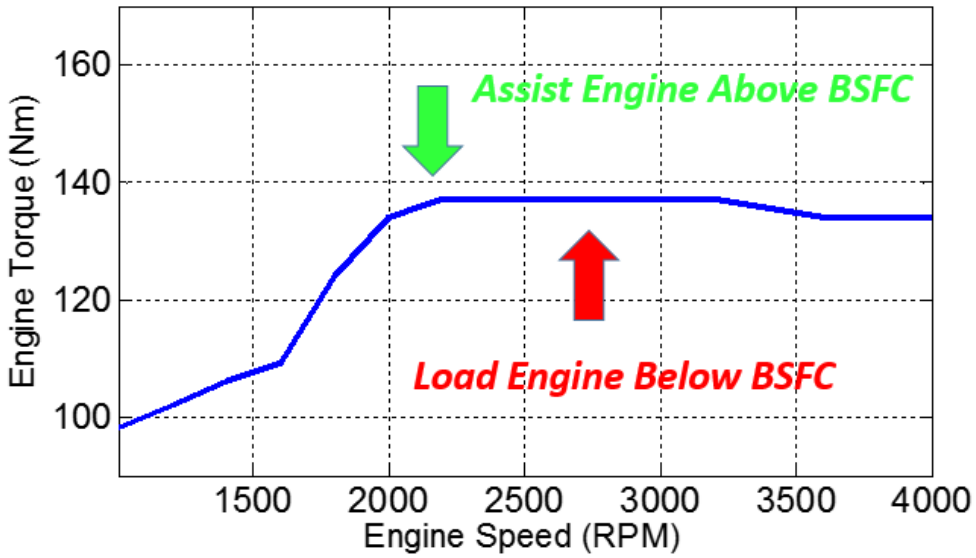

Figure 3-30: Minimum BSFC Line used for 84 kW Engine Operation

For managing regenerative braking, the braking command is calculated from a maximum brake force and the current brake pedal position (BPP). The motor is then saturated with the brake command. The leftover demand after the motor is commanded to friction braking. A summary matrix of the PTTR control strategy can be seen in Table 3-10. The driver demand high and low states are decided by an arbitrary power that is specific to each drive cycle used in the study. While more demanding drive cycles such as the US06 will require the engine to be on and putting power to the wheels to meet the drive schedule more often and require a lower power threshold, a more relaxed cycle such as the UDDS may not need the engine to meet the cycle and can have a higher power threshold. The power threshold is a value that was iterated to first meet the drive schedule, then most efficiently navigate each drive cycle. The mode descriptions are as follows:

Table 3-10: PTTR Propel Operation Decision Matrix

PTTR Propel Operating Strategy		Driver Demand	
		High	Low
SOC Level	High	Mode 4	Mode 1
	Low	Mode 3	Mode 2

Mode 1: Charge Depleting Mode. This state is only entered if the SOC is high and therefore the vehicle can entirely be driven on all electric. This mode will generally be used for low speeds where the engine assist is not required to propel the vehicle to meet driver demand.

Mode 2: Low Demand, Low SOC. With low SOC and low demand, the engine is operated along its most efficient operating line as discussed above. To determine the torque split, the characteristic torque and power limits are summed to find the total capability of the powertrain. Figure 3-28 shows the original operating torque curves for the engine and the motor, and the resulting total torque curve. In the case of Figure 3-31, a large motor and small engine are being used so the combined torque graph is heavily motor dominant.

With the overall torque capability, the APP determines what percentage of the total torque is required by the driver, and is then the engine is operated along the BSFC line to generate the engine command, while the motor command is determined based on the engine command. With low demand, the engine will generate enough energy to charge the battery, as well as assist with some vehicle propulsion, while the motor will either assist or load the engine, based on the operating point in Figure 3-30.

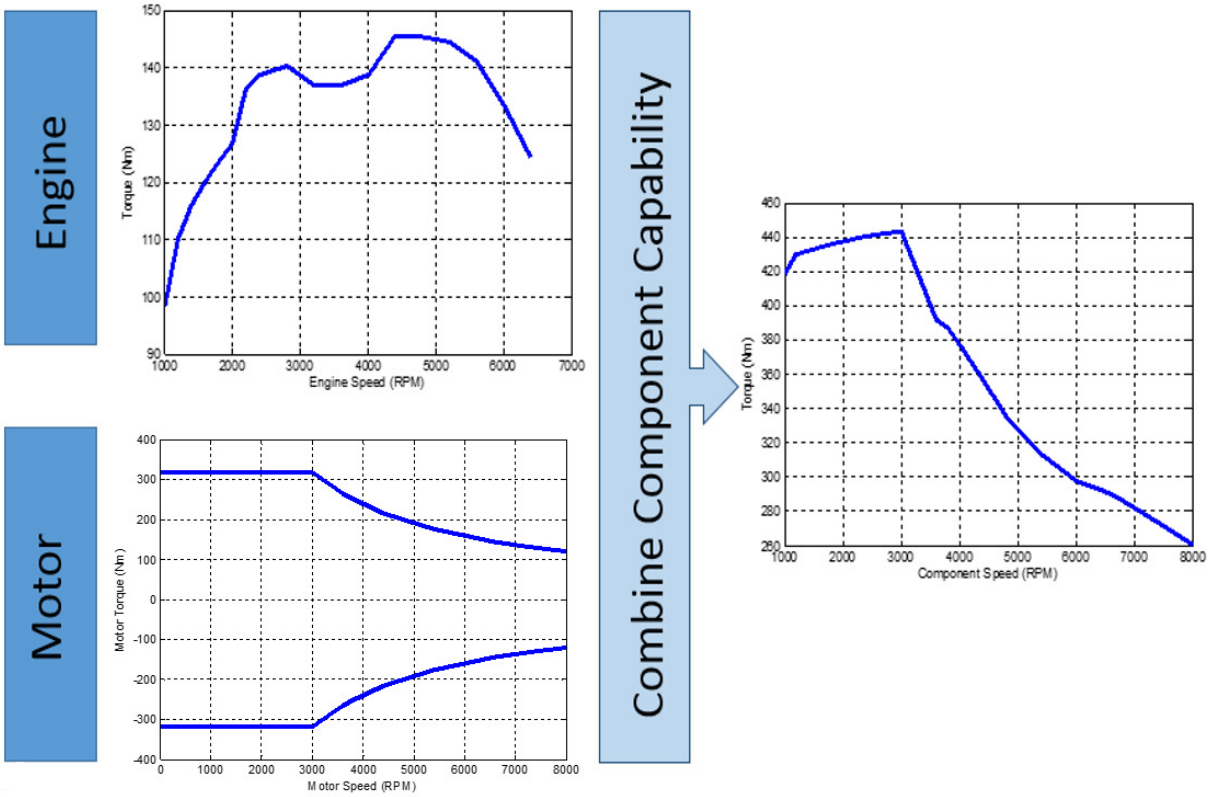

Figure 3-31: Sum of the Engine and Motor Torque Curves

Mode 3: High Demand, Low SOC. This "engine dominant" mode primarily attempts to meet driver demand using the engine because of the low SOC. In order to calculate the motor and engine command, the total torque capability is calculated in the same method as Mode 2. With the total torque, the driver demand is applied by multiplying the APP. The engine command is then calculated using the engine wide-open-throttle (WOT) curve. The remaining torque demand, if any, is then taken by the electric motor. This strategy minimizes the use of the electric motor when battery SOC is low, but operates the engine as if it was in a conventional vehicle, disregarding efficiency.

Mode 4: High Demand, High SOC. This "motor dominant" mode is similar to Mode 3, but instead of primarily using the engine to meet driver demand, the motor's full capability is first fully saturated and then uses the engine to command the remainder of the demand.

In addition to the propel modes, there is a final regenerative brake state, or Mode 5. The purpose of Mode 5 is to attempt to saturate all of the brake demand with the electric motor before engaging friction brakes. Mode 5 is only engaged if the brake pedal is engaged for

a period of longer than 5 seconds. In this mode, the engine is shut off and the motor is used to provide a majority of the brakes for the demand. This differs from other modes in that the braking in other modes (<5 seconds of braking) does not affect the state of the engine. This prevents the engine from continually being stopped and started while still taking advantage of engine start/stop capability. Battery SOC takes precedence in deciding which mode the vehicle operates in. Figure 3-32 shows the decision flow for how the PTTR controller operates.

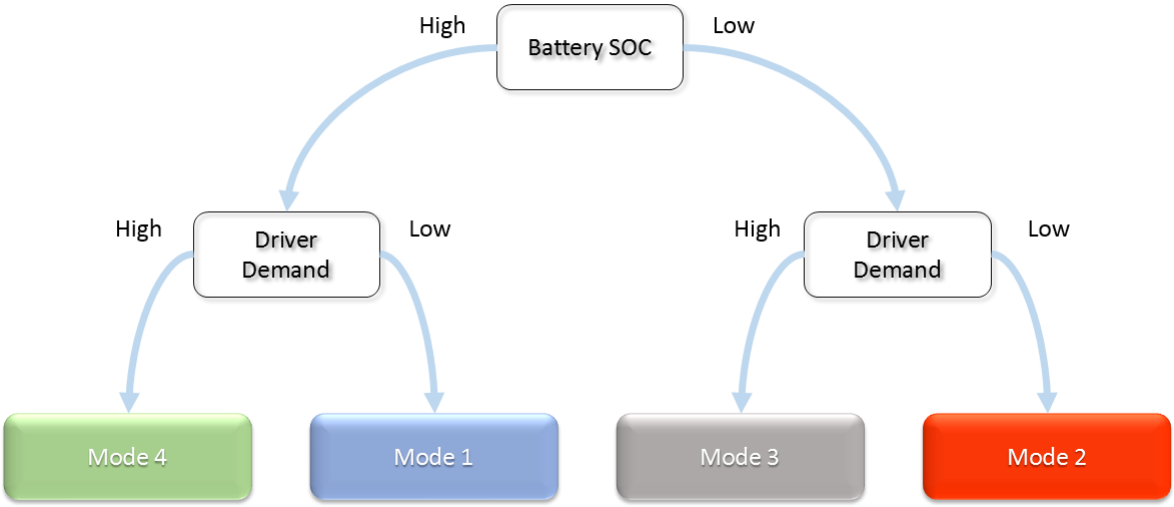

Figure 3-32: PTTR Decision Flow Chart

Figure 3-33 and 3-33 show examples of the PTTR strategy operation. In Figure 3-30, the vehicle is in an SOC high state where both all electric and motor dominant modes are to be used (Mode 1 & 4). During more demanding accelerations, mode 4 properly engages while in times of more steady speeds, all electric mode 1 takes over. During longer term decelerations, mode 5 is engaged where the engine is shut off.

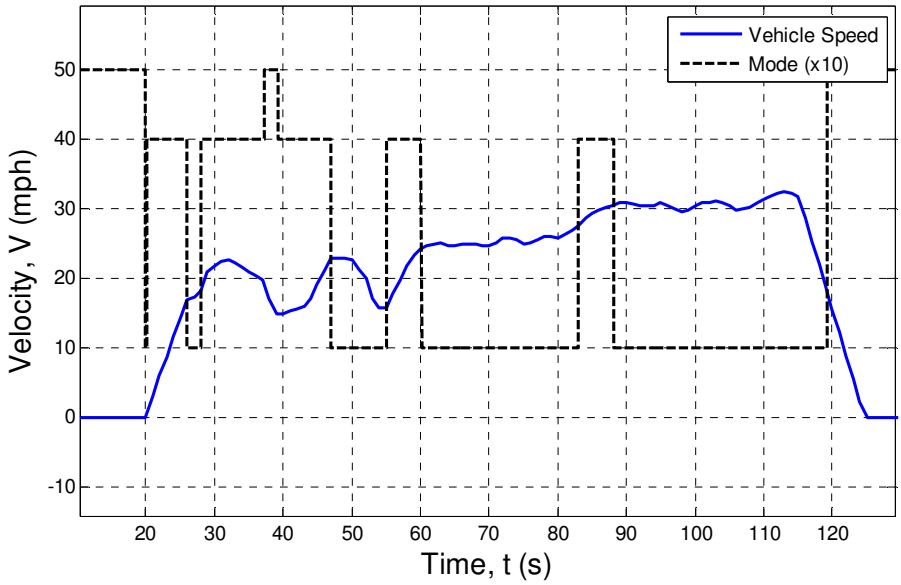

Figure 3-33: UDDS Hill 1, High SOC PTTR Operation

In Figure 3-34, the vehicle is in an SOC low state where modes 2 & 3 are primarily used for operation. In this case, the higher demand accelerations engage mode 3. The lower demand, more constant speeds engage mode 2. This is in accordance with the proposed control strategy and shows that the strategy is working as intended. In Figure 3-34, there is a short case of mode 4. This is due to the controller transitioning from SOC high state to SOC low state. Once again, mode 5 is used appropriately where the vehicle is engaged in a long brake state.

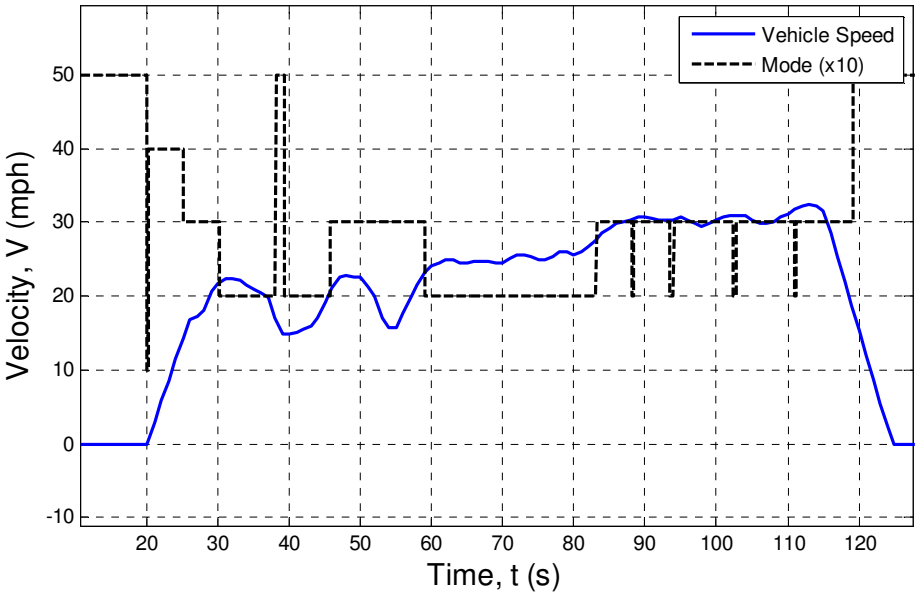

Figure 3-34: UDDS Hill 1, Low SOC PTTR Operation

Figure 3-35 shows the same drive cycle (UDDS hill 1) while also displaying the power outputs of both the engine and the motor for a PTTR hybrid. The model used to produce Figure 3-35 is described in Section 9.2. In this case, the engine does not have a 30 seconds on timer because the motor is not large enough to meet driver demand itself. Note that when the engine is on, it is acting along the minimum power limit (10 kW).

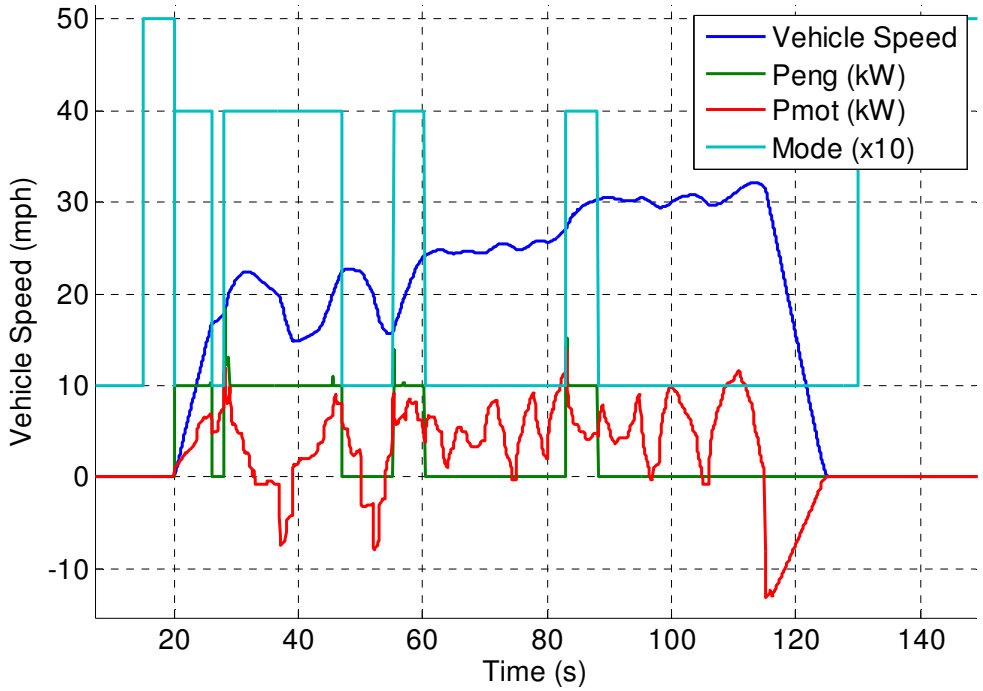

Figure 3-35: UDDS Hill 1, SOC High, PTTR Hybrid

The engine and motor behavior in the above figure shows the motor primarily driving the vehicle in the motor dominant mode (mode 4). The SOC is high enough to use mode 1 as well so whenever the demand is low, the engine is shut off. The engine is operated as a low power when the high demand state is initiated, which may be inefficient operation of the engine. Operating the engine efficiently is not taken into account in high demand states because the primary goal of the state is to meet driver demand, regardless of efficiency.

Figure 3-36 shows the SOC low operation of UDDS hill 1. The primary mode of operation for this portion is in mode 2. The load on the motor is negative for a majority of the operation to charge the battery. The engine is loaded with both the driver demand and the motor load to operate at an efficient point while charging the battery. When mode 3 is entered due to higher driver demand, the motor assists the engine in meeting driver demand, but the engine continues to carry a majority of the load.

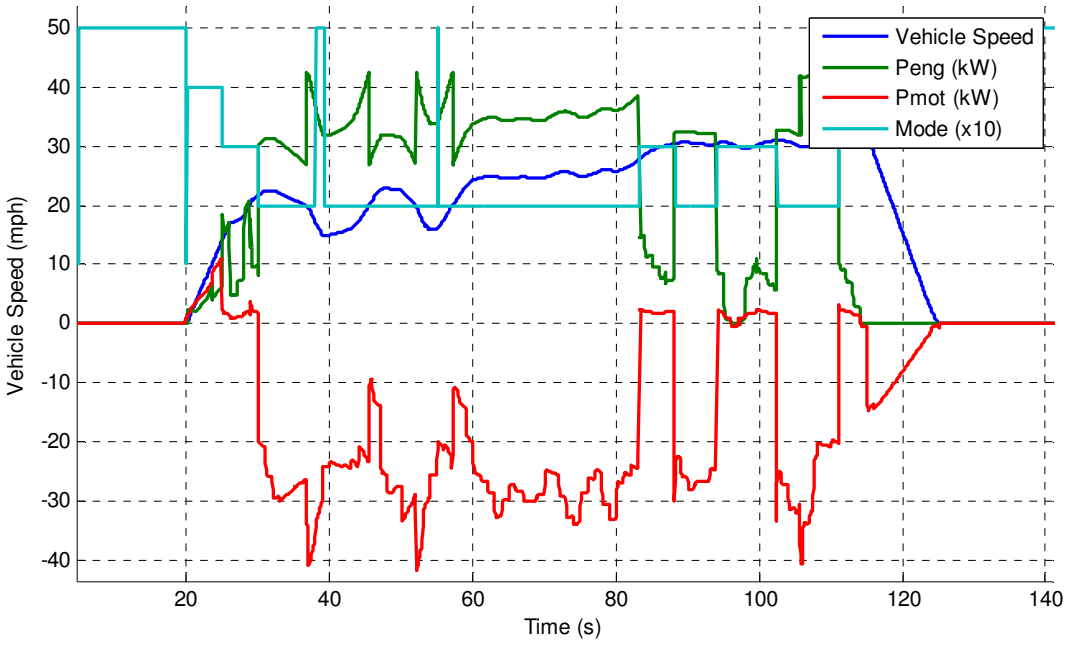

Figure 3-36: UDDS Hill 1, SOC Low, PTTR Hybrid

3.9. Model Validation

In order to validate the component models used in constructing the different powertrains throughout the study, results using the Series HEV are compared to data gathered by a modeling project undertaken by White. As discussed in Section 2.2, White's study is based on using simplified models in a 1 Hz spreadsheet to obtain powertrain design data such as energy consumption and performance. With this data, the results from this thesis and White's work can be directly compared.

To validate the models used, the base SHEV case discussed in Section 7.1 are directly compared. Table 3-11 shows the comparison for running a UDDS cycle using this thesis' SHEV model against White's SHEV model. Both models are using a basic thermostatic control strategy.

Table 3-11: SHEV Thermostatic Model Comparison

Base SHEV Comparison: UDDS	**Units**	**White SHEV**	**Ord SHEV**	**% Error**
Net Tractive Energy	Wh/km	67.5	66.3	1.78
Fuel Energy Consumption	Wh/km	487	482	1.03
Net Battery Energy	DC Wh/km	3.49	3.25	6.88
WTW GHG	g CO_2 eq/km	157	155	1.27
Range	km	664	661	0.45
Road load $\eta_{powertrain}$	%	13.9	14.1	1.44

As seen in the above table, the results using different component models are very similar with only the net battery energy exceeding 2% error. The net battery energy is supposed to be around zero for all cases to show charge balance in the model. Both models show a small value for net battery energy, so the error is insignificant. By comparing an identical hybrid model using a similar control strategy, the component models are validated for this work and can be applied to several different powertrains.

4. POWER & ENERGY REQUIREMENTS AT THE WHEELS

Prior to analyzing powertrain operation and efficiencies, vehicle glider energy requirements at the wheels are established without consideration for powertrain losses. These requirements can then be applied to any powertrain configuration on the same vehicle. The following section details the vehicle glider, drive cycle energy requirements, and peak/average power requirements.

4.1. Vehicle Glider Properties

The first step is to use the glider model to find the energy needed at the wheels to propel the vehicle through a given drive cycle. This is the energy required to power a specified vehicle without including any powertrain losses. Table 4-1 includes the given vehicle characteristics that are used to define the vehicle glider being modeled.

Table 4-1: Vehicle Glider Properties

Parameter	Value
Test Mass, m	1500 kg
Gross Vehicle Weight Rating (GVWR)	2000 kg
Drag Coefficient*Frontal Area ($C_d A_f$)	0.75 m^2
Coefficient of rolling resistance (C_{rr})	0.009
Rotating Inertia factor applied to test mass	1.04

These properties are used in Equation 4-1 to evaluate the energy requirements of a vehicle at a given speed, V, and acceleration:

$$F_{tr} = mgC_{rr} + \frac{1}{2}\rho C_d A_f V^2 + F_g + F_{inertial} \qquad \text{Equation 4-1}$$

Here F_{tr} is the tractive force required at a specific time to overcome the rolling resistance, aerodynamic drag, effects of grade, and vehicle inertia due to acceleration. In addition, g is the gravitational constant, ρ is the density of air, F_g is the force opposing a vehicle driving on a grade, and $F_{inertial}$ is the force required to accelerate the vehicle. This tractive force model scales with changes in vehicle test mass (due to powertrain) and is useful for estimating energy and power requirements for many driving conditions. Figure 3-1 details the relationship of these forces.

4.2. Energy at the Wheels

Using the vehicle characteristics described, several 1 Hz drive cycles are used to find the energy requirements at the wheels, using the equations describing the glider model. Along with energy at the wheels, other useful information is gathered such as peak tractive power, average tractive power, propelling energy and braking energy. The results for energy and power requirements at the wheels are listed in Table 4-2.

Table 4-2: Drive Cycle Results at the Wheels

Test Mass: 1500 kg	Units	UDDS	HwFET	Combined	US06
Positive propulsion energy	Wh/km	119.6	113.2	116.7	187.2
Negative (braking) energy	Wh/km	-55.4	-11.7	-35.8	-54.2
Net (road load) energy	Wh/km	64.2	101.5	81.0	133.0
Average positive propulsion power	kW	6.79	9.92	8.20	20.9
Peak power output	kW	33.1	27.4	30.5	84.5
Peak tractive force	kN	2.49	2.38	2.44	5.99
Percent idle time	%	17.8	0.52	10.0	5.87

The results presented in this table can be very useful in evaluating potential energy losses and savings in a vehicle. The positive propulsion energy is the minimum amount of energy required to propel a vehicle regardless of powertrain losses. Negative braking energy is representative of the energy lost during braking events of the corresponding drive cycle. Capturing some of this lost energy will increase overall vehicle efficiency. Also, peak and average power and force values help to size powertrain components.

4.3. Minimum Powertrain Efficiency

Table 4-3 details the required powertrain efficiency (calculated by Equation 1-1) to meet the energy consumption goal from Table 1-1. Since E_{tr} increases with vehicle mass, the efficiency required must increase as well.

Table 4-3: Required η_{PT} to Meet Combined Cycle Energy Consumption Goals

Parameter	Units	Base	PHEV	GVWR-BEV
Test Mass	kg	1500	1700	2000
Propel E_{tr}^{+}	Wh/km	117	127	143
η_{PT}^{+}	%	31.6	34.2	38.6
Road Load E_{tr}^{net}	Wh/km	81	86	93
η_{PT}^{net}	%	21.9	23.2	25.1

4.4. Average Power Requirements

To meet the performance requirements of ***EcoCAR 3***, acceleration tests are also run using the glider model. The competition requires a minimum 0-60 mph acceleration time of 11 seconds. To establish a base for performance requirements in terms of power and energy, the average power for an acceleration run as well as a constant 60 mph on a grade are calculated. In addition to the minimum acceleration time of 11 seconds, the average power required for an 8 second 0-60 mph acceleration is also calculated as it represents a more realistic acceleration time for a vehicle with similar properties. In order to calculate the average power required for both the minimum and target acceleration time, a discretized velocity model is used. The equation for the velocity trace used is:

$$V = V_m \left(\frac{t}{t_m}\right)^z \qquad \text{Equation 4-2}$$

where V_m is the target velocity (60 mph), and t_m is the target time in seconds. The exponent, z, is set equal to 0.6 to approximate the acceleration characteristics for most light duty vehicles. Time t is the input, and for this calculation a time step of 0.1 seconds is used. This model is unbounded in speed which leads to increasing power at the wheels. Actual vehicles are limited by peak power, and this prescribed velocity model provides an appropriate speed trace up to around the 400 m (¼ mile) mark. This prescribed velocity model is in very good agreement with the acceleration model results for a specific powertrain found in later sections.

All results can be found below in Table 4-4. The average power (over the whole 0-60 mph acceleration event) is provided for both acceleration times, as well for grades of 3.5% and 6% at 60 mph, and average power for cruising at 85 mph on a flat road. These performance results are what is required to propel the given vehicle glider at the wheels, and have no powertrain associated with them. The acceleration power represents a short-term or peak power requirement, while grade and cruise power represents typical continuous power requirement (often limited by thermal considerations).

Table 4-4: Average Power Requirements at the Wheels

Requirement	Power
Acceleration time of 11 seconds at test mass of 1500 kg	56 kW
Acceleration time of 8 seconds at test mass of 1500 kg	75 kW
Climb 3.5% grade at 60 mph at GVWR (2000 kg)	32 kW
Climb 6% grade at 60 mph at GVWR	45 kW
Cruise on 0% grade at 85 mph at GVWR	31 kW

An additional grade case is performed since a 6% grade at 60 mph more closely models industry standards for production vehicles. Cruising at 85 mph with no grade is close to the average power required for climbing a 3.5% grade at 60 mph. This result is due to the fact that the component of force that is caused by the grade is nearly equal to the additional aerodynamic force acting on the vehicle at the higher speed.

5. CONVENTIONAL VEHICLE PERFORMANCE & FUEL CONSUMPTION

As a starting point for vehicle powertrain modeling, a conventional vehicle model is generated. As discussed in section 3, both a power loss model and a torque-speed model are generated to attain and verify the base model results. Figure 5-1 shows the model powertrain configuration for a conventional vehicle.

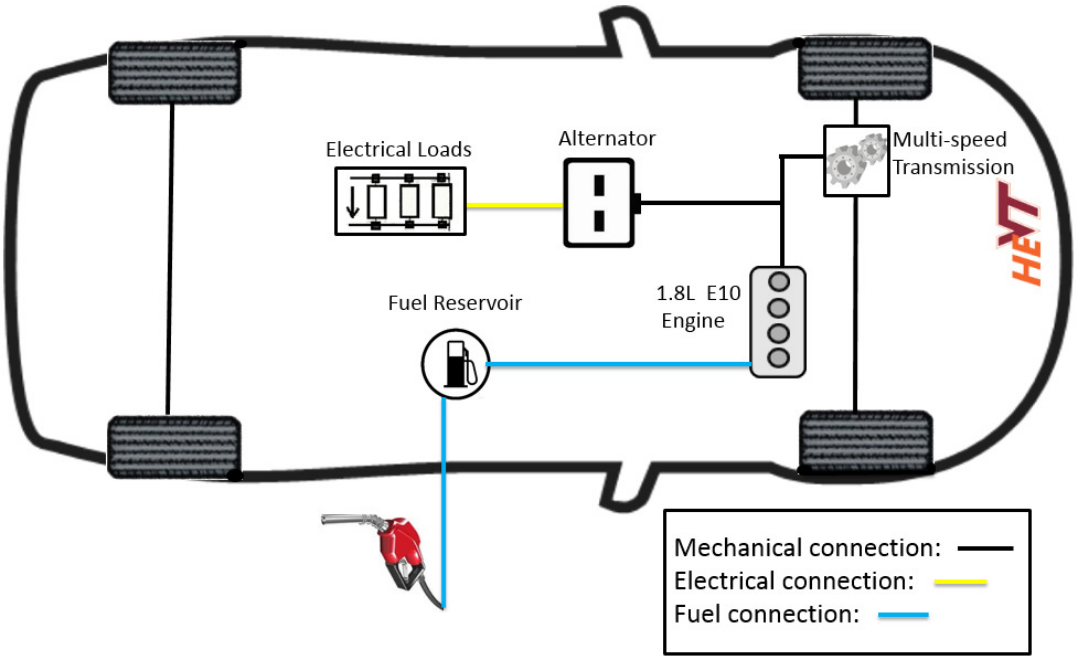

Figure 5-1: Conventional Vehicle Model Configuration

5.1. Base Engine Model

The conventional vehicle has characteristics similar to that of the 2013 Chevrolet Cruze LS. Engine sizing, performance, and fuel consumption model results should then be similar to this vehicle. To validate modeling results, the following data in Table 5-1 are found from the EPA Test Car Data site (EPA, 2013), and car magazine test data.

Table 5-1: 2013 Chevrolet Cruze LS Performance & Sizing

Engine Size & Type	1.8 L 16-Valve I-4 w/ DOHC & CVVT
Peak Power	103 kW @ 6300 rpm/156 Nm
Peak Torque	170 Nm @ 3800 rpm
Transmission	6-speed automatic
EPA Test Car Fuel Economy [City/Combined/Highway]	26.8/35.5/46.1 mpg (unadjusted)
Top Speed	108 mph (estimated)
0-60 mph Acceleration	9.3 s (estimated)
Curb Mass	1403 kg

First, the power loss method is used. Table 5-2 describes the component sizing and other variables attributed to the power loss and torque-speed conventional vehicle. The acceleration time is recorded by running the model with a maximum engine output until 60 mph was reached. In order to compare the advantages and disadvantages of each powertrain configuration, each model is run on the UDDS, HWFET, and US06 drive cycles. The results are displayed in Table 5-3. Running these cycles helps evaluate each configuration under different driving conditions.

Table 5-2: Conventional Vehicle Model Sizing & Performance

Test Mass	1500 kg
Top Speed	> 160 kph (100 mph)
0-60 mph Acceleration	7.6 s (Power Loss model) 9.1 s (Torque-Speed)
Highway Gradeability @ 60 mph @ Test Mass	> 6%
Powertrain Configuration	Conventional, E10 fuel, Automatic Transmission
Powertrain Sizing:	
Engine Peak Power	100 kW @ 6000 rpm
Engine Peak Torque	170 Nm @3800 rpm
Engine Peak Efficiency	35%
Multispeed Transmission Gearing – GM 6T30	**1st**: 4.58:1 **2nd**: 2.96:1 **3rd**: 1.91:1 **4th**: 1.44:1 **5th**: 1.0:1 **6th**: 0.74:1 **FD**: 3.87:1
E10 Fuel Tank Capacity	10 gal
Accessory Load	600 W

The coefficients used in the quadratic equation that the power loss model calculates losses from operates the engine along its most efficient points at a given power. The fuel economy numbers that are listed are reasonable, however they are higher than expected in comparison to Table 5-1. This difference can be attributed to high engine efficiency. These results represent what could be achieved using a continuously variable transmission (CVT) for the engine operating line, but without the typical losses of a CVT.

To generate more reasonable results using the power loss model, the loss equation parameters can be scaled to closer fit actual engine operation in the conventional vehicle that is being modeled. Table 5-4 shows the results for the power loss model with the characteristics of the engine model scaled to fit a more appropriate (non-optimum) operating line.

Table 5-3: 100 kW Optimum Engine Power Loss Conventional Vehicle

Test mass: 1500 kg Engine Size: 100 kW	**Units**	**UDDS**	**HwFET**	**Combined**	**US06**
Net Tractive Energy	Wh/km	64.5	101	81.0	133
Fuel Economy	mpgge	37.4	51.4	43.7	33.8
Fuel Energy Consumption	Wh/km	555	404	487	614
WTW GHG	g CO_2 eq/km	178	130	156	198
Range	km	602	827	703	543
Propel $\eta_{powertrain}$	%	13.2	26.1	19.0	22.9
Average η_{engine}	%	23.5	30.2	26.5	31.2

By scaling the coefficients in the power loss equation for the engine, more accurate results for the specified vehicle are generated. This shows that although the power loss model is simple, it is capable of generating useful results and is fairly simple to scale to a desired output.

Table 5-4: 100 kW Scaled Power Loss Conventional Vehicle

Test mass: 1500 kg Engine Size: 100 kW	**Units**	**UDDS**	**HwFET**	**Combined**	**US06**
Net Tractive Energy	Wh/km	65.5	101	81.5	133
Fuel Economy	mpgge	27.7	43.1	34.6	29.9
Fuel Energy Consumption	Wh/km	747	483	628	692
WTW GHG	g CO_2 eq/km	241	156	203	223
Range	km	447	692	557	483
Propel $\eta_{powertrain}$	%	8.7	20.9	14.2	19.2
Average η_{engine}	%	17.4	15.6	16.6	28.2

The conventional vehicle is also modeled using torque-speed engine and transmission components described in Section 3. This increases the complexity of the model, but does include more realistic limitations for the powertrain. This is reflected in the results table, as they are similar to that of the desired vehicle (Table 5-1) as well as the second scaled case for the power loss models. Table 5-5 provides a summary of results for the torque-speed version of the conventional vehicle model.

Table 5-5: 100 kW Torque-Speed Conventional Vehicle

Test mass: 1500 kg Engine Size: 100 kW	**Units**	**UDDS**	**HwFET**	**Combined**	**US06**
Net Tractive Energy	Wh/km	63.9	101	80.6	132
Fuel Economy	mpgge	27.7	41.6	34.0	24.7
Fuel Energy Consumption	Wh/km	739	498	636	839
WTW GHG	g CO_2 eq/km	241	160	205	297
Range	km	446	669	546	369
Propel $\eta_{powertrain}$	%	8.54	20.2	13.8	15.7
Average η_{engine}	%	17.5	25.1	20.9	24.3

Using a torque-speed base requires a higher fidelity model. It requires designing a basic shift strategy as well as imposing more limits; however it does increase the accuracy of the model, as seen in Table 5-5. With the engine efficiency constantly changing with the output torque and speed of the engine, the overall efficiency is lowered. Using a conventional vehicle, the performance goals of the competition are met, but the combined cycle energy consumption and WTW GHG goals are not met.

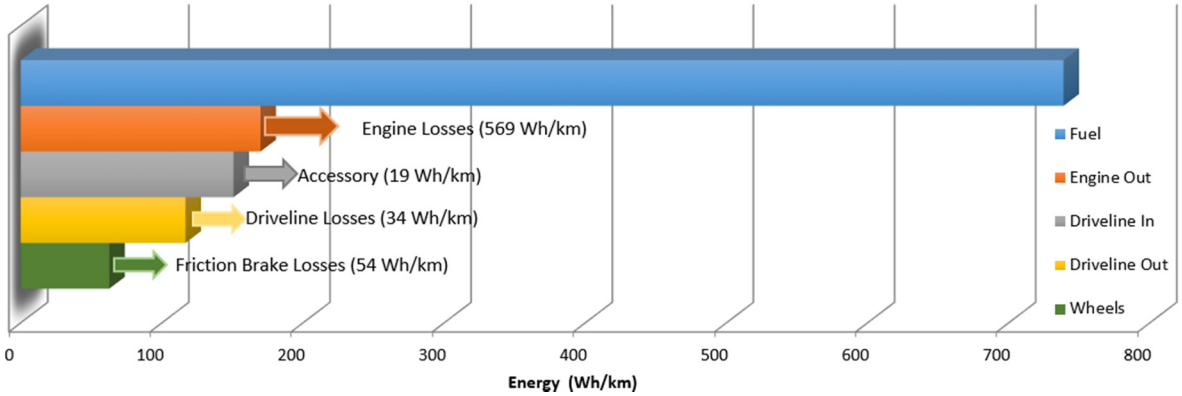

Figure 5-2: Conventional Vehicle Base Case Energy Balance for UDDS

To further validate the conventional vehicle base case model, an energy balance is completed to confirm that all of the energy contained in the fuel consumed is utilized to meet driver demand at the wheels or is consumed by losses. As shown for a UDDS case in Figure 5-2, of the total 739 Wh/km fuel energy consumption, 63.9 Wh/km supplies the net road load demand at the wheels. The remaining 676 Wh/km is consumed in total losses. Frictional brake losses include both engine idle losses and those associated with deceleration. While each bar represents the energy output from each vehicle component, the arrows demonstrate the losses from the previous energy output that are associated with that aspect. This validates that the energy flow for the model is accurate and that no energy has been lost or created in the model and calculations.

5.2. Gasoline Engine Sizing Study

With the scaled power loss and torque-speed model generating relatively accurate results for the conventional vehicle data, the engine size is now scaled by matching engine power

to performance requirements. To obtain a range of viable engine sizes, power and torque values are scaled to obtain a 0-60 mph time of about 8 and 11 seconds. Comparing the three engine sizes yields an important trade off that is prevalent throughout the competition, fuel economy versus performance. Table 5-6 shows the three engine sizes that are used, with the 100 kW engine serving as the base of the study. The test mass does not vary significantly with engine size in this range and is held constant so that all of the changes in acceleration and fuel consumption are due to the engine loading. The transmission gearing is also kept the same for all cases. Some minor differences in engine sizing could occur if the final drive ratio were adjusted.

To obtain the minimum 0-60 acceleration time of around 11 seconds, the base engine is scaled down by a factor of 0.84. To meet an 8 second acceleration time, which is seen as a higher performance vehicle, the engine is scaled up by a factor of 1.16. Even the small engine can meet a 6% grade (as expected from Table 4-4) and exceed a top speed of 160 kph. Table 5-7 and Table 5-8 show the results for using the smaller and larger versions of the engine running the same drive cycles as for the original engine.

Table 5-6: Scaling Gasoline Engine Sizes and Performance

Test	1500 kg		
Top Speed	> 160 kph (100 mph)		
0-60 mph Acceleration	10.8 s	9.1 s	8.2 s
Highway Gradeability @ 60 mph @ Test Mass	> 6%		
Powertrain Configuration	Conventional, E10 fuel, Automatic Transmission		
Powertrain Sizing:			
Engine Peak Power	84 kW	100 kW	116 kW
Engine Peak Torque	143 Nm	170 Nm	193 Nm
Engine Peak Efficiency	35%		
Multispeed Transmission Gearing – GM 6T30	Same as Table 5-2		

As expected, there is a significant trade-off between higher performance and higher fuel economy. The small 84 kW engine struggles with a slower 0-60 time, but reduces fuel consumption over the large 116 kW engine by up to 24%. The 84 kW engine operates in a more efficient range for the same drive cycles, therefore yielding a significantly higher overall powertrain efficiency. Figure 5-3 displays the fuel consumption of each engine versus the 0-60 times. As shown in the tables above, as the acceleration time increases, the fuel consumption decreases.

Table 5-7: 84 kW Torque-Speed Conventional Vehicle

Test mass: 1500 kg Engine Size: 84 kW	**Units**	**UDDS**	**HwFET**	**Combined**	**US06**
Net Tractive Energy	Wh/km	63.9	101	80.6	132
Fuel Economy	mpgge	32.3	46.2	38.6	25.7
Fuel Energy Consumption	Wh/km	639	449	554	808
WTW GHG	g CO_2 eq/km	206	145	179	260
Range	km	523	746	623	413
Propel $\eta_{powertrain}$	%	10.0	22.4	15.6	16.4
Average η_{engine}	%	20.5	27.8	23.8	25.5

Table 5-8: 116 kW Torque-Speed Conventional Vehicle

Test mass: 1500 kg Engine Size: 116 kW	**Units**	**UDDS**	**HwFET**	**Combined**	**US06**
Net Tractive Energy	Wh/km	63.9	101	80.6	132
Fuel Economy	mpgge	23.6	37.3	29.8	19.6
Fuel Energy Consumption	Wh/km	878	556	733	1057
WTW GHG	g CO_2 eq/km	283	179	236	340
Range	km	381	600	480	316
Propel $\eta_{powertrain}$	%	7.29	18.1	12.2	12.5
Average η_{engine}	%	14.9	22.5	18.3	19.5

Through all of the results stated in previous tables, none of the powertrain efficiencies reach the required goal of 31.6% (propel) for a conventional vehicle. This demonstrates that the conventional vehicle powertrain cannot meet the energy consumption target for the ***EcoCAR 3*** competition in Table 1-1 without other significant engine improvements.

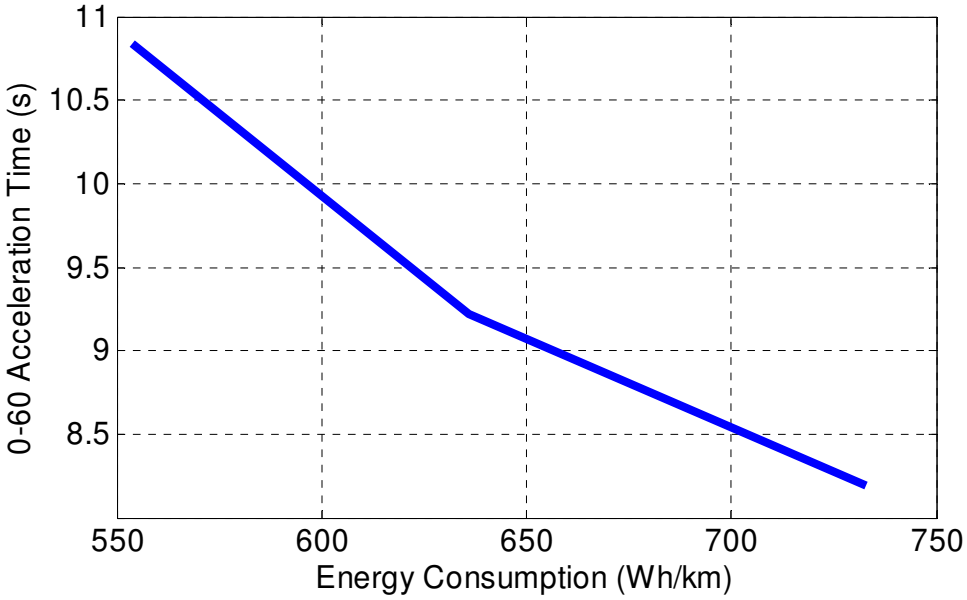

Figure 5-3: Acceleration Time vs. Combined Energy Consumption

Next, the idle and deceleration fuel use were analyzed. This analysis can prove useful in determining the benefits of advancements like engine idle stop and decel fuel cutoff. Based on the engine model used, the idle fuel rate is 0.15 g/s. This fuel rate is based on the power output so anytime the engine is producing near zero power, i.e. idle conditions or deceleration, the fuel is used at a rate of 0.15 g/s. Table 5-9 details the values used in calculating fuel savings.

When weighted together, these values give a combined cycle fuel energy use of 53 Wh/km during idle and decel conditions. Eliminating all of the non-propel fuel use during braking and idle results in fuel consumption reduction of 10% to 501 Wh/km for the 84 kW engine, but does not meet the fuel consumption target.

Table 5-9: Idle & Decel Fuel Cutoff Analysis for Conventional 84 kW Vehicle

Test mass: 1500 kg Engine Size: 84 kW	**Units**	**UDDS**	**HwFET**
Idle Time	s	244	4
Decel Time	s	368	83
Idle Fuel Rate	g/s	0.15	0.15
Fuel Energy	Wh	1050	150
Energy Use	Wh/km	86	9

5.3. Diesel Engine Model

A 95 kW diesel engine with the transmission gearing selected gives acceleration performance similar to the base conventional 100 kW gasoline engine (9.2 seconds) shown in Table 5-10. In an effort to consider a wide range of acceptable engine sizes, this base diesel engine is also scaled to match an 8 and 11 second 0-60 mph acceleration time. Using Table 1-2, the GHG emissions for a B20 diesel engine are calculated and produce 32% lower emissions than E10 gasoline. Additionally, a diesel engine has lower fuel consumption by about 23% making B20 very attractive.

To measure the performance of the diesel engine over a variety of driving conditions, the model is run over the UDDS, HwFET, and US06 drive cycles. Using these drive cycle results, the B20 diesel engine can be compared to the E10 gasoline engine over the same driving conditions. Table 5-11 shows the drive cycle results for the torque-speed diesel engine conventional vehicle model.

Table 5-10: Diesel Engine Conventional Vehicle Model Sizing & Performance

Test Mass	1500 kg
Top Speed	> 160 kph (100 mph)
0-60 mph Acceleration	9.2 s
Highway Gradeability @ 60 mph @ Test Mass	> 6%
Powertrain Configuration	Conventional, B20 fuel, Automatic Transmission
Powertrain Sizing:	
Engine Peak Power	95 kW @ 4000 rpm
Engine Peak Torque	283 Nm @ 2000 rpm
Engine Peak Efficiency	40.6%
Multispeed Transmission Gearing – GM F40-6	**1st**: 4.15:1 **2nd**: 2.37:1 **3rd**: 1.56:1 **4th**: 1.16:1 **5th**: 0.86:1 **6th**: 0.69:1 **FD**: 3.20:1
B20 Fuel Tank Capacity	10 gal
Accessory Load	600 W

It is well known that diesel engines perform with a higher efficiency than that of the conventional gasoline engine. Note that the fuel economy in Table 5-11 is not mpg of diesel, but mpg of gasoline equivalent. This value is to use to compare energy consumption to the gasoline conventional vehicle. Using the energy content value of gasoline from Section 1.6 (33.3 kWh/gal), the mpgge for the 95 kW diesel engine is:

$$555\,\frac{Wh}{km} = 894\,\frac{Wh}{mi}, \qquad \frac{33300\,\frac{Wh}{gal}}{894\,\frac{Wh}{mi}} = 37.2\,mpgge$$

Table 5-11 reflects this improvement in powertrain efficiency. This translates to lower fuel energy consumption than the gasoline engine conventional vehicle across all drive cycles. Not only does the diesel engine consume less energy per km than a gasoline engine, but also, according to Table 1-2, B20 diesel fuel also has a lower well to wheel greenhouse gas content per kWh than gasoline. This means that the B20 diesel engine conventional model has lower well to wheel greenhouse gas emissions than the base E10 gasoline engine model.

Table 5-11: 95 kW Diesel Engine Conventional Vehicle

Test mass: 1500 kg Engine Size: 95 kW	**Units**	**UDDS**	**HwFET**	**Combined**	**US06**
Net Tractive Energy	Wh/km	64.5	101	81.0	133
Fuel Economy	mpgge	37.2	51.4	43.7	33.8
Fuel Energy Consumption	Wh/km	555	404	487	614
WTW GHG	g CO_2 eq/km	160	116	140	177
Range	km	602	827	703	543
Propel $\eta_{powertrain}$	%	13.2	26.1	19.0	22.9
Average η_{engine}	%	23.5	30.2	26.5	31.2

5.4. Diesel Engine Sizing Study

After sizing the diesel engine to meet the acceleration performance of the base gasoline engine, the diesel engine is then scaled to match both an 8 and an 11 second 0-60 mph acceleration time. Table 5-12 shows the three engine sizes that are used, with the 95 kW engine serving as the base of the study. Similar to the gasoline engine sizing study, the 8 and 11 second engines represent the upper and lower limits of acceptable vehicle performance. Transmission gearing was left constant as the same transmission was used. Test mass was also unchanged as a result of negligible changes in mass from one engine size to another.

Table 5-12: Scaling Diesel Engine Sizes and Performance

Test Mass	1500 kg		
Top Speed	> 160 kph (100 mph)		
0-60 mph Acceleration	8.0 s	9.2 s	11.0 s
Highway Gradeability @ 60 mph @ Test Mass	> 6%		
Powertrain Configuration	Conventional, B20 fuel, Automatic Transmission		
Powertrain Sizing:			
Engine Peak Power	113 kW	95 kW	78 kW
Engine Peak Torque	336 Nm	283 Nm	232 Nm
Engine Peak Efficiency	40.6%		
Multispeed Transmission Gearing – GM F40-6	Same as Table 5-10		

To obtain the minimum 0-60 acceleration time of around 11 seconds, the base engine is scaled down by a factor of 0.82. To meet an 8 second acceleration time the engine is scaled up by a factor of 1.19. The 11 second engine represents a more efficient vehicle while the 8 second engine establishes a more performance based design. Table 5-13 and Table 5-14 summarize the drive cycle efficiency results for the 11 second and 8 second vehicles, respectively.

Table 5-13: 78 kW Engine Torque-Speed Conventional Diesel Vehicle

Test mass: 1500 kg Engine Size: 78 kW	**Units**	**UDDS**	**HwFET**	**Combined**	**US06**
Net Tractive Energy	Wh/km	64.1	101	80.7	133
Fuel Economy	mpgge	44.4	59.0	51.0	34.7
Fuel Energy Consumption	Wh/km	468	352	416	598
WTW GHG	g CO_2 eq/km	135	101	120	172
Range	km	714	950	820	559
Propel $\eta_{powertrain}$	%	25.5	32.0	28.4	31.1
Average η_{engine}	%	26.8	34.1	30.1	32.6

Table 5-14: 113 kW Engine Torque-Speed Conventional Diesel Vehicle

Test mass: 1500 kg Engine Size: 113 kW	**Units**	**UDDS**	**HwFET**	**Combined**	**US06**
Net Tractive Energy	Wh/km	64.1	101	80.8	133
Fuel Economy	mpgge	32.5	47.6	39.3	26.9
Fuel Energy Consumption	Wh/km	639	436	547	772
WTW GHG	g CO_2 eq/km	184	126	158	222
Range	km	523	766	632	433
Propel $\eta_{powertrain}$	%	18.7	25.9	21.9	24.1
Average η_{engine}	%	19.6	27.5	23.2	25.1

Similar to the results of the gasoline engine sizing study, a trade-off between performance and fuel consumption is evident. Figure 5-4 shows the acceleration times versus the combined energy consumption for the diesel cases.

For the smaller engine, the power demand for each of the drive cycles more closely corresponds to the most efficient operation point for the engine. As a result, the smaller engine operates at about 5% higher efficiency than the larger engine across all drive cycles. This improvement in efficiency corresponds to a 24% reduction in fuel consumption from the 8 second model to the 11 second model. While the combination of B20 fuel properties and diesel engine efficiency gives both lower fuel consumption and lower WTW GHG emissions than the base conventional E10 case, the B20 diesel conventional vehicle still cannot meet the competition goals.

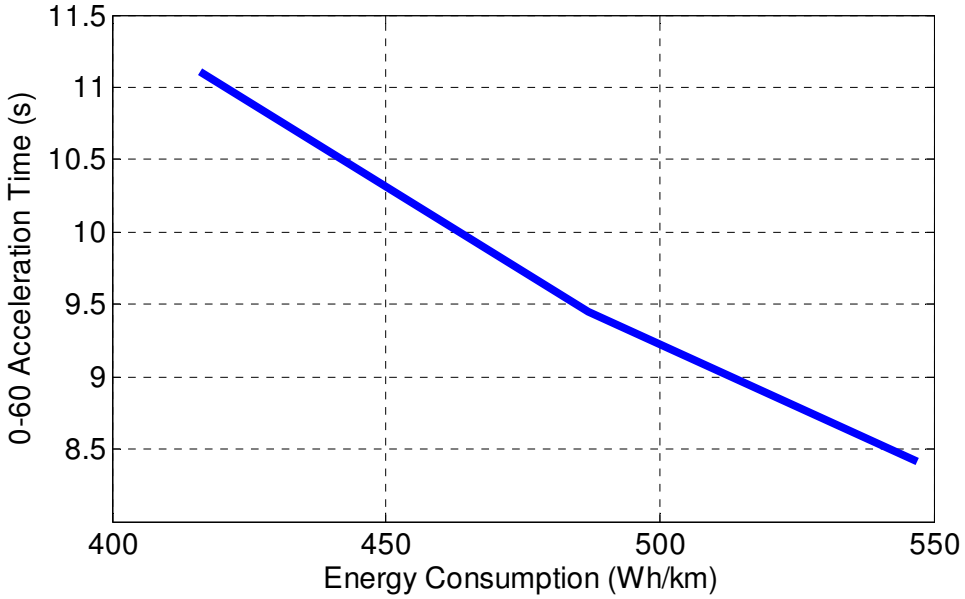

Figure 5-4: Acceleration Time vs. Combined Energy Consumption, Diesel

6. BATTERY ELECTRIC VEHICLE PERFORMANCE & ENERGY CONSUMPTION

A pure battery electric vehicle (BEV) powertrain configuration is modeled to evaluate the potential of a BEV to meet the competition energy consumption and GHG goals. Figure 6-1 is a diagram of the BEV model configuration.

The torque-speed characteristics of an electric motor allow a single speed transmission to suffice as a transmission in a BEV. This is modeled as a simple driveline with no shift strategy in both torque-speed and power loss models and only involves a constant torque loss based on 1.2% of maximum motor torque for the torque-speed loss model. The DC/DC converter is modeled as a pure loss to meet the accessory load of the vehicle. This model also includes regenerative braking. Some of the limits that control the level of regen available include a minimum vehicle speed cutoff, a maximum motor power, and a maximum tractive force. Table 6-1 provides a summary of the BEV powertrain and sizing to meet performance and range goals. The motor torque and gearing also allow for launch on a grade of greater than 30%.

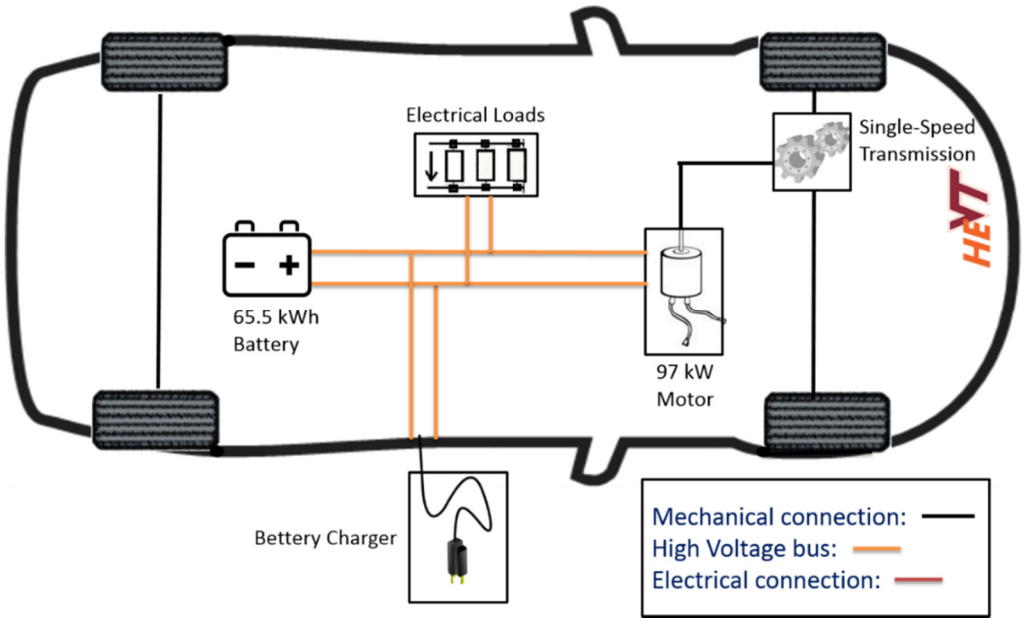

Figure 6-1: Battery Electric Vehicle Model Configuration

When sizing the drive motor and battery, the acceleration target and range both come into play. The 97 kW motor is chosen since it is able to meet the necessary peak power at the wheels to achieve the acceleration target and continuous power for highway gradeability. Range is the key characteristic when sizing the battery since enough energy must be present to complete the 320 km (200 mi) minimum range. This energy in turn sizes the battery power; the battery must be able to source enough power for the motor to meet the acceleration goal, but due to the energy sizing requirements, the available power is well above the required motor power. To ensure all criteria are met, a battery model is used to relate battery size and mass to the power and energy available from the battery. Using data for specific energy (Wh/kg) and specific power (W/kg) for both power and energy

batteries, the characteristics of lithium ion batteries as a function of mass are generated (Burke, 2007). Through analysis of these results, the energy battery mass in Table 6-1 is chosen for use in this BEV. Note that this same battery model is also used to size the battery systems discussed in later sections.

Table 6-1: Battery Electric Vehicle Powertrain Sizing to Meet Range Requirements

Test Mass	2000 kg (GVWR)
Top Speed	135 kph (85 mph)
0-60 mph Acceleration	11.0 s
Highway Gradeability @ 60 mph @ Test Mass	> 5%
Powertrain Configuration	Front Wheel Drive BEV
Powertrain Sizing:	
Motor Peak Power	97 kW @ 3000 rpm
Motor Peak Torque	310 Nm
Single Speed Transmission Gearing	7.05:1 (N/V = 94 rpm/mph)
Battery Energy Capacity	65.5 kWh
Battery Peak Power	218 kW
Battery Mass/ESS Mass	540/625 kg
Battery Usable Energy (95% - 10% SOC)	55.7 kWh
Regenerative Brake Fraction	85%
Accessory Load	600 W
Grid AC Charging System Efficiency	87%

Table 6-2 documents the battery model scaling parameters used throughout the modeling process. The main trade-off in battery development is between power and energy: batteries can be either high-power or high-energy, but not both. Often manufacturers will classify batteries using these categories. Depending on the battery requirements for a powertrain, an energy battery or power battery may be chosen, or something in between. For example, if the purpose of the battery is to meet the power demand of a traction motor, a power battery may be chosen. On the other hand, if the battery is to be designed for a specific charge depleting range, an energy battery may be more suitable to the situation. A 350 V nominal battery voltage is assumed and allows the internal resistance to be scaled inversely to Amp-hour or energy capacity. Thus a battery with twice the energy capacity has half the internal resistance. Further details of the battery model are seen in Section 3.6.

Table 6-2: Battery Model Scaling Parameters (Burke, 2007)

Battery Classification	Energy Battery	Power Battery
Specific Energy	120 Wh/kg	75 Wh/kg
Specific Power	400 W/kg	1200 W/kg
Internal Resistance	1.2 Ω-kWh	

To estimate the test mass for the BEV, the net increase for changing the powertrain from conventional to battery electric is approximated as the mass of the ESS. This is due to the engine and multispeed transmission being removed, and the comparable motor and single

speed transmission being added. Thus the conventional vehicle test mass (1500 kg, including two people) has the mass of the ESS added to it, but the BEV is still limited to GVWR. Note that using this component mass approximation, the battery/ESS sized to meet range (625 kg) would require an additional vehicle light-weighting of 125 kg to maintain a vehicle mass under GVWR of 2000 kg with only 2 people on board. Thus to achieve the goal of 4 passengers would require even more light-weighting (180 kg, or a total of 305 kg) which is not very practical for the vehicle. Table 6-3 shows the results of running the specified BEV for energy consumption values.

Table 6-3: Drive Cycle Energy Consumption Results for BEV

Test mass: 2000 kg Motor Size: 97 kW	**Units**	**UDDS**	**HwFET**	**Combined**	**US06**
Net Tractive Energy	Wh/km	76.5	113.7	93.2	145.3
Internal Battery Energy	DC Wh/km	171.3	176.26	173.5	241.4
AC Grid Energy	AC Wh/km	196.9	202.6	199.4	277.4
WTW GHG	g CO_2 eq/km	127.6	131.3	129.2	179.8
Range	km	325.1	315.9	320.9	230.7
Road load DC $\eta_{powertrain}$	%	44.6	64.5	53.6	60.2

The BEV has a high (road load) powertrain efficiency because it does not have the energy conversion losses of an IC engine. This lowers the vehicle energy use below the conventional vehicle results and also allows the goal of 370 Wh/km to be met and even exceeded by 170 AC Wh/km for the combined case. However, the WTW GHG is still comparable to the conventional vehicle because grid electricity has a high rate of GHG emissions per unit of energy. The low energy consumption combined with the high GHG of grid electricity does come close to the competition WTW GHG goal. As stated previously, the emissions goal for the modeling problem is 120 g/km for WTW GHG, and the minimum range requirement is 320 km (200 mi) for the competition.

This BEV design is able to meet the minimum combined range, but only with very significant mass reduction in other vehicle systems, and limited two-person mass capacity. At a test mass of 2000 kg with two people, and 435 kg of battery/500 kg ESS (so no extra lightweighting), the combined range is 160 miles. A BEV with room for 4 people at GVWR, but tested with two people at 1820 kg using 280 kg battery/320 kg ESS has a combined range of only 107 miles. This range is more typical of conventional vehicles converted to a BEV. The Tesla S is a dedicated, high-range (greater than 200 mi) BEV design using light-weight materials, and is also very expensive.

In addition to battery capacity sizing, regenerative ("regen") braking does play a large role in the ability of the BEV to meet the range requirement. Figure 6-2 shows how increasing the regen brake energy capture fraction also increases range. Since a higher regen fraction allows for more braking energy to be captured and stored in the battery (including losses along the way), it makes sense for range to be directly related to this fraction. The figure shows correlations for both the UDDS and US06 drive cycles. The UDDS has a higher range over all considering the US06 is much more aggressive and thus requires higher

energy use. In both cases however, regen is able to increase range thus solidifying the effectiveness of a well-planned regen braking control strategy.

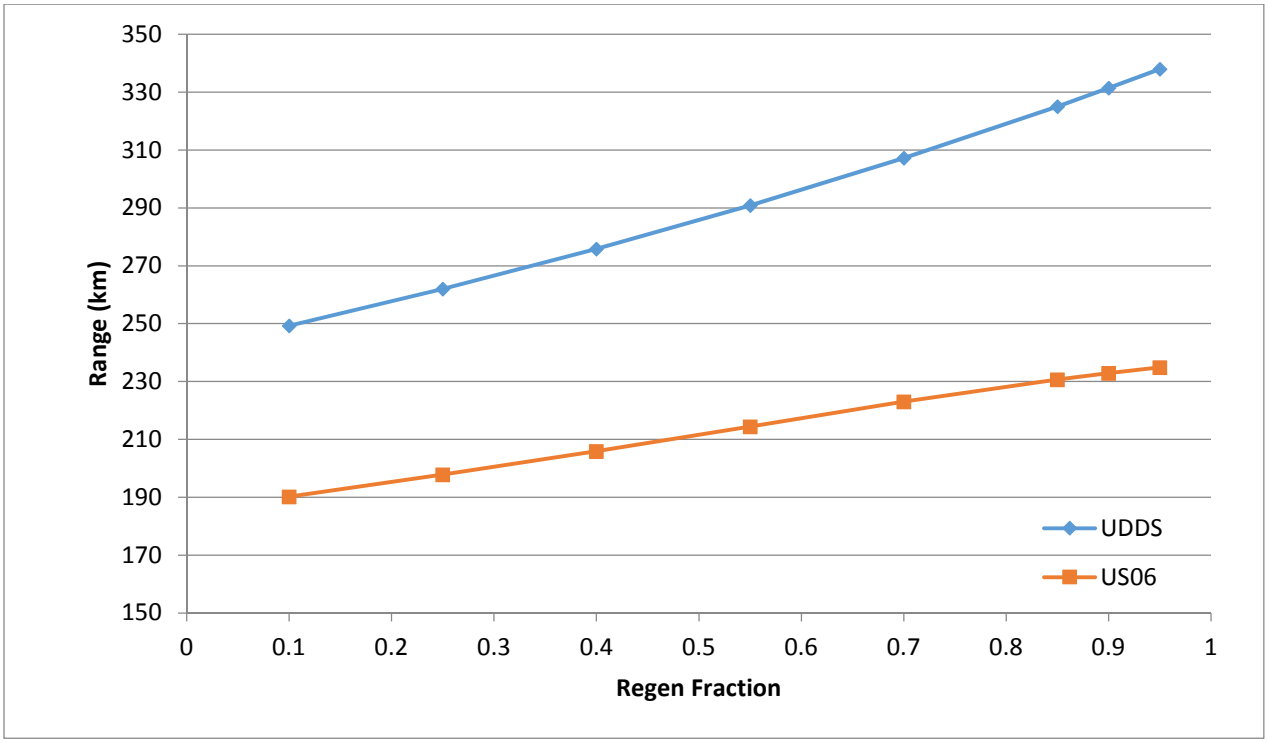

Figure 6-2: Regenerative brake fraction vs. range for BEV

To further validate the BEV model, an energy balance is completed to ensure that all the energy leaving the battery either meets driver demand at the wheels or is consumed by losses. As shown for the UDDS case in Figure 6-3, of the total 171 DC Wh/km net internal energy exiting the battery, 76 Wh/km supplies the net road load demand at the wheels (some discrepancy due to rounding values). The remaining 95 Wh/km is consumed as various component losses. The charger losses are not part of the vehicle model, and are calculated as a simple post-processing operation using the overall charging efficiency (87%) to find the total ac grid energy required to restore the battery internal energy to the initial SOC.

While each bar represents the energy output from each component, the arrows demonstrate the losses from the previous energy output that are associated with that aspect. This validates that the energy flow for the model is accurate and no energy is lost in calculation or is mysteriously created. Note that "Motor Elec." represents the energy on the electrical side of the motor while "Motor Mech." represents the energy on the mechanical side. This nomenclature is used to clarify locations since energy sometimes flows in both directions (propel and regen) through the vehicle powertrain.

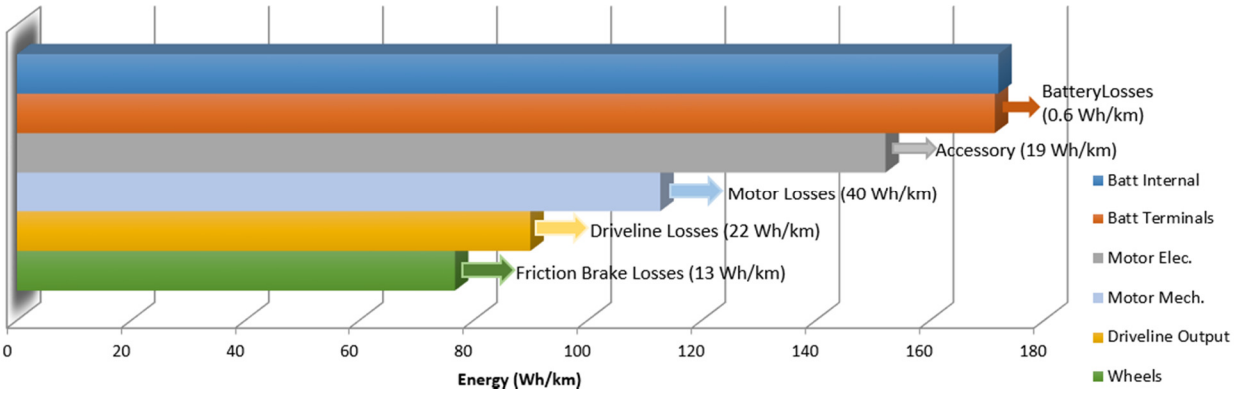

Figure 6-3: Battery Electric Vehicle Base Case Energy Balance for UDDS

7. SERIES HYBRID ELECTRIC VEHICLE PERFORMANCE & FUEL CONSUMPTION

The Series hybrid is the first configuration modeled that has multiple torque sources included. The powertrain configuration can be seen in Figure 7-1.

The Series model is driven by the traction motor coupled with a single speed transmission, similar to the BEV. An engine-generator, or genset, also has a fuel energy conversion path to the high voltage bus. This allows the genset to maintain energy in the battery while also supplying the traction motor that drives the vehicle. Regenerative braking is also possible in this configuration, using the traction motor to demand negative power and restore energy into the battery. More detail on the control strategy and model setup of the Series vehicle can be found in the Section 3.8.

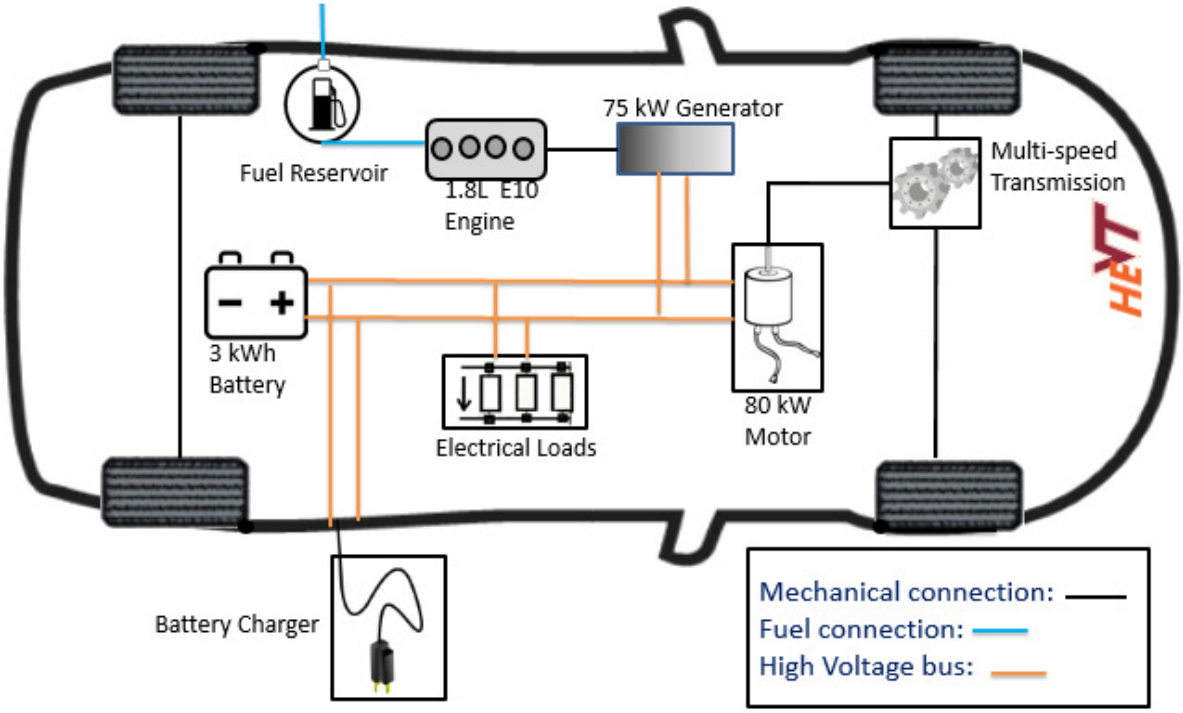

Figure 7-1: Series Hybrid Powertrain Configuration

7.1. Series Hybrid Base Case

The base Series hybrid case for this modeling problem requires that specified powertrain component sizes are used. This base case establishes a baseline for improving the powertrain by resizing the components as well as modifying the control strategy. The initial case for the Series hybrid is shown in Table 7-1. Note that the battery energy capacity is actually 3.1 kWh as opposed to the given 3.0 kWh due to the battery being sized for the appropriate maximum power of 50 kW.

Table 7-1: Base Series Hybrid Vehicle Powertrain Sizing

Test Mass	1633 kg
Top Speed	135 kph (85 mph)
0-60 mph Acceleration	11.0 s
Highway Gradeability @ 60 mph @ Test Mass	> 5%
Powertrain Configuration	Series HEV, E10 Fuel
Powertrain Sizing:	
Engine Peak Power	100 kW
Engine Peak Efficiency	35%
Generator Power (Peak/Continuous)	75/41 kW
Motor Peak Power	80 kW @ 3000 rpm
Motor Peak Torque	255 Nm
Single Speed Transmission Gearing	7.05:1 (N/V = 94 rpm/mph)
Battery Energy Capacity	3.1 kWh
Battery Peak Power	50 kW
Battery Mass/ESS Mass	42/50 kg
Battery Usable Energy (80% - 40% SOC)	1.2 kWh
Regenerative Brake Fraction	85 %
Accessory Load	600 W

To calculate the estimated Series HEV test mass, the conventional test mass of 1500 kg (including the 100 kW engine) has 63 kg added for the generator system, a net gain of 20 kg for the traction motor and single speed transmission in place of the 6 speed transmission, and 50 kg added for the ESS. This yields a total test mass of 1633 kg. The charge-balanced results of running the preliminary model are shown in Table 7-2.

Table 7-2: Base Series HEV Drive Cycle Energy Consumption Results

Test mass: 1633 kg Engine Size: 100 kW	**Units**	**UDDS**	**HwFET**	**Combined**	**US06**
Net Tractive Energy	Wh/km	66.3	103	82.8	136.8
Fuel Energy Consumption	Wh/km	482	524	524	735
Net Battery Energy	DC Wh/km	3.25	-1.56	1.08	-2.12
WTW GHG	g CO_2 eq/km	155	166	160	229
Range	km	661	617	641	441
Road load $\eta_{powertrain}$	%	14.1	21.3	17.3	18.8

Table 7-2 shows that the base Series hybrid powertrain is able to meet some of the design requirements such as range, acceleration, top speed, etc. The base case does not, however, meet the energy use or GHG WTW goals, and therefore does not serve as a viable option. In order to verify accurate modeling the values were measured for a charge balanced system as shown by the net battery energy being less than 1% of the fuel energy consumption. Note that one limitation of this model is that the US06 case experiences moments of high power demand unable to be supplied solely by the battery. Due to the simplified nature of this model, the issue is resolved by restricting the allowable SOC window to be ± 3% as

opposed to the 20% as for the other cycles. After exploring the effects this SOC window on the other drive cycles, the results do not significantly change, thus for this simple model the change in the SOC window for the US06 case is acceptable.

To further explore this case, different control strategies for the Series vehicle are used. In addition to the thermostatic model, a load-following Simulink model is also employed through the use of MATLAB. This model outputs very similar results when compared to the thermostatic model. All fuel consumption and loss values are very close to one another although there are slight variations mostly due to model assumptions and limitations discussed in Section 3.8. Overall, the thermostatic model is much more simplified, thus is more of an approximation. The fact that these models agree with each other validates that each model is producing valid results. Due to the fact that the results for the two strategies are similar, the results for the load-following case are found in Table A-1 in the of Appendix A.

To additionally validate the Series hybrid base case model, an energy balance is completed to confirm that all of the energy used from the fuel tank is utilized to meet driver demand at the wheels, or is consumed by losses. As shown for the UDDS case in Figure 7-2, of the total 486.8 Wh/km fuel energy consumption, 67.5 Wh/km supplies the net road load demand at the wheels. The remaining 418.3 Wh/km is consumed in total losses throughout the powertrain. It is important to note that the small net energy stored in the battery is displayed as a loss in the chart for simplicity since this is a Charge Sustaining model. While each bar represents the energy output from each vehicle component, the arrows demonstrate the losses from the previous energy output that are associated with that aspect. This validates that the energy flow for the model is accurate and that no energy has been lost or created in the model and calculations.

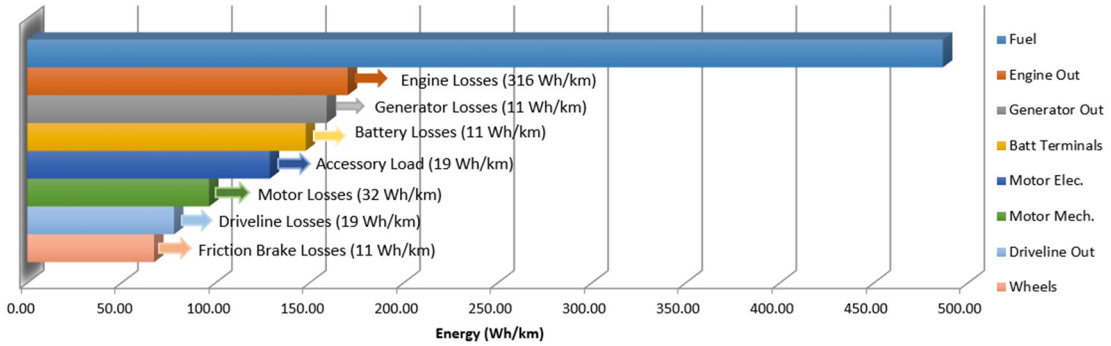

Figure 7-2: Series Hybrid Electric Vehicle Base Case Energy Balance for UDDS

Since this powertrain does not meet energy consumption and GHG goals, further investigation for the Series hybrid is done by resizing components to try to meet the design targets. Note that it is difficult to improve drastically because running with the base sizing yields an engine-generator efficiency of about 32%. Additional battery energy to allow use of grid electricity in a Charge Depleting mode can significantly reduce total energy consumption, but only slightly reduces GHG emissions.

7.2. Series Hybrid Sizing Study

After failing to reach all design targets with the Series base case, components are resized to achieve as many design targets as possible with a Series hybrid. Table 7-3 displays the variations between the base and improved case. The main changes are a downsized E85 engine with a higher efficiency, a larger drive motor, and larger battery sized to meet the motor peak power demand. With these new components, the mass increases but the acceleration time decreases with the increased motor and battery sizes. Highway gradeability is considered in this design as the 41 kW continuous power rating for the generator is ample power to exceed the required 32 kW at the wheels to maintain the 60 mph for 20 min on a 3.5% grade (Table 4-4). The mass estimation is consistent with the description for the base case. The only difference is the increased mass of the battery (and therefore ESS) since the masses for the smaller engine and larger motor approximately offset.

Table 7-3: Improved Series Hybrid Vehicle Powertrain Sizing

Test Mass	1633 kg	1692 kg
Top Speed	135 kph (85 mph)	
0-60 mph Acceleration	11.0 s	8.9 s
Highway Gradeability @ 60 mph @ Test Mass	> 5%	
Powertrain Configuration	Base Series HEV, E10 Fuel	Series PHEV, E85 Fuel
Powertrain Sizing:		
Engine Peak Power	100 kW	84 kW
Engine Peak Efficiency	35%	38.5%
Generator Power (Peak/Continuous)	75/41 kW	
Motor Peak Power	80 kW @ 3000 rpm	100 kW @ 3000 rpm
Motor Peak Torque	255 Nm	320 Nm
Single Speed Transmission Gearing	7.05:1 (N/V = 94 rpm/mph)	
Battery Energy Capacity	3.1 kWh	7.1 kWh
Battery Peak Power	50 kW	114 kW
Battery Mass/ESS Mass	42/50 kg	95/109 kg
Battery Usable Energy	1.2 kWh	5.7 kWh
Regenerative Brake Fraction	85 %	
Accessory Load	600 W	

7.2.1. Charge Sustaining Operation

With the much larger battery included in this improved case, the Series hybrid is able to have both Charge Depleting and Charge Sustaining operation modes. Table 7-4 displays the values for the charge balanced Charge Sustaining case. As shown here, values for fuel consumption and WTW GHG emissions decrease significantly, while efficiency increases when compared to the base case. This is mostly a function of the downsized E85 engine. Firstly, the smaller size also has a higher maximum efficiency at which it can be operated. Additionally, the fuel has been changed to E85 which has benefits when it comes to WTW GHG emissions. It is important to note that the range is decreased, however, this is a function of the lower energy density of E85 fuel. The vehicle still has an overall more

efficient powertrain but has less overall energy stored in the 10 gallon fuel tank. The energy consumption value, is improved by the Charge Depleting mode discussed in the next section.

Table 7-4: Improved Series HEV Drive Cycle Charge Sustaining Energy Consumption Results

Test mass: 1692 kg Engine Size: 84 kW	**Units**	**UDDS**	**HwFET**	**Combined**	**US06**
Net Tractive Energy	Wh/km	67.4	105	84.3	137
CS Fuel Energy Consumption	Wh/km	462	488	473	637
CS Net Battery Energy	DC Wh/km	-0.91	-1.15	-1.01	2.65
CS WTW GHG	g CO_2 eq/km	116	119	118	166
CS Range	km	506	491	499	361
CS Road load $\eta_{powertrain}$	%	14.7	21.4	17.7	21.2

When addressing the role of energy management strategies with the improved case shown here, the thermostatic and load-following cases again produce very similar results. This helps validate the values shown here and ensures confidence in the results for this powertrain. Again, since the values are so similar, the results for the load-following case are located in Appendix A.

7.2.2. Charge Depleting Operation

As mentioned above, an added benefit of this improved case is the addition of a Charge Depleting mode. The battery is now large enough to have both a large energy capacity and a large enough power to allow for full battery electric operation. This addition in battery capacity does come at the price of added mass. It is very important to consider the tradeoffs of a large battery before implementing one into the vehicle. The larger the battery, the higher the mass of the vehicle, which in turn, increases the resistance the powertrain must overcome to move the vehicle. In spite of this, added battery mass does allow for an offset in liquid fuel use which involves a much less efficient (much higher losses) energy conversion process, and the use of a much more efficient energy path to the wheels. The larger battery also provides a decrease in internal resistance, thus battery losses are also reduced making that energy path even more efficient than for a smaller battery. Overall, the added benefits outweigh the negative aspects for adding a larger battery to this improved case. Table 7-5 shows the values for the Charge Depleting mode of the Series HEV. As shown, a very low energy consumption allows for added range.

Table 7-5: Improved Series HEV Drive Cycle Charge Depleting Energy Consumption Results

Test mass: 1692 kg Engine Size: 84 kW	**Units**	**UDDS**	**HwFET**	**Combined**	**US06**
CD Net Battery Energy	DC Wh/km	164	173	168	243
CD AC Electrical Energy Cons.	Wh/km	188	199	193	279
CD Range	km	34.7	32.8	33.8	23.4

7.2.3. Utility Factor Weighting

To analyze vehicle energy consumption for a vehicle using two energy sources, it is necessary to take into account how often the vehicle is operating in each mode. The Society of Automotive Engineers J2841 definition of UF (SAE J2841, 2010) and the SAE J1711 test method (SAE J1711, 2010) are the standard way to analyze these operations.

J2841 establishes a value for weighting fuel and electric energy consumption for plug-in hybrid electric vehicles (PHEVs) on the basis of National Household Travel Survey (NHTS) data from 2005. In essence, PHEV charge-depleting energy consumption is weighted against the percentage of the fleet of vehicles that will use the CD range in a given day; the UF represents that percentage. The remaining percentage (1 – UF) is then used to weight the charge-sustaining energy consumption to represent the remaining drivers on that same day.

J1711 establishes a method for testing a vehicle to determine the point at which a CD PHEV transitions to its CS mode, so that the vehicle UF can be calculated. In the process, the CD and CS energy consumption values are quantified. Once the vehicle CD range and CS fuel consumption are measured, the UF can be assigned, and a value for the UF-weighted energy consumption can then be determined. The UF method is a fleet-average, combined city and highway factor. Equation 7-1 shows the method for calculating the utility factor based on charge depleting range, x. D_{norm}, C_1, C_2, etc. are known constants.

$$UF = 1 - e^{-\left[C_1*\left(\frac{x}{D_{norm}}\right)+ C_2*\left(\frac{x}{D_{norm}}\right)^2 + \ \ldots\right]} \qquad \text{Equation 7-1}$$

Using this equation and the charge depleting combined range from Table 7-5, the utility factor for the improved case Series HEV is 0.41. Other utility factor values are included in Table 7-6. Figure 7-3 shows the J1711 plot for the improved series case.

Table 7-6: Improved Series HEV UF Weighted Energy Consumption Results

Parameter	Value
CD Range	33.8 km
Utility Factor	0.41
UF Weighted Fuel Consumption	280 Wh/km
UF Weighted Grid Electrical Energy Consumption	80 AC Wh/km
UF Weighted Total Energy Consumption	360 Wh/km
UF Weighted WTW GHG	120 g CO_2 eq/km

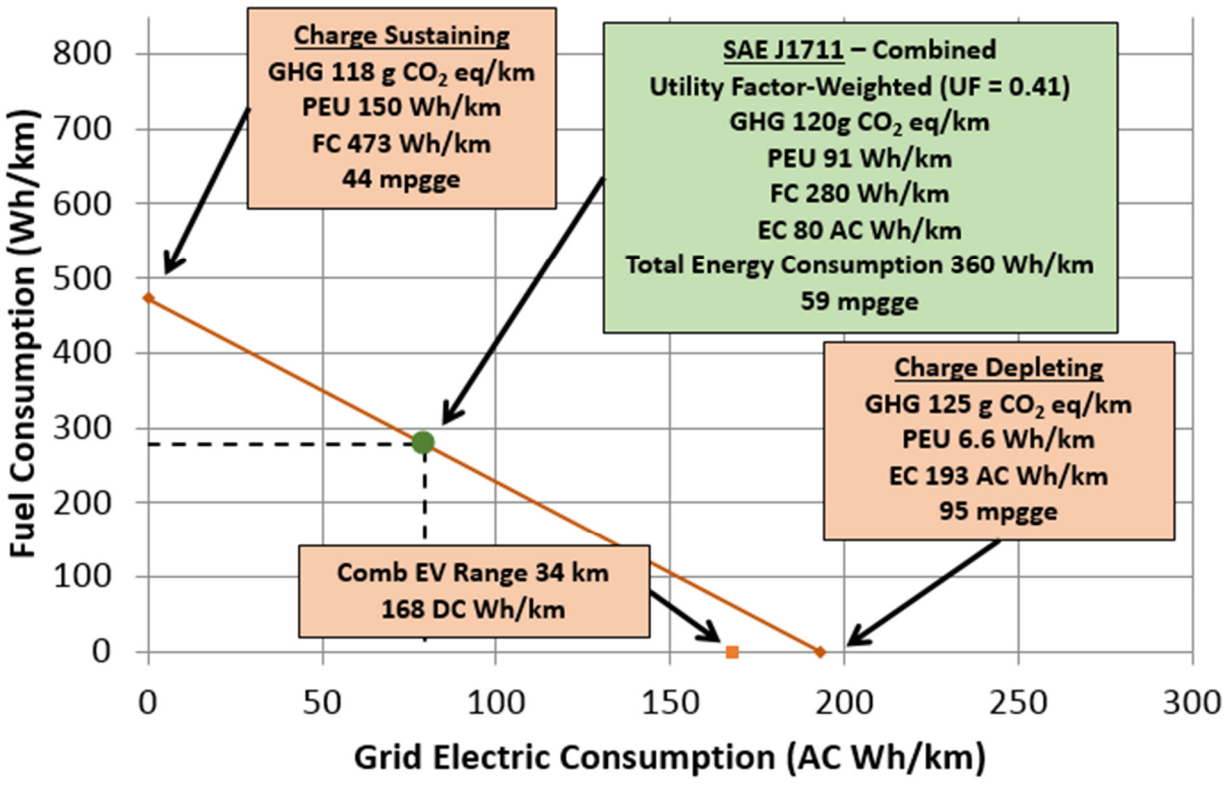

Figure 7-3: J1711 Plot of Improved Series Hybrid Vehicle

These results show that this Series HEV is able to just barely meet the total energy consumption goal and the WTW GHG goal. Since this does meet all design goals, it will be further discussed in Section 9.4 below.

8. INNOVATIVE TECHNOLOGIES TO REDUCE ENERGY CONSUMPTION

HEVT explored many options for reducing vehicle energy consumption. An overview of many possible technologies is provided by Ricardo, Inc. (2011). After a literature review of both existing and prototypical technologies, HEVT narrowed the search down to three: active noise control, turbocharging, and waste heat recovery with thermoelectric generators. The following sections are a discussion of these three technologies and their application.

8.1. Active Noise Control

Exhaust noise reduction is traditionally controlled by passive mufflers. The noise cancelation occurs in a chamber with two tubes that cause destructive interference. While effective for noise reduction, the chamber allows for the pressure to build up from the inlet to the outlet causing a decrease in engine efficiency.

Noise cancelation in an electronic muffler is generated by an acoustical source through a loudspeaker. The sound waves from the acoustical source are located at the end of the exhaust pipe and are directed towards the incoming sound waves using pressure to cause destructive interference (Huang et al., 2003). The electronic muffler does not require a chamber, thus eliminating the pressure build-up and increasing the engine efficiency.

An electronic muffler prototype has been designed and tested on a Fiat Marea SW 1900 JTD car at Perugia University Acoustic Laboratory, resulting in low frequency noise reduction and improvements in engine efficiency and fuel consumption. Data from the testing showed a 2% reduction in fuel consumption as well as an average of 9.5 dB decrease in noise when compared to performance with the stock muffler (Rossi, 2002). This data is similar to results released more recently. The German Company Eberspächer tested a 2.0 L four-cylinder gasoline engine, comparable in size to HEVT's own engine. They indicated a back pressure reduction of 8 kPa resulting in a 1.8% increase in engine power (Krüger et al., 2007). Efficiency would not be affected by a change in weight as the design would be similar in weight to the traditional muffler. Despite the potential reduction in fuel consumption, HEVT decided the improvement in fuel economy was too small to justify the complexity of the design.

8.2. Turbocharging

Turbochargers are used in the automotive industry to increase the output of an IC engine without the need to increase cylinder capacity. Traditionally, turbochargers were used to increase the potential of already powerful IC engines. Today, however, turbochargers allow manufacturers to adopt smaller, more efficient engines while maintaining performance. A turbocharged engine is more thermally efficient than a naturally aspirated one because it makes use of the heat and flow from the exhaust, energy that is normally wasted. Since the turbo makes use of waste exhaust heat, a greater amount of fuel is converted to useful work.

In a study affiliated with Honeywell International, Petitjean et al. (2004) compared fuel economy data of naturally aspirated gasoline engines to that of turbocharged gasoline

engines. The study found that the combination of turbocharging and engine downsizing of 30% could improve fuel economy by 8-10% (Petitjean et al., 2004). Without engine downsizing, improvements in fuel economy are minimal. The team decided that without engine downsizing, turbocharging alone would be insufficient in cutting fuel consumption.

8.3. Waste Heat Recovery

Waste heat recovery may prove vital in the ongoing search for increased engine efficiency. With most automobile engines operating at an average overall efficiency of about 25%, there is a great deal of lost energy. Much of this lost energy comes in the form of waste heat. Some of this heat is evacuated by coolant but about 40% of the fuel combustion energy is lost in exhaust heat. This leads to exhaust manifold temperatures of about 250 °C (Chuang and Chau, 2009). By recovering a fraction of this heat, overall fuel consumption can be decreased. This recovery may be achieved with thermoelectric (TE) generators.

The benefits of thermoelectric power generators are numerous. TE generators allow the accessory loads to be either reduced or eliminated from the drivetrain so that full power of the engine may be translated to the driveshaft. Furthermore, TE generators are extremely reliable due to their lack of moving parts. Recently, the European Union funded Power Driver Project has simulated a prototype which will produce 300 W. This prototype resulted in fuel savings of 2.5% over the NEDC drive cycle (Ricardo, 2013). An ***EcoCAR 3*** vehicle will likely need closer to 600 W of power to meet all accessory loads.

8.4. Modeling of the Potential for Conventional Vehicle Fuel Consumption Reduction

In a mathematical model of a TE generator from the Nissan Research Center, Nissan Motor Company estimated a maximum power density of about 1.2 kW/m^2 (Ikoma et al., 1998). For accessory loads of 600 W, this would mean a surface area of about 0.5 m^2 and a weight of approximately 91 kg. While this power density was calculated with a temperature difference of 396 °C during normal driving conditions, increased manifold temperatures could increase this temperature differential. Additionally, the cold side of the TE generator may be included in the coolant system of the vehicle leading to an even greater temperature differential. Maximizing this temperature differential would result in the smallest unit possible for the vehicle. This increased load on the coolant system would have little to no effect on its performance resulting in only a small modification without the need to enhance the existing system (Chuang et al., 2009). To model the effects of a thermoelectric generator on fuel consumption, the base case conventional vehicle was modeled without an accessory load met from engine fuel use. The results, shown in Table 8-1, show a decrease in combined fuel energy consumption of 7.1%. This case assumes that the thermo electric generator could fully eliminate the vehicle accessory load losses without any additional mass.

Table 8-1: Base Conventional Vehicle without Accessory Load

Test mass: 1500 kg Engine Size: 100 kW w/o Accessory Load	**Units**	**UDDS**	**HwFET**	**Combined**	**US06**
Net Tractive Energy	Wh/km	63.9	101	80.6	132
Fuel Economy	mpgge	30.0	44.2	36.4	25.3
Fuel Energy Consumption	Wh/km	691	469	591	820
WTW GHG	g CO_2 eq/km	222	151	190	264
Range	km	483	711	586	407
Propel $\eta_{powertrain}$	%	9.24	21.4	14.7	16.8
Average η_{engine}	%	18.9	26.6	22.3	24.6

This would be an ideal case but not a realistic one. A second case is run while iterating the vehicle mass. The goal is to figure out how much increase in mass will cause the vehicle to have the same combined fuel energy consumption as the base case conventional vehicle. This iteration resulted in a mass increase of 340 kg as shown in Table 8-2.

Table 8-2: Conventional Vehicle with Increased Mass to Replace Accessory Load

Test mass: 1840 kg Engine Size: 100 kW w/o Accessory Load	**Units**	**UDDS**	**HwFET**	**Combined**	**US06**
Net Tractive Energy	Wh/km	82.0	109	94.1	151
Fuel Economy	mpgge	27.8	41.5	33.9	22.0
Fuel Energy Consumption	Wh/km	749	500	637	942
WTW GHG	g CO_2 eq/km	243	161	206	303
Range	km	448	668	547	354
Propel $\eta_{powertrain}$	%	9.65	21.8	15.1	15.9
Average η_{engine}	%	20.5	27.4	23.6	27.5

This result means that any technology that would be able to supply enough power to meet the accessory load would be of no net benefit if it had a mass equal to or greater than 340 kg. Considering that the expected mass of a TE generator capable of 600 W is 91 kg, the energy consumption savings could be well worth it.

8.5. Conclusions for Fuel Consumption Reduction Technologies

Ultimately the team decided that waste heat recovery is the best option due to its proven effectiveness and relative simplicity of implementation. Active noise control simply isn't developed enough to provide sufficient energy recovery and be practical for HEVT's vehicle. Turbochargers offer enticing rewards but at the cost of complicated implementation, and depend on particular engine availability. Waste heat recovery provides a balance between practicality and performance. While TE generators do provide a decrease in energy consumption, there is still a long way to go to reach the energy consumption goal listed in Table 1-1.

9. PROPOSED POWERTRAIN DESIGN TO MEET *ECOCAR 3* DESIGN TARGETS

The advantage of a hybrid powertrain is clear from the series hybrid vehicle results, however the series configuration does generate significant electrical losses especially at high speeds due to the arrangement of the powertrain components. All mechanical energy from the engine must be converted to electrical energy to be used to propel the vehicle in a series hybrid. To give both the engine and the motor torque sources the ability to propel the vehicle, and also avoid the required conversion losses from mechanical to electrical, a parallel hybrid powertrain is proposed to meet the ***EcoCAR 3*** goals.

Figure 9-1 shows a basic layout of the parallel hybrid configuration. Only one electric motor is present and is used both to propel the vehicle as well as generate electric energy for the battery. The primary use of the electric motor is varied based on motor/battery sizing and the case being tested.

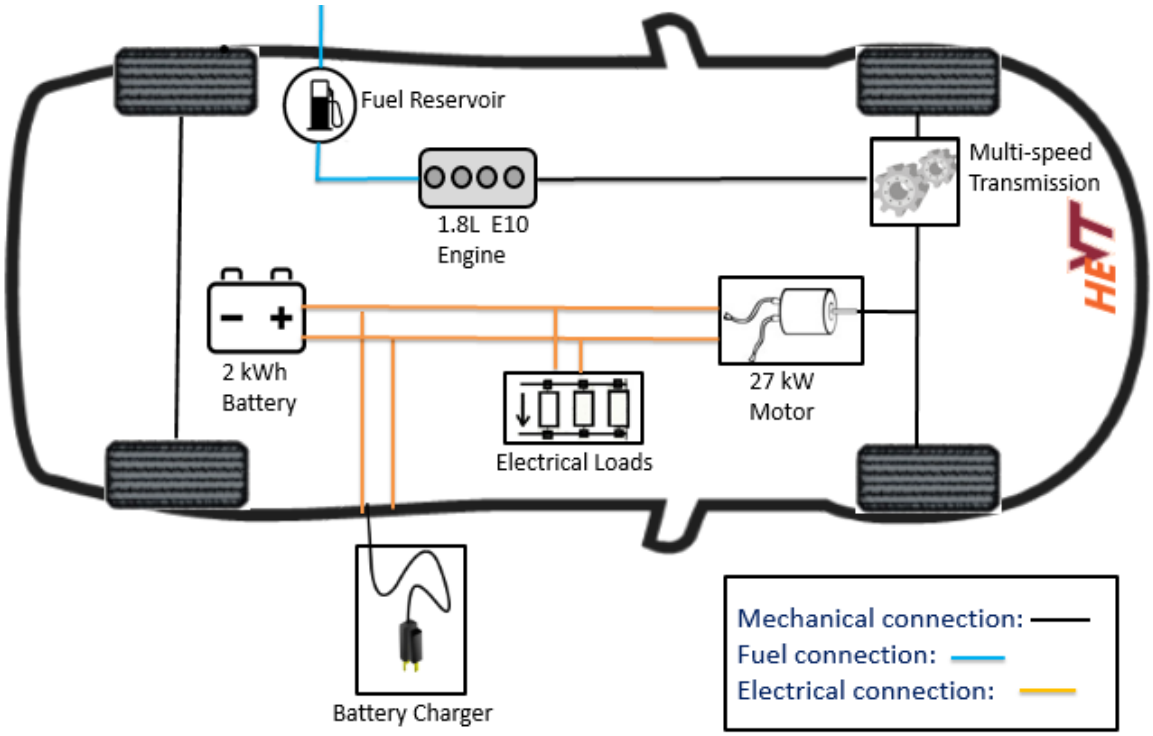

Figure 9-1: Parallel Hybrid Powertrain Configuration

In order to fully explore the ability of a parallel hybrid, several variations of different component sizing are used. Initially, a belted alternator starter (BAS) motor is directly coupled to the engine to allow for engine start-stop capability as well as minor torque assistance for the engine when required. The BAS motor also allows for some regenerative braking. Table 9-1 lists the powertrain sizing for three cases, including the BAS motor case.

Table 9-1: Parallel Hybrid Vehicle Powertrain Sizing

Test Mass	1520 kg	1550 kg	1692 kg
Top Speed	>85 mph		
0-60 mph Acceleration	7.95 s	7.92 s	5.2 s
Highway Gradeability @ 60 mph @ Test Mass	> 5%		
Powertrain Configuration	BAS, E85 Fuel	PTTR HEV, E85 Fuel	PTTR EREV, E85 Fuel
Powertrain Sizing:			
Engine Peak Power	100 kW	84 kW	84 kW
Engine Peak Efficiency	38.5%		
Multispeed Transmission Gearing – GM 6T30	Same as Table 5-2		
Motor Peak Power	16 kW	27 kW	100 kW
Motor Peak Torque	61 Nm	130 Nm	320 Nm
Single Speed Transmission Gearing	7.05:1 (N/V = 94 rpm/mph)		
Battery Energy Capacity	1.8 kWh	2.8 kWh	7.1 kWh
Battery Peak Power	18 kW	32 kW	114 kW
Battery Mass/ESS Mass	15/18 kg	27/32 kg	95/109 kg
Battery Usable Energy (95% - 10% SOC)	1.4 kWh	2.2 kWh	5.7 kWh
Regenerative Brake Fraction	85%		
Accessory Load	600 W		

9.1. Case 1 – BAS Parallel, E85 Fuel

The BAS motor is sized in order to reach a 0-60 performance time of 8 seconds. From previous conventional results, a 116 kW engine is used to reach this performance goal. A 100 kW engine plus a 16 kW motor yields similar performance values of the 116 kW engine without having the less efficient results of the large engine. The battery is sized to accommodate the BAS motor and allow for some electrical assistance as well as regenerative braking. The motor and the battery yield a net increase in mass of 20 kg from the base conventional vehicle. Table 9-2 shows the drive cycle energy results for the BAS motor parallel hybrid.

Comparing the results to the 100 kW conventional vehicle (Table 5-5) some improvement is shown. This is due to the limited ability of a small electric motor. While it provides the ability for engine start/stop and some regenerative braking, the engine operation is not dramatically altered and still operates primarily in inefficient regions and yields somewhat similar results.

Table 9-2: Case 1 Parallel Hybrid Vehicle Drive Cycle Energy Consumption Results

Test mass: 1520 kg Engine Size: 100 kW Motor Size: 16 kW	**Units**	**UDDS**	**HwFET**	**Combined**	**US06**
Net Tractive Energy	Wh/km	64.4	101	81	132
Fuel Energy Consumption	Wh/km	731	456	607	747
Net Battery Energy	DC Wh/km	-1.3	2.6	0.5	-2.2
WTW GHG	g CO_2 eq/km	191	119	159	195
Range	km	457	731	580	447
Road load $\eta_{powertrain}$	%	16.6	24.7	20.2	24.9
Average η_{engine}	%	21.3	31.6	25.9	30.0

Figure 9-2 shows the engine operation points for a UDDS cycle using the case 1 PTTR configuration. The engine operation rarely operates along the BSFC, which as discussed previously, is the desired operation point for the engine. To improve the engine operation, the motor size must be further increased.

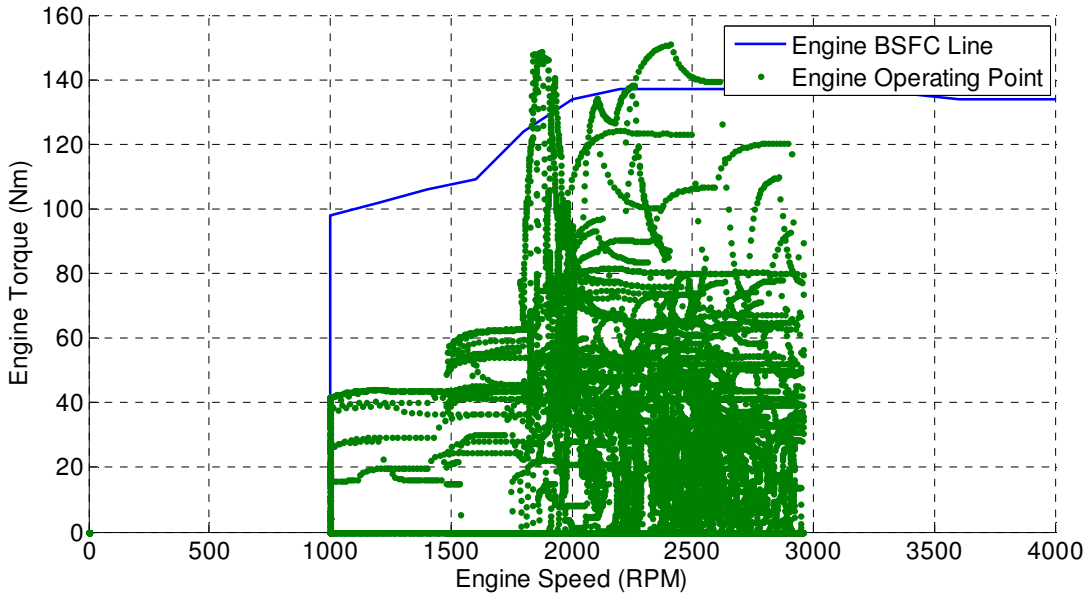

Figure 9-2: UDDS Engine Operating Points, PTTR Case 1 (BAS)

9.2. Case 2 – Parallel through the Road, E85 Fuel

To improve the performance of the parallel configuration, the motor and battery size is increased to allow for more use of the electric machine to propel the vehicle, maintain performance with a downsized engine, as well as more advanced system controls to load the engine to a higher efficiency region. To improve engine efficiency, the downsized 84 kW engine with E85 fuel is used with a peak efficiency of 38.5%. Using this engine, the minimum brake specific fuel consumption (BSFC) line is drawn to characterize engine operation. A description of this operation is in Section 3.8.

With the engine primarily operating along the minimum BSFC line, the overall efficiency of the vehicle increases. To meet the same 0-60 performance goal of 8 seconds with a smaller engine, a larger electric motor is needed than in the previous case. A 27 kW motor is sized to assist the engine in reaching an 8 second performance goal, as well as a larger battery to accommodate a larger motor, and capture significant regenerative brake energy on the UDDS. With both the motor and engine coupled to the wheels, the vehicle is modeled as a parallel through the road hybrid. This configuration keeps the electrical and mechanical components separated on their own individual axle, while the mechanical connection between them is the road. Table 9-1 includes the powertrain specifications for the second case parallel.

Though operating the engine along the minimum BSFC line does increase the engine efficiency, this will not always meet driver demand. Because of the power limit of the motor, the engine will also resume normal operation, if needed, along with electric assist to meet driver demand. Table 9-3 shows the drive cycle results for the case 2 parallel hybrid vehicle.

Table 9-3: Case 2 Parallel Hybrid Vehicle Drive Cycle Energy Consumption Results

Test mass: 1550 kg Engine Size: 84 kW Motor Size: 27 kW	**Units**	**UDDS**	**HwFET**	**Combined**	**US06**
Net Tractive Energy	Wh/km	65.2	102	81.8	133
Fuel Energy Consumption	Wh/km	409	401	405	618
Net Battery Energy	DC Wh/km	-1.6	-0.5	-1.1	1.4
WTW GHG	g CO_2 eq/km	107	105	106	161
Range	km	815	833	823	541
Road load $\eta_{powertrain}$	%	31.7	34.1	32.8	31.6
Average η_{engine}	%	36.7	37.9	37.2	32.3

Case 2 shows significant improvement in powertrain efficiency because the engine is operating at its highest efficiency for some portions of the drive cycles. However, because the electric motor is still relatively small, it cannot meet all of the driver demand itself and the engine is needed to assist the motor to meet driver demand. The lack of power from the motor sometimes causes the engine to operate away from the minimum BSFC line, decreasing engine efficiency. Figure 9-3 shows hill 2 of the UDDS cycle for PTTR case 2. In the case shown, the SOC state is high, therefore if the motor was larger and could meet the driver demand alone, the engine would not need to be turned on. Instead, Figure 9-3 shows the engine being used to propel the vehicle along with the electric motor. The operation of the engine in this case is not along the BSFC for some portions.

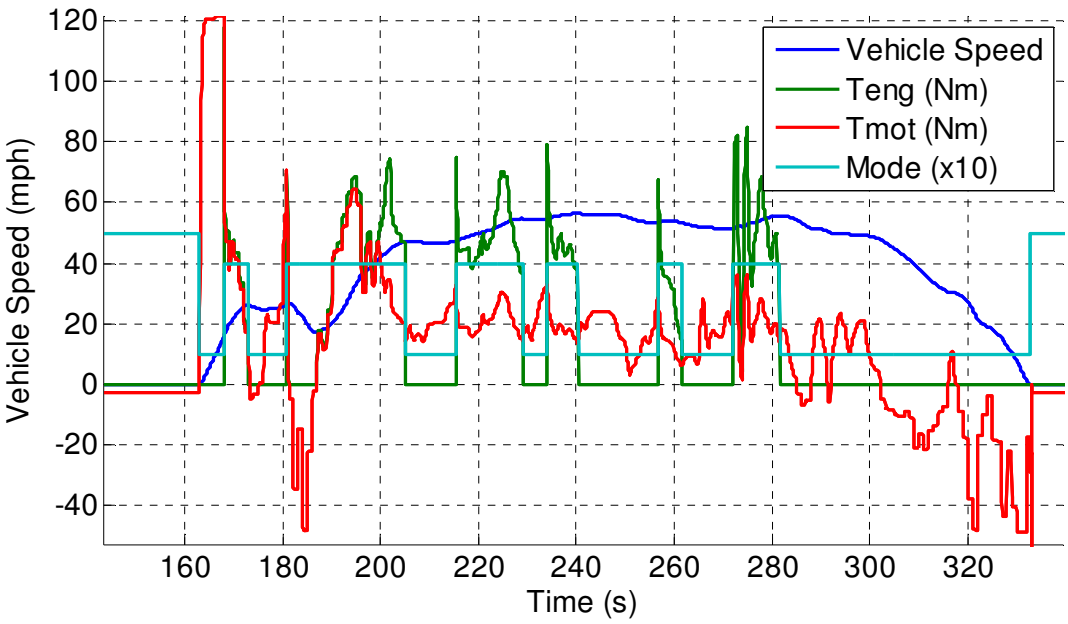

Figure 9-3: UDDS Hill 2, SOC High, PTTR Case 2 Torque Split

Figure 9-4 shows the operating points of the engine for the UDDS cycle relative to the desired BSFC operating line. Once again, the example case is run in an SOC high state. Because the motor cannot produce the torque required to meet the driver demand, the engine is used to assist the motor in propelling the vehicle. The engine operation when it is assisting the motor (mode 4) is determined by the leftover driver demand that the motor cannot handle. Because of this, the engine operates at a low torque in assisting the motor when battery SOC is high. Figure 9-4 shows the engine does not always along the BSFC line, but also spends a significant amount of time operating based on assisting driver demand.

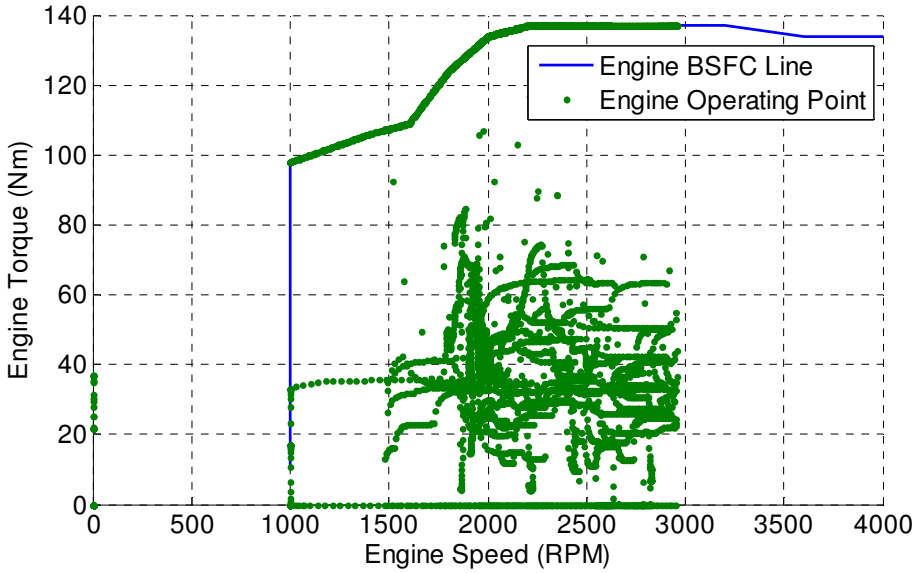

Figure 9-4: UDDS Engine Operating Points, SOC High, PTTR Case 2

Case 2 does make improvements over case 1 in that it is able to operate the engine more efficiently at some points, while case 1 has to use the engine alone to meet driver demand, and will not operate the engine efficiently.

The improvements are clear in comparing Figure 9-2 to 9-4 where Figure 9-2 does not operate with any regard to efficiency, while Figure 9-4 is able to operate efficiently at some points. Table 9-4 compares the component losses for cases 1 and 2.

Table 9-4: Case 1 & 2 Component Losses

UDDS Losses	Case 1	Case 2
Engine Loss (kJ)	17701	16021
Motor Loss (kJ)	57	846
Battery Loss (kJ)	27	191

The engine in case 2 produces significantly less losses than in case 1. The electric components do produce more losses because they are used more in case 2, but the fuel energy saved by operating the engine more efficiently compensates more than enough to make up for the increased motor and battery losses.

9.3. Case 3 – PTTR Plug-In, E85 Fuel

To further improve the parallel design, the same engine is kept to meet the continuous grade requirement, however the motor and battery power are increased. To allow an electric-only charge depleting mode and compare the improved Series HEV to the parallel HEV, the same motor and battery power are used for this case. Sizing the battery and motor *power* for EV mode results in enough battery *energy* to enable a charge depleting range. The series generator is replaced with a 6 speed transmission for parallel mode, and

the test mass is the same at 1692 kg. With a large motor and battery, all drive cycle demand can be met by the motor, and the engine is only used in charge sustaining mode.

9.3.1. Charge Sustaining Operation

Table 9-1 also lists the powertrain component sizing for the case 3 parallel HEV. The charge sustaining drive cycle results are shown in Table 9-5. The charge sustaining results are similar to that of case 2 with a slight improvement due to the higher engine operating efficiency. The higher engine operating efficiency also is significantly higher than that of the case 2 series HEV. The primary advantage of the EREV versus the case 2 parallel HEV is that it now has approximately 34 km (21 mi) combined charge depleting range before entering charge sustaining mode, and can efficiently use stored grid electric energy. Figure 9-5 shows the SOC of case 3 on a constant 60 mph cruise cycle to demonstrate the CD and CS operation. In Figure 9-5, the initial battery SOC is set to 95% (0.95). For the first portion of the run, the vehicle operates all electrically in CD range. When the SOC reaches the bottom limit of the target SOC, charge sustaining takes over. From here, the SOC is maintained in a window around the target SOC.

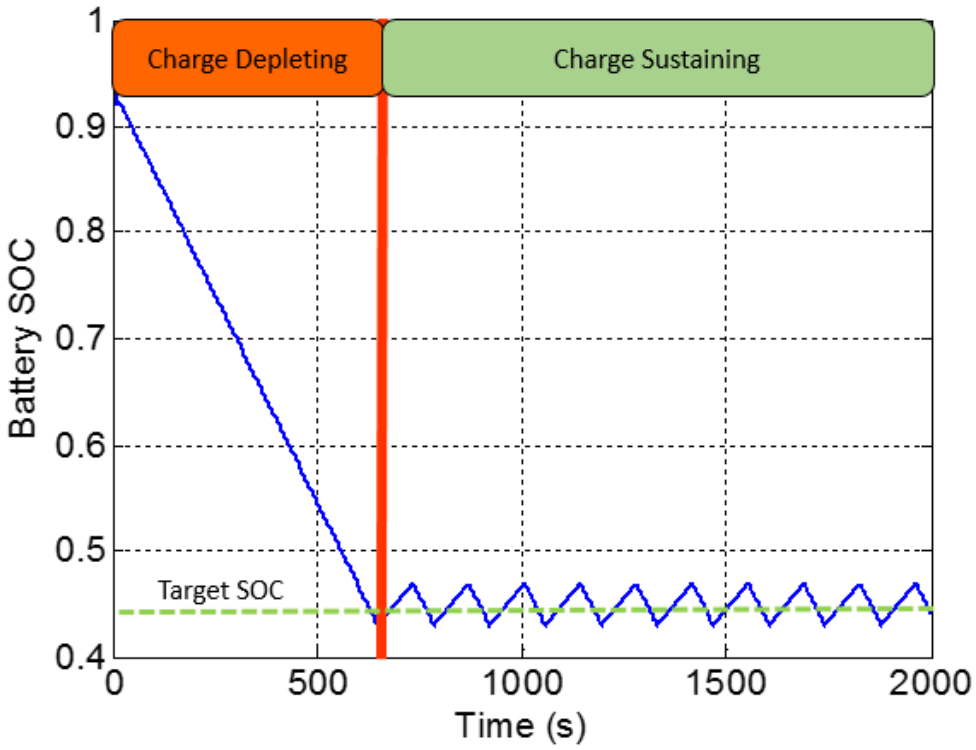

Figure 9-5: CD and CS operation of a Plug-In Hybrid

Table 9-5: Case 3 Parallel Hybrid Vehicle Drive Cycle CS Energy Consumption Results

Test mass: 1692 kg Engine Size: 84 kW Motor Size: 100 kW	**Units**	**UDDS**	**HwFET**	**Combined**	**US06**
Net Tractive Energy	Wh/km	68.8	106	85.5	137
Fuel Energy Consumption	Wh/km	396	391	394	571
Net Battery Energy	DC Wh/km	2.2	1.5	1.9	-0.4
WTW GHG	g CO_2 eq/km	103	102	103	149
Range	km	842	854	847	541
Road load $\eta_{powertrain}$	%	33.3	34.5	33.8	34.8
Average η_{engine}	%	37.9	38.2	38.0	38.4

Table 9-5 shows charge sustaining advantages over case 2 because of the improved capability of the electric motor. Because case 3 now has a charge depleting mode, the charge sustaining operation must be compared to case 2, while keeping in mind the advantage of having an all-electric range as well. Figure 9-6 shows the CS operation of case 3 for UDDS Hill 2. Because of the enlarged motor, the vehicle can operate in low demand mode for the entire UDDS cycle. As seen in Figure 9-5, the engine and motor are both loaded beyond the requirement to meet the drive cycle in order to run the engine at an efficient point and use the motor to load the engine and maintain battery SOC. The engine is shut off at some points in the figure because of the strategy discussed in Section 3.8. Once the SOC reaches the upper limit of the SOC window, the engine is shut off until the lower limit of the SOC window is reached. Although there is no fuel penalty for engine start-stops implemented in the model, the amount of energy saved by having the engine off intermittently is advantageous for energy consumption because of the general poor efficiency of engines.

Figure 9-7 shows the engine operating points for case 3 on a UDDS drive cycle. As stated before, a high demand state is not required because the larger motor size and capability. This allows the engine to either operate completely along the BSFC line, or be turned off. The efficiency improvement can be seen in comparing the results tables for case 2 and 3 (Tables 9-3 and 9-5). In addition to a more efficient CS mode, case 3 also has the advantage of a CD mode.

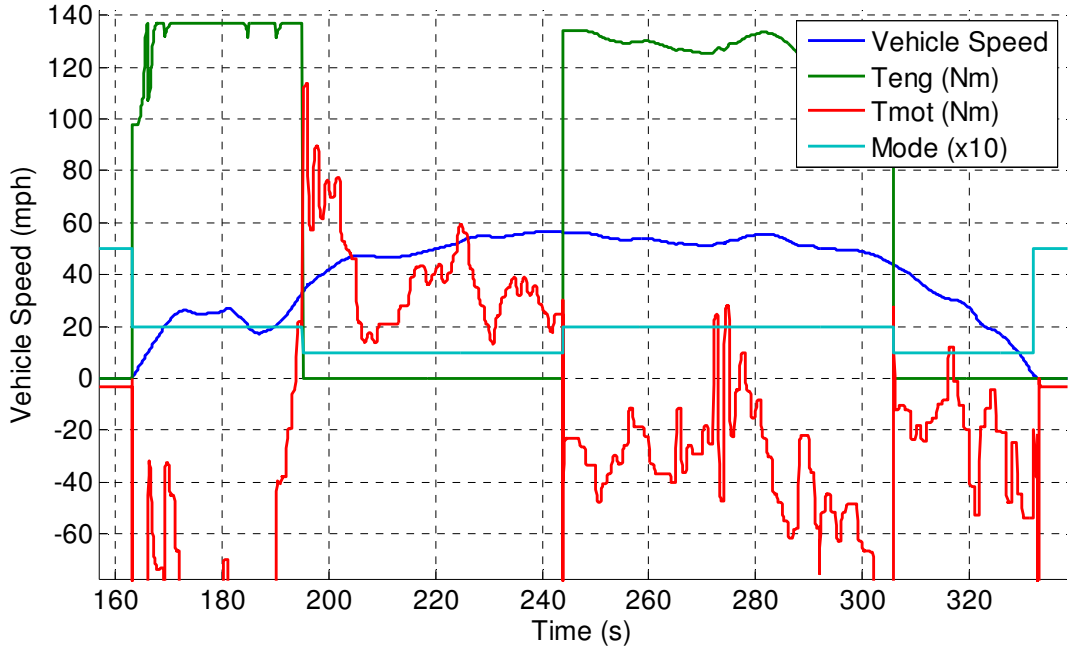

Figure 9-6: UDDS Hill 2, PTTR Plug-In CS Torque Split

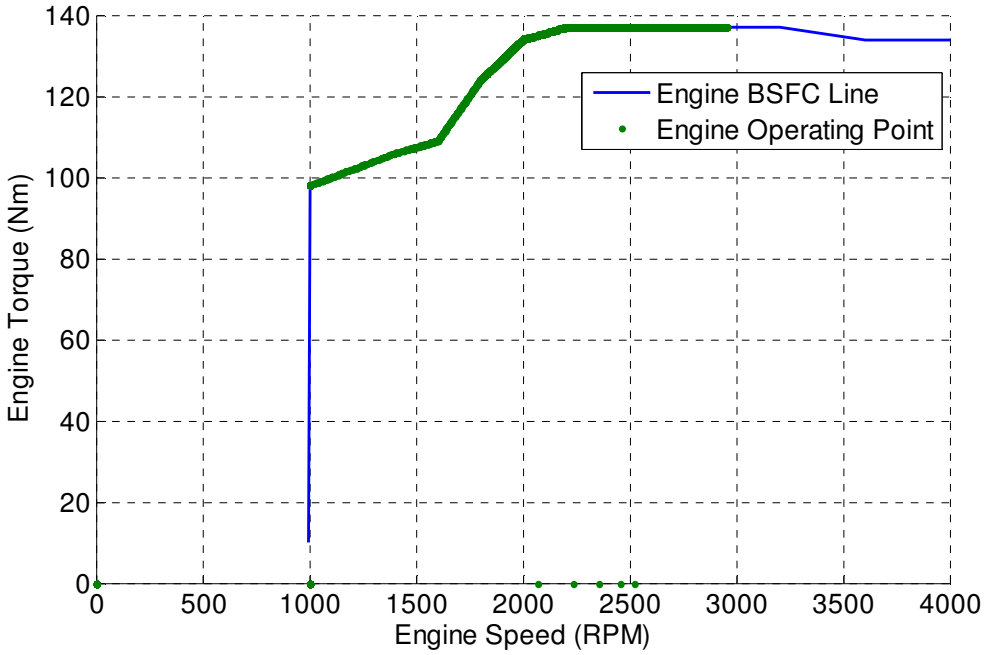

Figure 9-7: UDDS Engine Operating Points, PTTR Case 3 CS

9.3.2. Charge Depleting Operation

As discussed for the series hybrid case, an added benefit of this case is the addition of a Charge Depleting mode. Note that the results in Table 9-6 are very similar to the series hybrid charge depleting results because of the similar test mass and electric drivetrain.

Table 9-6: Case 3 Parallel Hybrid Vehicle Drive Cycle CD Energy Consumption Results

Test mass: 1692 kg Engine Size: 84 kW Motor Size: 100 kW	**Units**	**UDDS**	**HwFET**	**Combined**	**US06**
CD Net Battery Energy	DC Wh/km	165	179	171	246
CD AC Electrical Energy Cons.	Wh/km	191	206	198	284
CD Range	km	35.7	33.5	34.7	24.5

9.3.3. Utility Factor Weighting

Using equation 5-1 and the charge depleting range from Table 9-6, the utility factor for the case 3 parallel EREV is 0.41. Note that the values here are very similar to the improved series HEV case (Table 7-5) because the vehicle test mass and electric powertrain are identical. Other utility factor values are included in Table 9-7. These results show that this parallel HEV is able to meet the both the total energy consumption goal and the WTW GHG goal.

Table 9-7: Case 3 Parallel Hybrid Vehicle UF Weighted Energy Consumption Results

Parameter	**Value**
CD Range	34.7 km
Utility Factor	0.41
UF Weighted Fuel Consumption	230 Wh/km
UF Weighted Grid Electrical Energy Consumption	83 AC Wh/km
UF Weighted Total Energy Consumption	313 Wh/km
UF Weighted WTW GHG	114 g CO_2 eq/km

These values are more easily viewed and illustrated using a J1711 plot as in Figure 9-8. This plot compares Fuel Consumption and Electric Consumption of different operating modes of a hybrid electric vehicle. The charge depleting operating point lies along the x-axis because there is no fuel use during charge depleting operation. Similarly, since charge sustaining results are charge balanced, the net electric consumption is minimal. Additionally, as discussed in the series hybrid utility factor discussion, the utility factor describes how a fleet's energy consumption can tend towards the charge sustaining or charge depleting values. A UF of 1 would be a completely battery electric vehicle and a UF of zero would be a non-plug-in hybrid powertrain

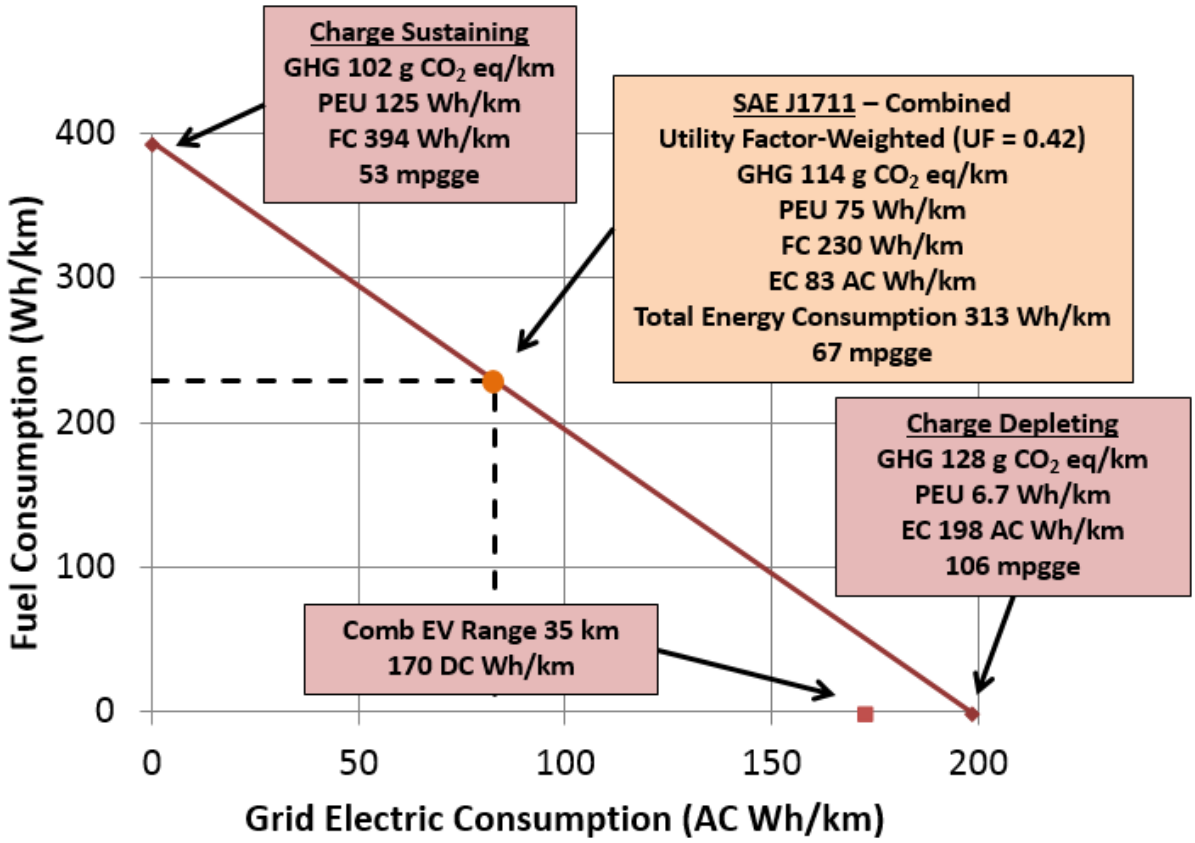

Figure 9-8: J1711 Plot of Case 3 Parallel Hybrid Vehicle

Ultimately, these results help to show that the parallel hybrid vehicle with parameters denoted in Table 9-1 has the ability to meet all of the design goals and is the powertrain in the proposed powertrain.

9.4. Case 4 – Improved Series HEV Plug-In, E85 Fuel

As described in Section 7.2 above and shown in Table 9-9, the improved Series HEV is able to meet all of the design targets given with the utility factor weighted values and thus is used as one of the three cases considered to be built for EcoCAR 3. As discussed earlier, this design is a large benefit over the BEV since range is achieved while maintaining a reasonable mass. Cost is also an important consideration. This vehicle will be more expensive than a conventional vehicle with the addition of the battery pack and two electric machines, however the increased efficiency along with consumer acceptability balances that tradeoff with the added CD mode and efficient CS mode. Unfortunately, the motors in a Series HEV cannot be scaled down to reduce cost since the power is required to meet acceleration and gradeability goals, but again, tradeoffs must be made to meet targets. As documented previously, the CS performance for the series is also not as beneficial as the PTTR CS performance. Although the improved series case does have higher efficiency than a conventional vehicle, it generates higher losses than the PTTR case. Table 9-8 documents the motor, generator, and battery losses for case 3 and 4.

Table 9-8: Component Loss Comparison for Case 3 & 4 HwFET Cycle

	Series HEV (Case 4)	PTTR HEV (Case 3)
Motor Loss (kJ)	1642	752
Generator Loss (kJ)	898	0
Battery Loss (kJ)	224	211
Total Electrical Loss (kJ)	2764	963

Table 9-8 shows higher losses for case 4 than case 3. The higher motor loss is as expected because, as discussed earlier, the motor must be used to drive the vehicle at all times for the series. The engine has no direct method of transferring power to the wheels, therefore the motor will be have higher losses because of the energy conversion. The generator also has significant losses compared to the PTTR where no generator is present. The engine losses are not listed because both series and parallel are able to run the engine at a high efficiency and generate comparable results.

Figures 9-9 shows the highway fuel economy test (HwFET) drive cycle. The primary reason PTTR has advantages over series is operating constantly at high speeds. While both operate similarly in a city cycle, the ability for the engine power to be directly coupled to the wheels shows the PTTR is superior at higher sustained speeds.

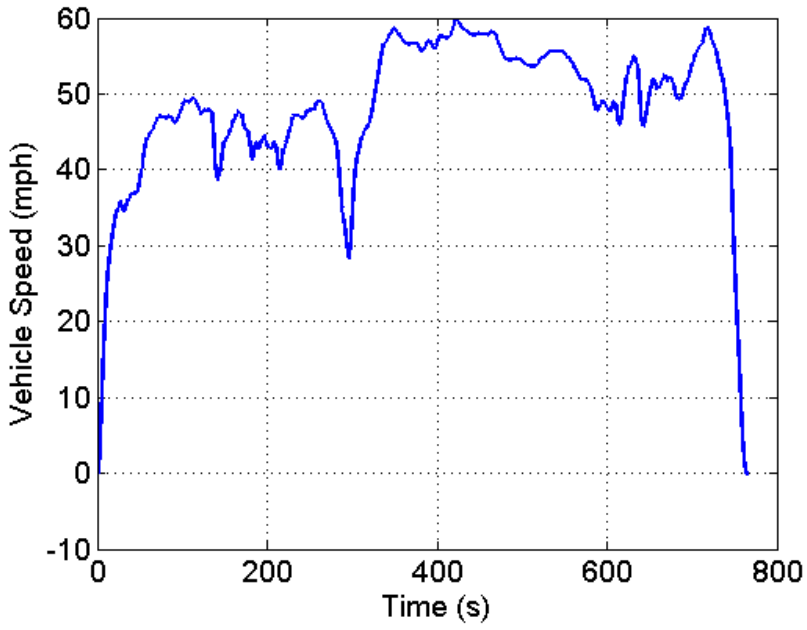

Figure 9-9: HwFET Drive Cycle

9.5. Case 5 – PTTR Plug-In, B20 Fuel

One more powertrain is proposed to meet the design targets. This case is identical to Case 3 (described in Table 9-1) with the exception of the engine and fuel selection. Since the

effects of B20 have already been studied in Section 3 and diesel engines operate at a higher efficiency than E10 and E85 engines, this higher engine efficiency proves to be very useful in reducing the total energy consumption of the vehicle, especially in the stronger hybrid configurations where the engine load can be controlled and results in high engine and powertrain efficiency. Table 9-3 and Table 9-5 show that the average η_{engine} is very close to the maximum engine efficiency for those cases. Although B20 has a slightly higher WTW GHG contribution, the increased powertrain efficiency reduces CS fuel consumption and keeps the GHG emission below the target for the utility factor weighted results (shown in Table 9-9). Unfortunately, due to the complex exhaust after-treatment systems, the noise, vibration, and harshness issues that are associated with diesel engines, and VT's lack of experience with diesel systems, this is not the powertrain of choice. Cost will be discussed further in the next section since this powertrain is quite similar to the chosen case.

9.6. Chosen Powertrain

Based on the discussion in previous sections, the team's chosen powertrain which meets all of the design targets is the PTTR PHEV with E85 fuel as detailed in Section 9.3. The Series powertrain was not chosen due to the better fuel consumption and GHG values of the PTTR, and using B20 fuel was discounted because of factors related to team experience. Exhaust emissions for the E85 engine have been considered through engine sizing and loading. Table 9-9 details how this powertrain compares to the design targets. The E85 PTTR PHEV modeled here can meet or exceed all categories with its utility factor weighted results. The only category of concern is luggage capacity. Since mechanical packaging is not addressed in this problem and this category is fully dependent on final component selection and packaging, it is unrealistic to estimate a value now. However, through the team's history in AVTC competitions, luggage capacity has always been achievable by using a portion of the trunk to house the ESS and to leave the remainder of the trunk as consumable space which could house luggage.

Table 9-9: Powertrain Comparisons to Design Targets

Category	Units	Target	E85 PTTR PHEV	B20 PTTR PHEV	E85 Series PHEV
Energy Consumption	Wh/km	< 370	313	297	360
WTW GHG emissions	CO_2 eq/km	< 120	114	115	120
Passenger Capacity	--	4	4		
Luggage Capacity	ft^3	> 8	*Dependent on packaging		
Range	km	> 320	880	1050	530
Top Speed	kph	> 135	> 135		
0-60 mph Accel Time	s	< 11	5.2	5.5	8.9
Gradeability [GVWR]	%	> 3.5	> 5		

Mass considerations have been discussed throughout the study, beginning with a conventional vehicle mass of 1500 kg and adding mass considerations for an ESS and a drive motor. One of the advantages of a parallel powertrain is the flexibility of the placement of the electric powertrain relative to the IC engine/transmission drivetrain. This allows some of the trunk space to house the ESS if needed. Features usually appealing to consumers include the drive quality and acceleration of a vehicle. With an electric drive mode, the drive quality can be improved and the acceleration performance is very attractive as it uses two propulsion sources.

Although the cost of this chosen powertrain would be greater than a conventional vehicle, the benefits, as in the Series case, greatly outweigh the negatives. The added benefit of this PTTR setup is that unlike for the Series case, the motor and battery can be scaled down for cost considerations. This obviously affects the fuel consumption and GHG emission values, as well as some of the other targets, but since both torque sources reach the wheels, both can be used to achieve the driver demand. Thus cost vs performance is able to be balanced to some degree for added benefits in both areas. While the additional powertrain components may cause a marked up price for the vehicle itself, the fuel cost savings would be large (it consumes 64% less fuel than the base conventional vehicle).

10. SUMMARY & CONCLUSIONS

This paper has demonstrated the use of model-based design in the powertrain selection phase of vehicle development. By developing both power loss and torque-speed models, the models themselves are validated and display the tradeoffs between model fidelity and user understanding. While the torque-speed models are preferred for use because of their ability to be configured, the power loss models do provide semi-accurate results. By developing component models in MATLAB/Simulink, several powertrain configurations are able to be explored. The main interest is in the hybrid powertrains where more advanced work is required. The development of different series control strategies once again displayed the usefulness of simple, yet effective models. The thermostatic strategy is extremely simplified, but provided nearly identical results to the more advanced load-following model. The parallel powertrain requires a more advanced control strategy for torque security and to ensure efficient use of the engine along with a shift strategy. Once the models are fully developed, they are applied to meet goals proposed by the ***EcoCAR 3*** competition.

The conventional vehicle models provide baseline results and allow for analysis of areas of improvement such as idle engine stop and decel fuel cutoff. Experimentation with conventional fuels showed that B20 offers energy consumption and WTW GHG emissions improvements over E10 due to higher peak engine efficiencies but still does not meet design targets. Battery electric powertrains, when compared to conventional vehicles, help to set bounds for the abilities of the hybrid powertrains that are modeled. When developing the series hybrid model, many components from previous models (i.e. engine from conventional vehicle, battery and drive motor from BEV) are used to increase overall vehicle efficiency and the improved case is able to meet all design targets. Lastly, a parallel powertrain is modeled and three powertrains are deemed viable to meet the design targets:

- Parallel through the Road Plug-In Hybrid Electric Vehicle using E85 and grid electricity
- Parallel through the Road Plug-In Hybrid Electric Vehicle using B20 and grid electricity
- Improved Series Plug-In HEV using E85 and grid electricity

Of these powertrains, the E85 PTTR PHEV powertrain is chosen as the potential powertrain to build during the competition because of its simplicity and the school's experience with the powertrain in previous competitions. The components required for this powertrain are very feasible in a competition setting, and the driveability can be refined using the hybrid vehicle supervisory controls. Diesel powertrains are ruled out due to complex exhaust after-treatment systems, the noise, vibration, and harshness issues that are associated with diesel engines, lack of experience with diesel systems as well as emissions test facilities.

Future work that could build off of what is done in this thesis is to further develop the control strategy in the parallel model. Currently the gear shifting strategy is built off of speed and not driver demand. A more advanced shift strategy could improve the model fidelity, providing more accurate results. Another area of improvement could be with the

power threshold parameter in the parallel strategy. This parameter is just a set constant obtained by a short study to examine what was ideal for each drive cycle. Generating an alternative solution to determining high and low demand states would improve the model strategy. The component models presented could also be used to construct further more advanced powertrains, such as a series-parallel model where the advantages of series and parallel hybrids are applied in the proper situations. This would once again involve developing a more advanced control strategy for the models.

REFERENCES

Alley, R. Jesse, Douglas J. Nelson, Eli White, P. Christopher Manning (2013), "VTool: A Method for Predicting and Understanding the Energy Flow and Losses in Advanced Vehicle Powertrains", SAE paper 2013-01-0543, *SAE 2013 International World Congress*, April 16-18, Detroit, MI.

Alley, R. Jesse, Jonathan King, Douglas J. Nelson, and Eli White, (2012), "Hybrid Architecture Selection and Component Sizing to Reduce Emissions and Petroleum Energy Consumption", SAE Paper 2012-01-1195, *SAE 2012 International World Congress*, April 24-26, Detroit, MI.

Burke, Andrew F. (2007), "Batteries and Ultracapacitors for Electric, Hybrid, and Fuel Cell Vehicles", *IEEE Proceedings - Special Issue on Electric, Hybrid & Fuel Cell Vehicles*, Vol 95, No.4, April 2007, pp. 806-820.

EcoCAR 2: Plugging In To The Future, http://www.ecocar2.org/.

Ehsani, M., Gao, Y., and Emadi, A. (2010), "Modern Electric, Hybrid Electric, and Fuel Cell Vehicles: Fundamentals, Theory, and Design", Second Edition, Wiley.

EPA Test Car List Data (2013), http://www.epa.gov/otaq/tcldata.htm.

GREET (Greenhouse Gases, Regulated Emissions, and Energy Use in Transportation) Model (2013), http://greet.es.anl.gov/.

Hsiao, Y.Y. Chang, and W.C. Chen, S.L. (2010), "A mathematic model of thermoelectric module with applications on waste heat recovery from automobile engine", *Energy*, Volume 35, Issue 3, March 2010, pp. 1447-1454.

Hwang, Yoha, Lee, John Min, and Kim, Seung-Jong (2003), "New active muffler system utilizing destructive interference by difference of transmission paths", *Journal of Sound and Vibrati*on, Volume 262, Issue 1, 17 April 2003, pp. 175-186.

Ikoma, K., Munekiyo, M., Furuya, K., Kobayashi, M., Izumi, T., and Shinohara, K. (1998), "Thermoelectric module and generator for gasoline engine vehicles", *Proceedings XVII International Conference on Thermoelectrics*, 1998, pp. 464-467, 24-28 May 1998.

King, Jonathan and Douglas J. Nelson (2013), "Model-Based Design of a Plug-In Hybrid Electric Vehicle Control Strategy", SAE Paper 2013-01-1753, *SAE 2013 International World Congress*, April 16-18, Detroit, MI.

King, C. John, (2012), "Model-Based Design of a Plug-In Hybrid Electric Vehicle Control Strategy", MS Thesis in Mechanical Engineering, Virginia Tech, Blacksburg, VA.

Krüger, J., Castor, F., and Jebasinski, R. (2007), "Active Exhaust Silencers - Current Perspectives and Challenges" SAE Technical Paper 2007-01-2204.

Lai, Jih-Sheng (Jason), and Douglas J. Nelson (2007), “Energy Management Power Converters in Hybrid Electric and Fuel Cell Vehicles”, *IEEE Proceedings - Special Issue on Electric, Hybrid & Fuel Cell Vehicles*, Vol 95, No.4, April 2007, pp. 766-777.

Mahapatra, Saurabh, Tom Egel, Raahul Hassan, Rohit Shenoy, and Michael Carone, (2008), “Model-Based Design for Hybrid Electric Vehicle Systems”, SAE Paper 2008-01-0085, SAE .

Manning, P. Christopher, Eli White, R. Jesse Alley, Jonathan King, Douglas J. Nelson (2012), "Vehicle System Design Process for a Series-Parallel Plug-in Hybrid Electric Vehicle*", SAE International Journal of Alternative Powertrains*, 1(2):503-524, Dec. 2012, doi:10.4271/2012-01-1774.

Manning, P. Christopher, Eli White, Douglas J. Nelson (2013), "Development of a Plug-In Hybrid Electric Vehicle Control Strategy Employing Software-In-the-Loop Techniques", SAE paper 2013-01-0160, *SAE 2013 International World Congress*, April 16-18, Detroit, MI.

Marco, J., and E. Cacciatori, (2007), “The Use of Model Based Design Techniques in the Design of Hybrid Electric Vehicles”, 2007 3rd Institution of Engineering and Technology Conference on Automotive Electronics, June 28-29, Warwick, UK.

Nam, E. and Sorab, J. (2004), *"*Friction Reduction Trends in Modern Engines*,* SAE Paper 2004-01-1456, 2004, doi:10.4271/2004-01-1456.

National Training and Education Resource (NTER): Model Based Design Curriculum, https://nwtp.sri.com/

Ord, David, Eli White, Peter Manning, Abhijit Khare, Lucas Shoults, Douglas Nelson (2014), "Powertrain Design to Meet Performance and Energy Consumption Goals for EcoCAR 3", SAE paper 1024-01-1915, *SAE 2014 International World Congress*, April 8-10, Detroit, MI.

Petitjean, D., Bernardini, L., Middlemass, C., and Shahed, S. (2004), "Advanced Gasoline Engine Turbocharging Technology for Fuel Economy Improvements" SAE Technical Paper 2004-01-0988.

Pisu, P., and Rizzoni, G.(2007) , *“*A Comparative Study of Supervisory Control Strategies for Hybrid Electric Vehicles*”*, *IEEE Transactions on Control System Technology*, Vol. 15, No. 3, May 2007.

Ricardo, Inc. (2013), “PowerDriver Passes Key Milestones towards Fuel Saving through Waste Heat Recovery”, Ricardo.com, 21 Aug. 2013.

Ricardo, Inc. (2011), “Computer Simulation of Light-Duty Vehicle Technologies for Greenhouse Gas Emission Reduction in the 2020-2025 Timeframe”, EPA Report 420_R_11-020.

Rossi, Frederico (2002), “Active Noise Control Technique To Improve Engine Efficiency”, Proceedings of Energy and Environment, 2002, Italy.

SAE J1711 (2010), Recommended Practice for Measuring the Exhaust Emissions and Fuel Economy of Hybrid-Electric Vehicles, Including Plug-in Hybrid Vehicles.

SAE J2841 (2010), Utility Factor Definitions for Plug-In Hybrid Electric Vehicles Using Travel Survey Data.

Simpson, G. Andrew and Geoffrey R. Walker, (2003), "A Parametric Analysis Technique for Design of Fuel Cell and Hybrid-Electric Vehicles", SAE Paper 2003-01-2300, SAE.

Wang, Qing, Wei Liang, Mind Kuang, and Ryan McGee, Ford Motor Company, (2011), "Vehicle System Controls for a Series Hybrid Powertrain", SAE Paper 2011-01-0860, SAE.

White, H. Eli (2014), "An Illustrative Look at Energy Flow Through Hybrid Powertrains for Design and Analysis", MS Thesis in Mechanical Engineering, Virginia Tech, Blacksburg, VA.

Yu, Chuang, and K.T. Chau (2009), "Thermoelectric automotive waste heat energy recovery using maximum power point tracking", *Energy Conversion and Management*, Volume 50, Issue 6, June 2009, pp. 1506-1512.

Zhang, B, and Mi, C. (2011), "Charge-Depleting Control Strategies and Fuel Optimization of Blended-Mode Plug-In Hybrid Electric Vehicles", *IEEE Transactions on Vehicular Technology*, Vol. 60, No. 4, May 2011.

APPENDIX A: LOAD FOLLOWING RESULTS

Table A-1: Base Series HEV Simulink Model Energy Consumption Results

Test mass: 1633 kg **Engine Size: 100 kW**	**Units**	**UDDS**	**HwFET**	**Combined**	**US06**
Net Tractive Energy	Wh/km	66.3	103	82.8	136
Fuel Energy Consumption	Wh/km	485	521	501	752
Net Battery Energy	DC Wh/km	1.09	-1.65	-0.14	1.94
WTW GHG	g CO_2 eq/km	156	168	161	242
Range	Km	659	618	641	430
Road load $\eta_{powertrain}$	%	13.7	19.8	16.5	18.1

Table A-2: Improved Series HEV Simulink Model Energy Consumption Results

Test mass: 1692 kg **Engine Size: 84 kW**	**Units**	**UDDS**	**HwFET**	**Combined**	**US06**
Net Tractive Energy	Wh/km	67.2	104	83.9	137
Fuel Energy Consumption	Wh/km	465	489	476	635
Net Battery Energy	DC Wh/km	-0.75	-1.05	-0.89	2.56
WTW GHG	g CO_2 eq/km	122	128	124	166
Range	Km	508	502	505	358
Road load $\eta_{powertrain}$	%	14.4	21.3	17.6	21.6